EXTRACTION OF CELLULOSE FROM AGRICULTURAL WASTE FOR WATER PURIFICATION

by

Ntombizanele Jafta

Submitted in accordance with the requirements for the degree

MASTER OF HEALTH SCIENCES IN ENVIRONMENTAL HEALTH (M_HSEN)

in the

Department of Life Science

Faculty of Health and Environmental Sciences

at the

Central University of Technology (Bloemfontein campus)

Supervisor: Dr M.J. Mochane
Co-supervisor: Dr T.C. Mokhena

August 2021

DECLARATION

I, NTOMBIZANELE JAFTA, student number , do hereby declare that this research project submitted to the Central University of Technology, Free State for the Master of science in Environment, is my own independent work; and complies with the Code of Academic Integrity, as well as other relevant policies, procedures, rules and regulations of the Central University of Technology, Free State; and has not been submitted before to any institution by myself of any other person in fulfilment (or partial fulfilment) of the requirements for the attainment of any qualification.

_____

N. JAFTA

DEDICATION

This work is dedicated to my late grandmother, Nozigigaba Jafta, my parents, Sandile Jafta and Mathabo Jafta, and the entire Jafta and Shomaele clan.

ACKNOWLEDGEMENTS

First and foremost I would like to thank God Almighty for the gift of life.

Throughout my study and the writing of this dissertation I have received a great deal of support and assistance. I would like to thank the Central University of Technology and the National Research Fund for their generous support and the grant that assisted me immensely on this journey.

I would like to extend a special word of thanks to my supervisors, Dr M.J. Mochane and Dr T.C. Mokhena. Your expertise was invaluable in formulating the research questions and methodology and your insightful feedback pushed me to sharpen my thinking and to take my work to the desired level. Dr Mochane, thank you for supporting me. You provided me with the tools that I needed to choose the right direction and to successfully complete this dissertation.

I would also like to acknowledge Mr T.P. Makhele for his continuous support and for his assistance with my laboratory work. I also thank everybody in the Life Science Department for your guidance and motivation, more especially Mr K. Lebelo, Ms T. Tsolo, Mrs M. Mokgadi. Thank you for your encouragement, support, interest, and valuable inputs. I would also like to thank my colleagues at DUT, UCT, CSIR, UNISA, and UOFS for assisting me with the analyses of the data.

In addition, I would like to thank our research team and most importantly Tiisetso Mokoena. I shall forever be grateful to you for your daily motivation and your assistance when I had to complete this dissertation.

I give special and loving credit to my parents for raising me with love, guidance, support, responsibility, and a lot of encouragement. Moreover, I could not have completed this dissertation without the support of my brother, Jabulane Jafta, sister, Lindiwe Shomaele, aunt, Bekiwe Mahlae, and grandmother Nomateketwa Shomaele. Lastly to my extended family, and all my lovely friends, thank you for engaging with me in stimulating discussions as well as happy distractions to rest my mind when I needed a break. Enkosi.
“Veni, Vidi, Vici”.

ABSTRACT

The escalating demand for clean water and rising water shortages due to population growth, improper use, and expanding urbanisation have become a global issue. In most parts of the world freshwater contains of contaminants such as heavy metal ions that are detrimental to human health. Water treatment has thus become important for the removal of any contaminants in water to render it safe for consumption. Continuous membrane and/or filter processes have been shown to be effective in water treatment. In this study, agricultural residue in the form of cellulose based maize stalks was used to extract cellulose which is a renewable and environmentally friendly adsorbent material that contains nano- and micro cellulose membranes. The membranes were prepared from cellulose nanofibers and CNT in the absence and presence of sodium lauryl sulfate (SLS) via vacuum filtration process. To Improve the stability and absorption of contaminants, carbon nanotubes were added into the cellulose membranes. Furthermore, to enhance the dispersion of SWCNTs into the cellulose membranes, SLS was used, and the resultant composite was “termed” the modified composites. The membranes were analysed by means of SEM, transmission electron microscopy (TEM), X-ray diffraction (XRD), Fourier Transform Infrared spectroscopy (FTIR), UV-vis spectroscopy (UV), and thermogravimetric analysis (TGA). The ratios of the investigated cellulose membranes were categorized as follows: cellulose: non-SLS SWCNT 1:0.3, 1:0.5 and 1:1, as well as: cellulose: CNT: SLS 1:0.3:1, 1:0.5:1 and 1:1:1. SEM and TEM images showed that the presence of sodium lauryl sulfate (SLS) resulted in a better dispersion of the carbon nanotubes within the cellulose matrix with few agglomerates of carbon nanotubes being visible. According to the XRD, the incorporation of carbon nanotubes in the form of single-walled carbon nanotubes (SWCNT) and their modification in the form of SLS seemed to cause little or no change in the peak positions. However, the addition of SWCNTs decreased the crystallinity index of the cellulose i.e. 71.5% to 67.1% for cellulose: CNT 1:0.3. The presence of SLS in the composites was demonstrated by symmetric stretching 2843 cm^{-1} and asymmetric stretching 2910 cm^{-1} as became evident using FTIR. Generally, as much as the SLS modified system for cellulose (CNT 1:0.3 composites) showed high removal efficiency, the presence of the SLS-based system seemed to hinder the formation of porous structure in the cellulose membrane and, as a result, reduced the adsorption of the dye. The removal efficiency showed that bromophenol blue dye (46.9%) was most adsorbed by cellulose when compared with dylon

dye (2.6%). All investigated samples were found to be resistant to calcium carbonate ($CaCO_3$), sodium hydroxide (NaOH), and nitric acid (HNO_3).

TABLE OF CONTENTS

LIST OF TABLES

LIST OF FIGURES

LIST OF SYMBOLS AND ABBREVIATIONS

AC	Activated carbon
AFM	Atomic Force Microscopy
AMBAC	Composite Bioadsorbent
APS	Aminopropyl triethoxysilane
BC	Bacterial cellulose
BET	Brunauer–Emmett–Teller
Ca	Calcium
CA	Cellulose acetate
CAN	Ceric ammonium nitrate
CB	Cellulose beads
CC	Cellulose carbamate
CCB	Carboxylated cellulose beads
Cl	Chlorine
CMC	Carboxymethyl cellulose
CNC	Cellulose nanocrystal
CNF	Cellulose Nanofibril
CNT	Carbon nanotubes
CNW	Cellulose nanowiskers
COOH	Carboxylic acid
CP	Chemically pure
Cr	Chromium
Cr(VI)	Chromium six
DMAc	N,N-dimethylacetamide
ECH	Epichlorohydrin
EPS	Extracellular polymetric substance
F	Fluorine
Fe_3O_4	Ferrosoferric oxide/Iron (II,III) oxide
Fe-CCB	Iron-carboxylated cellulose beads
$FeCl_3$	Iron chloride
FESEM	Field emission scanning electron microscope
FTIR	Fourier Transform Infrared spectroscopy

GMA	Glycidyl methacrylate
GO	Graphene oxide
GO-Zr	Graphene oxide-zirconium
GPa	Gigapascal
HPH	High-pressure homogenization
KOH	Potassium hydroxide
MBR	Membrane bioreactor
MC	Methylcellulose
Mg	Magnesium
MGO	Magnetic graphene
MO	Methyl orange
MPa	Megapascals
MPMWCNT	Magnetic polymer multi-wall carbon nanotubes
MWCNT	Multi-walled carbon nanotubes
NaBr	Sodium bromide
NaClO	Sodium hypochlorite
$NaClO_2$	Sodium chlorite
NaDDBS	Dodecyl-benzene sodium sulfonate
NaOH	Sodium hydroxide
$ND\text{-}NH_2$	Amino-functionalized nanodiamond
ND-PEG	Polyethylene glycol grafted nanodiamond
nm	Nanometer
OH	Hydroxide
OM	Optical microscope
PA	Polyamide
Pb^{2+}	Lead (II) ion
PEI	Polyethylenimine
PGMIC	Poly (1-glycidyl-3-methylimidazolium chloride)
PMA	Polyacrylamide
PQC	Polyethyleneimine and quaternized cellulose
PSF	Polysulfone
qe	Equilibrium adsorption potential
RGO	Reduced graphene oxide
SANS	South African National Standard

SBF	Sugarcane bagasse
SDS	Sodium dodecyl sulfate
SEM	Scanning electron microscope/microscopy
SEM-EDS	Scanning electron microscopy and energy dispersive X-ray spectroscopy
SLS	Sodium lauryl sulfate
SWCNT	Single-walled carbon nanotube
TEDA	Tetraethylenepentamine
TEM	Transmission electron microscope
TEMPO	2,2,6,6-Tetramethylpiperidyl-1-Oxyl
TGA	Thermogravimetric analysis
Ti^{+4}	Titanium
TiO_2	Titanium dioxide
TMC	Trimethyl chloride
TOCN	TEMPO-oxidized cellulose nanofiber
TOCNF	Tempo-mediated oxidized cellulose nanofibers
UF	Ultrafiltration
UV	Vinyl-triethoxy silane
UV-vis	Ultraviolet-visible spectroscopy
XRD	X-ray diffraction analysis
XRF	X-ray fluorescence
ZnO	Zinc oxide
Zr(OH)4	Zirconium hydroxide
ZrO_2	Zirconium dioxide

Chapter 1: General Introduction

1.1 Background to the study introduction

Water is an important renewable resource for sustaining life on earth [1,2]. The growing demand for clean water supplies has become a global concern due to population growth, excessive usage, and urban development. Researchers have warned that the lack of clean water, as well as growing water scarcity, could worsen significantly by the year 2050 [3]. In addition to direct human use, water contributes about 70% of fresh water worldwide for agricultural applications [4]. Water quality is determined by the concentration of inorganic and organic content and includes physical, chemical, and biological parameters [5,6,7]. The quality of drinking water is a crucial component for sustainable socio-economic growth and development, but a multitude of ill water management practices and harmful land uses have had a detrimental effect on marine and soil habitats worldwide [8]. Moreover, with the ongoing and escalating water crisis in South Africa, maintaining good water quality is vital for sustainable development. Water quality is not only a pivotal factor in promoting biological safety, but it is also an indicator of water suitability for maintaining numerous industrial applications and processes [7,9,10]. The quality of water depends on various factors including local geology, the environment, human uses such as waste disposal and industrial contamination, and it's used as a heat sink of water bodies [11]. When these factors exist in excess or in combination, they contribute to water pollution.

Water pollution is known as "the addition of contaminants to water that alter its natural properties [and] that make it unfavourable for life" [12]. This is a global issue that desperately needs attention and prevention [12,13]. Most incidences of water pollution do not start in the water itself, but virtually any human activity will affect the quality of the water environment [14]. Major drivers of water contamination are manufacturing, mining, building, transportation, and anthropogenic sources, with particular culprits being industrial and commercial activities [15,16,17]. Pollutants that impact untreated water include microorganisms (viruses, protozoa, and bacteria), organic chemicals (pesticides, herbicides, and industrial processes), inorganic pollutants (salt and metals), and radioactive contaminants [18,20]. When present in water, the pollutants listed above degrade the quality of the water and contribute to severe environmental

problems [18,19,20]. It is thus undeniable that eradicating water contamination calls for immediate action to ensure future prevention [21,22,23].

Clean water is the most desirable and important compound that most species need to sustain life. When dissolved in water, elements such as calcium (Ca), magnesium (Mg), chlorine (Cl), and fluorine (F) pose little threat to species when they are in low concentrations and comply with South African National Standard (SANS) 241 [24]. However, large concentrations of dissolved metals in water can pose a significant risk to public health because they may be harmful and are undetectable without laboratory analysis [25]. Several factors are responsible for heavy metal accumulation in aquatic systems such as weathering and the degradation of heavy metal-rich soil and rock, smelting, anthropogenic activities in mining, and the use of heavy metals or heavy metal-containing substances [26,27]. Based on the above information, effective water treatment to illuminate pollutants has become a matter of major concern.

Assessing metallic pollution in the environment is fraught with many problems due to the rapidly increasing variability of metal concentrations over time and space [28]. Sediments are potential reservoirs of absorbed heavy metals that are suspended in them. Earlier studies have shown that metals are either picked up from the soil via roots or are suspended in untreated river water that is used for irrigation. Moreover, heavy metal pollution of fresh water supplies and produce poses a major risk to human health [30-32]. Many adverse health effects associated with heavy metals have been established, but humans' and animals' exposure to heavy metals in water has continued unabated and is even increasing in various parts of the world, particularly in less developed countries [33]. Arsenic, mercury, and lead are the three main 'rogue' metals or metalloids that have a strong correlation to adverse health effects in humans (Table 1.1). Arsenic, which is graded as Class A, is notoriously carcinogenic as it can accumulate in the human body with severe adverse effects [34]. Its cumulative effects on the human body include skin inflammation, skin hyperpigmentation, and skin and internal organ cancer [34,35], while its acute symptoms are respiratory, gastrointestinal, and cardiovascular failure [35].

Water intake is the only mechanism to access drinking water and controlling heavy metals in water is therefore critical. Tchounwou *et al*. [36] noted that water samples have been analysed in South Africa that have indicated hazardous concentrations of various metals such as antimony, arsenic, cadmium, chromium, mercury, nickel, and selenium. All of these metals/metalloids have severe impacts on human health, with arsenic being of most concern.

Table 1.1: Health effects caused by heavy metals

Metals	Acute Health Effects	Chronic Health effects
Arsenic	• Death caused by upper respiratory, pulmonary, and abdominal pains as well as gastrointestinal and cardiovascular failure.	• Nervous damage and sensory loss in the peripheral nervous system and eventually death.
Organic and Inorganic mercury	• Neurological and renal disturbances may occur. • Acute mercury exposure may give rise to lung damage.	• Chronic poisoning is characterised by neurological and psychological symptoms such as tremors, changes in behaviour, restlessness, anxiety, sleep disturbance, and depression.
Lead	• Headache, irritability, abdominal pain • Pain and various symptoms related to the nervous system	• In encephalopathy, the affected person may suffer from acute psychosis, confusion, and reduced consciousness. • suffering from memory loss, prolonged reaction time, and reduced ability to understand.

Sources: Adapted from ATSDR, 2017; Järup, 2003 [34,33]

Constraints caused by the inappropriate use of, or a lack of water put pressure on the already limited supply of food globally. Moreover, existing water purification methods such as (1) physical processes, such as filtration, sedimentation, or distillation; (2) biological processes, such as sand filters, active carbon; (3) chemical processes, such as flocculation, chlorination, the use of ultraviolet light. The technologies are very costly, and this has prompted researchers to find new ways of extracting toxins from water. Heavy metal ions that are commonly found in wastewater also tend to persist in the environment where they are extremely toxic even at lower levels [37-40]. It is against this background that an inexpensive, efficient, robust, and eco-friendly method for the removal of pollutants in the form of dyes and heavy metal ions from wastewater is urgently required.

Well-known water treatment methods include chemical precipitation, electrochemical degradation, photo-degradation, ion exchange, membrane filtration, bio-removal, and adsorption [41-44]. Among these, adsorption is considered ideal for industrial wastewater treatment due to its high absorption capacity, ease of use, and economic viability [45,46]. Various high-capacity adsorbents such as activated carbon, alumina nanoparticles, modified metal oxides, silica mesoporous substances, and cellulose adsorbents have been investigated in recent years [47-49]. Cellulose-based adsorbents in particular have attracted increasing attention because they are biodegradable, renewable, inexpensive, biocompatible, eco-friendly, and highly stable in the presence of most organic solvents [50-52].

Agricultural residues are primarily composed of cellulose, hemicellulose, and lignin [53,54], as shown in Figure 1.1 [55]. Agricultural residues are sourced from coconuts, sugarcane bagasse, and maize stalks, to name a few. Cellulose, which possesses all the mechanical properties of natural fiber, is stored in micro-fibrils that are enclosed by hemicellulose and lignin [14,53,54,56]. Cellulose is one of the world's most abundant, natural, and renewable macromolecules and is commonly found in various biomass forms [57]. Natural cellulose fibers may be used for different applications such as in the textile and pulp and paper industries. They are also used as composites and components and have multiple other industrial applications [58]. Selective application of cellulose include; osmotic drug delivery systems, bioadhesives and muco adhesives, compression tablets as compressibility enhancers, liquid dosage forms as thickening agents and stabilizers, granules and tablets as binders, semisolid preparations as gelling agents and many other applications.

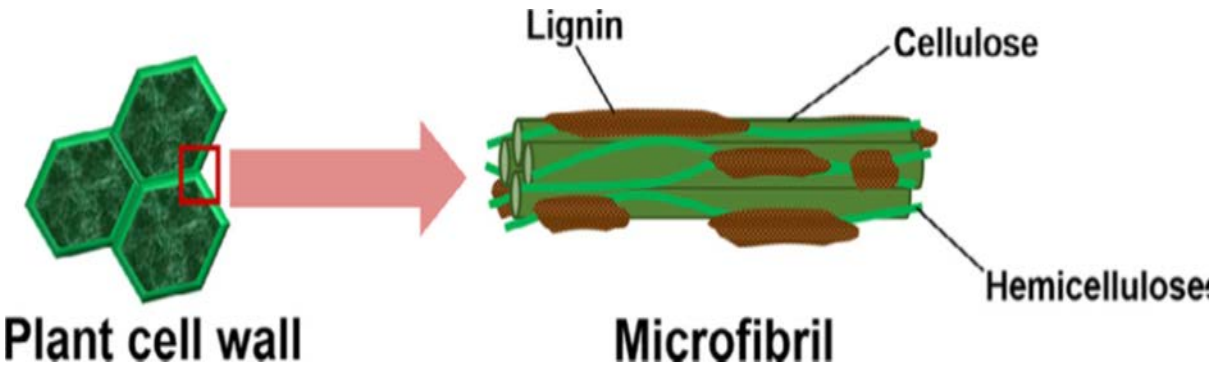

Figure 1.1: Main structure of the plant cell wall in lignocellulosic biomass which consists of lignin, hemicellulose, and cellulose [55]

There are different methods used for water treatment, such as using adsorbents or a continuous membrane and/or filter process. In recent years, cellulose and its applications have attained high favour in both research and industrial areas due to its attractiveness in terms of mechanical properties, high surface area, rich hydroxyl groups for modification, and natural properties with 100% environmental friendliness [59,60]. Nanocellulose is commonly classified as cellulose nanomaterials consisting of nanometrically dimensioned fibrils that are obtained primarily through mechano-chemical treatments [55,61]. These treatments effect the regeneration of materials with special properties such as strength and chemical inertia and with wide surface areas. Moreover, it is accessible for surface modification through plentiful hydroxyl group which is composed of, renewable and environmentally safe adsorbent material in the form of nano- and micro-cellulose was used for contaminant adsorption in the current study. The desirable adsorbent material was obtained by extracting nanocellulose (nanofibers) from agricultural waste, specifically maize stalks [62-64].

Cellulose is extracted from plant fibers using some of the chemical and mechanical methods and they could be extracted in nano and micro forms by alkalization, bleaching and acid hydrolysis process. For an example, Ranganagowda *et al.* [65] reported-on extraction of cellulose from areca fibers using formic acid at 20% v/v as well as hydrogen peroxide (viz 10% v/v) and 65% yield of cellulose was obtained. Furthermore, cellulose was extracted from sisal fiber by two methods/procedure which included acid hydrolysis, chlorination, alkalization, and bleaching [Juan I. Mora´n][66]. The extraction method led to the production of cellulose. The production of nanocellulose was formed by the acid hydrolysis of the extracted cellulose.

Khenblouche [67] and co-workers reported on the extraction of microcellulose fibers from the retama raetam stems. The microcellulose were extracted from retama raetam stems by employing 7 wt% sodium hydroxide which was followed by bleaching treatment. The microcellulose were found to be highly crystalline with a crystallinity of 77.8%, and its crystallite size was reported to be 3.62 nm. The acid hydrolysis and mechanical treatments of cellulose extracted waste newspaper was reported by Takagi *et al.* [68]. The obtained cellulose nanofibers were in the form of thick whisker-like structures with a diameter in the range 10-40 nm.

The nanocellulose based membranes have been reported to be promising materials for water purification, however, there are challenges that are associated with these membranes, such as cost-effective upscaling, stability, and biofouling. In this study, carbon nanotubes were added

into the cellulose membranes in order to improve the stability and adsorption behaviour of the cellulose membranes. Nanocellulose was extracted from maize stalks in this project to build a filtration membrane for treating wastewater. The research aimed to establish how nanocellulose and its modified surface structures impacted the adsorption of water contaminants such as heavy metals and dye. A combination of the above-mentioned properties makes nanocellulose an outstanding substrate for high-performance membranes and filters to extract pollutants selectively from both industrial and drinking water sources.

1.2 Research Aims

Nanocellulose (nanofibers) was extracted from maize stalks to create a filtration membrane for wastewater treatment, specifically to investigate how nanocellulose structures affected the adsorption of different contaminants and to understand the effect of carbon nanotubes on the adsorption efficacy of cellulose. The membranes were prepared from cellulose nanofibers and CNT in the absence and presence of sodium lauryl sulfate (SLS) via vacuum filtration process.

1.3 Research Objectives

The objectives of this study were to investigate:

- The effectiveness of cellulose/CNT and cellulose/CNT/SLS membranes against anionic bromophenol and commercial dye;
- The chemical resistance of cellulose/CNT and cellulose/CNT/SLS membranes; and
- The effect of CNT and CNT/SLS on the thermal stability of the selected cellulose membrane.

1.4 Thesis Organisation

This thesis is structured as follows:

Chapter 1: Introduction

Chapter 2: Literature Review

Chapter 3: Materials and Methods

Chapter 4: Results and Discussions

Chapter 5: Conclusion

1.5 References

1. Wolf, A.T. (2007). Shared waters: conflict and cooperation. Annual. Review of Environment and Resources, 32(1), 241–269.
2. Fthenakis, V.M., & Kim, H.C. (2010). Lifecycle uses of water in U.S. electricity generation. Renewable and Sustainable Energy Reviews. 14(7), 2039–2048.
3. Galvan, F.R.V., & Barranco, J.C., Galvan, S., Batlle, S.F., & Garcia, F. (2018). "We are Intech Open, the world' s leading publisher of open access books built by scientists, for scientists in the top 1%". *Intech open*, i, [tourism], 13.
4. Duan, W., Takara, K., He, B., Luo, P., Nover, D., & Yamashiki, Y. (2013). Spatial and temporal trends in estimates of nutrient and suspended sediment loads in the Ishikari River, Japan, 1985 to 2010. *Science of the Total Environment, 461*, 499–508.
5. Wang, Y.B., Liu, C.W., Liao, P.Y., & Lee, J.J. (2014). Spatial pattern assessment of river water quality: implications of reducing the number of monitoring stations and chemical parameters. *Environmental Monitoring and Assess*ment, 186(3), 1781–1792.
6. Jiang, X., Xu, S., Liu, Y., & Wang, X. (2015). River ecosystem assessment and application in ecological restorations: a mathematical approach based on evaluating its structure and function. *Ecological Engineering*,76, 151–157.
7. Manickum, T., John, W., Terry, S., & Hodgson, K. (2014). Preliminary study on the radiological physiochemical quality of the Umgeni water catchment and drinking sources in Kwazulu-Natal, South Africa. *Journal of Environmental Radioactivity,* 137, 227−240. http://dx.doi.org/10.1016/j.jenvrad.2014.07.015 .
8. Xing, Z., Fong, D.A., Lo, E.Y., & Monismith, S.G. (2014). Thermal structure and variability of a shallow tropical reservoir. Limnology and Oceanography, 59(1), 115–128.

9. Khan, S., Cao, Q., Zheng, Y.M., Huang, Y.Z., & Zhu, Y.G. (2008). Health risks of heavy metals in contaminated soils and food crops irrigated with wastewater in Beijing, China. *Environmental. Pollution*, 152(3), 686-692.
10. Duan, W., He, B., Nover, D., Yang, G., Chen, W., Meng, H., Zou, S., & Liu, C. (2016). Water quality assessment and pollution source identification of the eastern Poyang Lake basin using multivariate statistical methods. *Sustainability*, 8(2), 133–147.
11. Gopal, K., & Agarwal, A.K. (2003). *River pollution in India and its management*. New Delhi: APH Publishing Corporation.
12. Bai, J., Huang, Y., Gong, Q., Liu, X., Li, Y., Gan, J., Zhao, M., Shao, Y., Zhuang, D., Liang,L. (2018). Preparation of porous carbon nanotube/carbon composite spheres and their adsorption properties. *Carbon*, 137, 493–501.
13. Woodford, C. (2015). Water pollution: an introduction. http://www.explainthatstuff.com/waterpollution.html [accessed 2015/01/10].
14. Zimmerman, T., Pohler, E. and Schwaller, P. (2005) Mechanical and morphological properties of cellulose fibril reinforced nanocomposites. *Advanced Engineering Materials*, 12, 1156-1161. http://dx.doi.org/10.1002/adem.200500157
15. Van Landeghem, M.M., Meyer, M.D., Cox, S.B., Sharma, B., & Patino, R. (2012). Spatial and temporal patterns of surface water quality and ichthyotoxicity in urban and rural river basins in Texas. *Water Research*. 46(20), 6638–6651.
16. Zhao, Y., Song, K., Li, S., Ma, J., & Wen, Z. (2016). Characterization of CDOM from urban waters in North-Eastern China using excitation-emission matrix fluorescence and parallel factor analysis. *Environmental Science and Pollution Res*earch, 23(15), 15381–15394.
17. Singh, K.P., Malik, A., Mohan, D., & Sinha, S. (2004). Multivariate statistical techniques for the evaluation of spatial and temporal variations in water quality of Gomti River (India): a case study. *Water Research*, 38(18), 3980–3992.
18. Hambright, K.D., Zamor, R.M., Easton, J.D., Glenn, K.L., Remmel, E.J., & Easton, A.C. (2010). Temporal and spatial variability of an invasive toxigenic protist in a North American subtropical reservoir. *Harmful Algae*, 9(6), 568–577.
19. He, W., Lee, J., & Hur, J. (2016). Anthropogenic signature of sediment organic matter probed by UV-visible and fluorescence spectroscopy and the association with heavy metal enrichment. *Chemosphere*, 150, 184–193.
20. Kowalkowski, T., Zbytniewski, R., Szpejna, J., & Buszewski, B. (2006). Application of chemometrics in river water classification. *Water Research*, 40(4), 744–752.

21. Schwarzenbach, R.P., Egli, T., Hofstetter, T.B., Von Gunten, U., & Wehrli, B. (2010). Global water pollution and human health. *Annual Review of Environment and Resources*, 35(1), 109–136.
22. State Environment Protection Administration of China (SEPA). (2002). *Methods for water and wastewater monitoring and analysis in China* (4th ed.). Beijing: China Environmental Science Press.
23. Kasel, D., Bradford, S.A., Simůnek, J., Heggen, M., Vereecken, H., & Klumpp, E. (2013). Transport and retention of multi-walled carbon nanotubes in saturated porous media: effects of input concentration and grain size. *Water Res*earch, 47(2), 933–944.
24. South African National Standard (SANS). (2015). Drinking water, 241, 1−2. Published by SABS Standards Division. www.sabs.co.za
25. Pearson, D., Weindorf, D.C., Chakraborty, S., Li, B., Koch, D.J., Van Deventer, D.P., de Wet, D.J., & Kusia, N.Y. (2018). Analysis of metal-laden water via portable X-ray fluorescence spectrometry. *Journal of Hydrology,* (561), 267−276.
26. Rai, P.K. (2008). Heavy metal pollution in aquatic ecosystems and its phytoremediation using wetland plants: an eco-sustainable approach. *International journal of Phytoremediation*, 10(2), 131–158.
27. Hartmann, J., West, A.J., Renforth, P., Kohler, P., La Rocha, C.L., Wolfgladrow, D., Durr, H.H., & Scheffran, J. (2013). Enhanced chemical weathering as a geoengineering strategy to reduce atmospheric carbon dioxide, supply nutrients, and mitigate ocean acidification. *Reviews of Geophysics*, 51(2), 113–149.
28. Ali,H., Khan,E., Ilahi,I.(2019). Environmental Chemistry and Ecotoxicology of Hazardous Heavy Metals: Environmental Persistence, Toxicity, and Bioaccumulation. *Journal of chemistry*,2019,1-14.
29. Chaney, R.L., Li, Y.-M., Brown, S.L., Homer, F.A., Malik, M., Angle, J.S., Baker, A.J.M., Reeves, R.D., & Chin, M. (1999). Improving metal hyperaccumulator wild plants to develop commercial phytoextraction system: Approaches and Progress (Chapter 7). *Phytoremediation of contaminated soil and Water*. CRC Press http://www.crcnetbase.com/doi/abs/10.1201/9781439822654.ch7
30. Khan, S., Cao, Q., Zheng, Y.M., Huang, Y.Z., & Zhu, Y.G. (2008). Health risks of heavy metals in contaminated soils and food crops irrigated with wastewater in Beijing, China. *Environmental Pollution*, 152(3), 686e692. https://doi.org/10.1016/j.envpol.2007.06.056

31. Sipter, E., Rozsa, E., Gruiz, K., Tatrai, E., Morvai, V. (2008). Site-specific risk assessment in contaminated vegetable gardens. *Chemosphere*, 71(7), 1301e1307. https://doi.org/10.1016/j.chemosphere.2007.11.039.
32. Amin, N., Hussain, A., Alamzeb, S., & Begum, S. (2013). Accumulation of heavy metals in edible parts of vegetables irrigated with wastewater and their daily intake to adults and children, District Mardan, Pakistan. *Food Chemistry*, 136(3), 1515-1523. https://doi.org/10.1016/j.foodchem.2012.09.058
33. Järup, L. (2003). Hazards of heavy metal contamination. *British Medical Bulletin*, 68, 167–182. https://doi.org/10.1093/bmb/ldg032
34. Agency for Toxic Substances and Disease Registry (ATSDR). (2017). Arsenic. https://www.atsdr.cdc.gov/index.html
35. Farzan, S.F., Karagas, M.R., & Chen, Y. (2013). In utero and early life arsenic exposure in relation to long-term health and disease. *Toxicology and Applied Pharmacology*, 272(2), 384−390.
36. Tchounwou, P.B., Patlolla, A.K., & Centeno, J.A. (2003). Carcinogenic and systematic health effects associated with arsenic exposure: a critical review. *Toxicologic. Pathology.*, 31(6), 575-588. https://doi.org/10.1080/01926230390242007
37. Feng, Q., Wu, D., Zhao, Y., Wei, A., Wei, Q., & Fong, H. (2017). Electrospun AOPAN/RC blend nanofiber membrane for efficient removal of heavy metal ions from water. *Journal of Hazardous Materials*, 344, 819–828.
38. Ji, W.B., Yap, S.H.K., Panwar, N., Zhang, L.L., Lin, B., Yong, K.T., Tjin,S.C., Ng,W.J., Majid,M.B.A. (2016). Detection of low-concentration heavy metal ions using optical microfiber sensor. *Sensors and Actuators B, Chemical*, 237, 142–149.
39. Setyono, D., & Valiyaveettil, S. (2016). Functionalized paper: a readily accessible adsorbent for removal of dissolved heavy metal salts and nanoparticles from water. *Journal of Hazardous Materials*, 302, 120–128.
40. Zou, T., Wang, C., Tan, R., Song, W., & Cheng, Y. (2017). Preparation of pompon-like ZnO-PANI heterostructure and its applications for the treatment of typical water pollutants under visible light. *Journal of Hazardous Materials*, 338, 276–286.
41. Chakraborty, A., Bhattacharyya, S., Hazra, A., Ghosh, A.C., & Maji, T.K. (2016). Post-synthetic metalation in an anionic MOF for efficient catalytic activity and removal of heavy metal ions from aqueous solution. *Chemical Communications*, 52, 2831–2834.

42. Peng, W., Li, H., Liu, Y., & Song, S. (2017). A review on heavy metal ions adsorption from water by graphene oxide and its composites. *Journal of Molecular Liquids*, 230, 496–504.
43. Salleh, M.A.M., Mahmoud, D.K., Karim, W.A.W.A., & Idris, A. (2011). Cationic and anionic dye adsorption by agricultural solid wastes: a comprehensive review. *Desalination*, 280, 1–13.
44. Zhang, P., Gong, J.L., Zeng, G.M., Deng, C.H., Yang, H.C., Liu, H.Y., Huan, S. (2017). Cross-linking to prepare composite graphene oxide-framework membranes with high-flux for dyes and heavy metal ions removal. *Chemical Engineering Journal*, 322, 657–666.
45. Fakhre, N.A., & Ibrahim, B.M. (2017). The use of new chemically modified cellulose for heavy metal ion adsorption. *Journal of Hazardous Materials*. 343, 324–331.
46. Yang, Q., Lu, R., Ren, S.S., Chen, C., Chen, Z., & Yang, X. (2018). Three-dimensional reduced graphene oxide/ZIF-67 aerogel: effective removal cationic and anionic dyes from water. *Chemical Engineering Journal*, 348, 202–211.
47. Bai, J., Huang, Y., Gong, Q., Liu, X., Li, Y., Gan, J., Liang,J. (2018). Preparation of porous carbon nanotube/carbon composite spheres and their adsorption properties. *Carbon*, 137, 493–501.
48. Islam, M.S., Choi, W.S., Nam, B., Yoon, C., & Lee, H.J. (2017). Needle-like iron, oxide@CaCO3 adsorbents for ultrafast removal of anionic and cationic heavy metals ions. *Chemical Engineering Journal*,307,208-219.
49. Xu, S., Lv, Y., Zeng, X., & Cao, D. (2017). ZIF-derived nitrogen-doped porous carbons as highly efficient adsorbents for removal of organic compounds from wastewater. *Chemical Engineering Journal*, 323, 502–511.
50. Martins, B.F., Toledo, P.V.O.D., & Petri, D.F.S. (2017). Hydroxypropyl methylcellulose based aerogels: synthesis, characterization and application as adsorbents for waste-water pollutants. *Carbohydrate Polymers*, 155, 173–181.
51. Suhas Gupta, V.K., Carrott, P.J.M., Singh, R., Chaudhary, M., & Kushwaha, S. (2016). Cellulose: a review as natural, modified and activated carbon adsorbent. *Bioresource Technology*, 216, 1066–1076.
52. Maatar, W., Alila, S., & Boufi, S. (2013). Cellulose based organogel as an adsorbent for dissolved organic compounds. *Industrial Crops and Products*, 49, 33–42.

53. Vignon, M.R., Heux, L., Malainine, M.E., & Mahrouz, M. (2004). Arabinan-cellulose composite in Opuntia ficus-indica prickly pear spines. *Carbohydrate Res*earch, 339(1), 123–113.
54. Rong, M.Z., Zhang, M.Q., Lui, Y., Yang, G.C., & Zeng, H.M. (2001). The effect of fibers treatment on the mechanical properties of unidirectional sisal-reinforced epoxi composites. *Composites Science and Technology*, 61, 1437–1144.
55. Phanthong, P., Reubroycharoen, P., Hao, X., Xu, G., Abudula, A., & Guan, G. (2018). Nanocellulose: extraction and application. *Carbon Resources Convention.*,1,32-43.
56. Mandal, A., & Chakrabarty, D. (2011). Isolation of nanocellulose waste sugarcane bagasse (SCB) and its characterization. *Carbohydrate Polymers*, 86, 1291−1299.
57. Fengel, D., & Wegner, G. (1989). *Wood-chemistry, ultrastructure, reactions*. Berlin, New York: Walter de Gruyter.
58. Klemm, D., Heublein, B., Fink, H.P., & Bohn, A. (2005). Cellulose: fascinating biopolymer and sustainable raw material. *Angewandte Chemie* [International Edition], 44, 3358–3393.
59. Park, N., Choi, S., Oh, J., & Hwang, D. (2019). Facile extraction of cellulose nanocrystals. *Carbohydrate Polymers*, 223, 115114.
60. Kopania, E., Wietecha, J., & Ciechańska, D. (2012). Studies on isolation of cellulose fiber from waste plant biomass. *Fiber & Textiles in Eastern Europe*, 20(6B 96), 167−172.
61. Dufresne, A. (2013). Nanocellulose: a new ageless bionanomaterial. *Material. Today*, 16, 220−227.
62. Dufresne, A. (2012). Nanocellulose: potential reinforcement in composites. *Natural Polymers, Nanocomposite*, 2, 1−32.
63. Eichhorn, S.J., Dufresne, A., Aranguren, M., Marcovich, N.E., Capadona, J.R., Rowan, S.J., Peijs, T. (2010). Review: current international research into cellulose nanofiber and nanocomposites. *Journal of Material Sci*ence, 45, 1−33.
64. Jamshaid, A., Hamid, A., Muhammad, N., Naseer, A., Ghuari, M., Iqbal, J., Shah, N. (2017). Cellulose-based materials for the removal of heavy metals from wastewater: an overview. *Chem Bio Eng*, 4, 1–18.
65. Ranganagowda,R,P.G., Kamath,S.S., Bennehalli,B.(2019). Extraction and Characterization of Cellulose from Natural Areca Fiber. *Material Science Research India*,16, (1) ,86-93.
66. Mora´n, J.I., Alvarez, V.A., Cyras, V.P.,Va´zquez,A.(2008). Extraction of cellulose and preparation of nanocellulose from sisal fibers. *Cellulose,* 15,149–159.

67. Khenblouche, A., Bechki, D., Gouamid, M., Charradi, K., Segni, L., Hadjadj, M., & Boughali, S. (2019). Extraction and characterization of cellulose microfibers from Retama raetam stems. *Polímeros: Ciência e Tecnologia*,29(1), e2019011. https://doi.org/10.1590/0104-1428.05218

68. Takagi,H., Nakagaito,A.N., Shahril,M.,Bistamam,A.(2013). Extraction of cellulose nanofiber from waste papers and application to reinforcement in biodegradable composites. *Journal of Reinforced Plastics and Composites*, 0(00), 1–5.

Chapter 2: Literature Review

2.1 Cellulose-Based Materials and their Classifications

The applications of cellulose in the industrial sector is steadily increasing. Amongst these applications is wastewater treatment, which has received tremendous interest in recent years. There are different classifications of cellulose depending on the methods and techniques of preparation, shapes, and sizes [1]. Generally, there are three classifications of nano-cellulosic materials which are the following [2]:

- cellulose nanocrystals (CNCs)
- cellulose nanofibrils (CNFs)
- bacterial nanocellulose (BC or BNC).

A comparison of these different forms of nanostructured cellulose is presented in Table 2.1.

Table 2.1: Comparison of the different types of nanocellulose

Nanocellulose	Shape	Typical sources	Advantages
Cellulose nanocrystals (CNCs)	Cylindrical rods	Hardwood, plants, agricultural residues, etc.	High surface area, excellent mechanical properties, low density, low coefficient of thermal expansion
Cellulose nanofibrils (CNFs)	Complex fibers structure with thin fibrils	Hardwood, softwood, plants, agricultural residues	Low density, high surface area, and good mechanical strength
Bacterial nanocellulose (BNC)	Ribbon shaped	Low molecular weight sugars such as glucose	Excellent mechanical strength, high purity, great stability

Source: 3, D. Tranche, 2018; published by the AIMS Press.

2.1.1 Cellulose nanocrystals (CNCs)

Cellulose nanocrystals, also known as cellulose whiskers, are rod-like structures that are acquired from lignocellulosic fibers and are generally obtained using the acid hydrolysis process [1]. Cellulose from various plants and other lignocellulosic materials are used to extract these nanocrystals. Cellulose nanocrystals have a crystalline structure which limits their flexibility [1]. These nanocrystals have a nanosized distribution scale and they are usually 4–55 nm in diameter and 90–400 nm in length, but a particular study [4] found that the diameter of the nanocrystals was 4−7 nm and that they were 150−450 nm in length. Such nanocrystals are for instance extracted from maize stalk leftovers [4]. Similarly, Siró *et al*. [5] reported that the nanocrystals in their study had a diameter of 2−20 nm and a length of between 100−200 nm. Valenti *et al*. reported a nanocrystal mean length of 1.8 μm with a thickness of 22.6 nm for 0.5 wt.% nanocellulose incorporated in polyhydroxyalkanoates matrix [6].

Cellulose nanocrystals have a high aspect ratio and present a disproportionate number of hydroxyl groups on their surface. They also exhibit additional properties such as strong transparency, ultrafine structure, high purity level, and excellent mechanical strength. For example, their Young's modulus ranges between 100–140 and a tensile strength of 7500 MPa [7]. These properties make these nanosized materials effective for various applications in the biomedical, food and paper, and pharmaceutical industries [8,9].

2.1.2 Cellulose nanofibrils (CNFs)

In earlier studies CNFs were isolated from plant sources such as wood pulp in a process that included the pre-treatment and homogenisation of the pulp under high pressure [1]. This technique has been successfully utilised for the isolation of CNFs, but it is energy-consuming [10,11]. More effective processes have subsequently been developed using both mechanical and chemical techniques that have resulted in CNFs of superior quality [10].

Using a mechanical process, the fibers structure obtained from the cellulosic sources is removed and chemically treated to eradicate hemicellulose and lignin [12]. Before converting the strands into CNFs, the cellulose fibers must be subjected to intense mechanical crushing to remove volatile compounds such as, terpenoids, amino acids, fatty acid derivatives, benzenoid, and phenylpropanoid chemicals from the divider of the plant unit [1,13,14,15]. Typically, the

dimensions of the filaments range from 2–80 nm, depending on the breaking-down force [16]. The morphology of CNFs is characterized by prolonged masses of rudimentary nanofiber with anisotropic and isotropic reciprocating regions. These CNFs, as already stated, require intense mechanical shearing. However, to encourage the defibrillation process, a preliminary treatment of strands is required [1]. Pre-treatment is typically done using synthetic substances or, conversely, enzymes that precede the mechanical procedure to achieve CNFs that have the most desirable properties [1].

CNFs have a complex fibers structure with thin fibrils woven together in a web-like manner, while CNCs are small, rod-like structures. CNFs have an average length of 200–1800 nm and a diameter of 6–100 nm. CNFs contain more amorphous regions than CNCs as they form long, flexible fibers networks. CNCs are obtained through acid hydrolysis which is a process that removes the amorphous regions from the cellulosic structure, thus making them highly crystalline [1]. The removal of amorphous regions makes CNCs more crystalline than CNFs. In terms of aspect ratio, CNFs have a much higher aspect ratio than CNCs [1].

In addition to its biodegradability attributes, the principal property of the nanosized fibrils is their higher strength compared to other natural and synthetic fibers [1]. According to Mariani *et al*. [17], the tensile strength of CNF suspension films was 7.4-72.6 MPa while their Young's modulus was 1.2-10.2 GPa. Other key characteristics of CNF films include their high specific surface and good mechanical properties. CNFs have a variety of potential applications in the biomedical field (tissue engineering), scaffolding, paper and film industries, and the electronic and energy sectors (catalysts and sensors, coatings, membranes, and composites), and they have also been used for environmental remediation, water treatment, hydrogels, and as superabsorbent polymers [1].

2.1.3 Bacterial cellulose (BC)

The cellulose fibres extracted from bacteria sources exhibit a ribbon-like shape and have a width below 100 nm. It was reported [18] that the cellulose derived from *Asaia bogorensis* showed a bead-like rather than a ribbon-like shape. Contrary to the production/preparation techniques used for other nanocellulose, bacterial cellulose synthesis is conducted using the biosynthesis process which yields a gel-like, swollen, aqueous, flexible membrane [1].

Stanislawska [19] mentions that fiber from the extracellular matrix of bacteria combine with the aqueous region to form bundles of fibres, further creating a three-dimensional structure.

Although BCs may have potential for several applications, their disadvantages are that they require extended processing time, are costly to produce, and require arduous large-scale production and application processes [1]. Various other authors agree that the production of these nanomaterials requires an expensive and time-consuming cultivation medium which restricts large-scale production [11,20].

2.2 Extraction of cellulose and nanocellulose from Natural Fiber

Cellulose is the major constituent of most plant materials and is thus extracted from plant fiber using both mechanical and chemical methods. Both nano- and micro-cellulose are produced in three steps: alkalization, bleaching, and acid hydrolysis. Vu *et al.* extracted cellulose from Vietnam's rice straw by employing the ultrasound-assisted alkaline treatment process [21]. It was shown that, when extracting cellulose sourced from rice straw using ultrasound irradiation in the presence of an alkaline solution at high temperatures, enhanced production was achieved when the time was increased from 10−30 minutes. Sun *et al.* [22] extracted cellulose from sugarcane bagasse with ultrasonic irradiation in the presence of alkali and alkaline peroxide. According to the authors, 44.7% yield of cellulose was obtained from the alkaline treatment and 45.9% from the peroxide treatment. In another study, Feng *et al.* [23] used an environmentally friendly process for the extraction of cellulose nanofibrils from sugarcane bagasse using the ultra-sonification method combined with various mechanochemical pre-treatments. These pre-treatments included the continuous explosion of steam, a hydrothermal diluted alkali-catalyzed (0.4 wt.% NaOH) treatment, and hydrogen peroxide bleaching [20]. Using very small amounts of chemical reagents, existing pre-treatments have effectively eliminated non-cellulosic constituents from the raw fiber with a yielding suspension of 0.6wt% and a crystallinity index of 71.2% [20]. Nie *et al.* [24] extracted cellulose nanofibrils from unbleached sugarcane bagasse pulps that were pre-treated by xylanase and subjected to low-temperature pre-treatment involving various cold alkali concentrations [24]. Through ultra-micro grinding and high-pressure homogenization, the cellulose nanofiber (CNF) had a diameter of 13−30 nm and an average fibre diameter of 39.71 nm.

According to the literature [25,26], cellulose nanocrystals may be derived from purified cellulose fiber after the complete dissolution of non-crystalline fractions using the hydrolysis process. Lignin content is normally left in the cellulose fibers after alkali treatment, which may impede CNC extraction and result in poor surface wettability between the material of the polymer matrix and the natural fibers. In most cases, lignin is the hardest chemical component to remove from lignocellulose fiber [27]. In this case, bleaching is an additional step that is necessary to further eliminate the residual cementing material in the alkali retted fiber, primarily lignin. This method is known as delignification [28].

Sulfuric acid treatment of cellulosic materials is another method that has been commonly used in the acid hydrolysis process for the fabrication of cellulose nanocrystals [28]. The acidic sulfate groups formed during acid hydrolysis are simultaneously added and left on the surface of developed cellulose crystals by esterifying the cellulose surface hydroxyl group [28]. Sheltami and co-workers [29] extracted cellulose from mengkuang leaves. The crystallinity of the cellulose was found to be 69.5%. The extracted cellulose was treated with alkaline and bleaching agents, while concentrated sulfuric acid was used to isolate cellulose nanocrystals from the cellulose. Table 2.2 summarises different extraction methods and sources of cellulose.

Table 2.2: **Different extraction methods and sources of cellulose and nanocellulose**

Source	Method	Summary of findings	Refs
Raw cotton liner	Acid hydrolysis	Increased crystallinity index of 91%. Nanocrystals were 177 nm long and 12 nm wide with an aspect ratio of 19.	[30]
Reused wastepaper	Alkaline and bleaching treatments followed by acid hydrolysis for isolation of CNCs	CNC length ranged from 100 nm− 300 nm. The crystallinity index of extracted CNC was 75.9%	[31]
TEMPO-oxidized jute fiber	TEMPO selectively oxidized pre-treatment	Cellulose nanowhiskers with a super-thin diameter (3–10 nm) in the form of a stable and transparent dispersion with high crystallinity,	[32]

	combined with mechanical homogenization	carboxylate functional groups, and high surface areas.	
Rice husk	Alkali and bleaching treatments (acid hydrolysis treatment)	Cellulose nanocrystals with a diameter ranging from 10−15 nm were obtained.	[33]
Vietnam's rice straw	Ultrasonic irradiation	Cellulose showed high thermal stability with 5% degradation. The yield increased with increased sonication time from 10−30 min under the set conditions.	[21]
Sisal fiber	Acid hydrolysis, chlorination, alkaline extraction, and bleaching	Purified cellulose sisal fiber of about 100–500 µm and several microfibrils with diameters in the range of 8–12 µm were obtained.	[34]
Natural areca fibers	Formic acid and hydrogen peroxide	The cellulose was found to contain α-cellulose to an extent of 92.8% with 70% crystallinity. Cellulose fibers diameter was 9.6 nm and the yield was 65%.	[35]
Cassava bagasse	Sulfuric acid hydrolysis	Cellulose whiskers were extracted. The degree of crystallinity was found to be 43.7−54.1%. Yield content was 30 wt.%. Length and diameter were 1150 and 15 nm respectively.	[36]
Rice husk	Sulfuric acid hydrolysis	Cellulose whiskers were obtained with a yield of 74%. The cellulose varied in size from 6−14 nm in width and 100–400 nm in length.	[37]

Dry softwood pulp	Shear's homogenization process	The diameters of the CNFs ranged between 16−28 nm. The CNFs exhibited a slightly higher crystallinity and lower thermal stability dry pulp fiber.	[38]

Park *et al.* [39] suggest that a simple method for the extraction of cellulose nanocrystals (CNCs) is to employ high-pressure homogenization (HPH) and to regulate the temperature of the production process. The proposed process was evaluated and compared with normal acidic hydrolysis [39]. The latter study showed a simple and green CNC extraction method that employed HPH without acidic hydrolysis. CNCs with high crystallinity, which increased linearly with increasing temperatures over 20 passes, were developed by temperature controlled HPH. Rod-like cellulose nanocrystals with a width of 4−14 nm and a length of 60−320 nm were obtained. Flauzino Neto *et al.* [40] investigated the production of cellulose nanocrystals from cellulose extracted from soy hulls. The nanocrystals were obtained by acid hydrolysis. The hydrolysis was performed at 40°C and the resulting nanocrystals were characterised by high crystallinity. The results showed that more drastic hydrolysis conditions (40 minutes) resulted in shorter nanocrystals while some harm to the cellulose crystalline structure occurred [40]. Cellulose nanocrystals with a length ranging from 100−200 nm and 15 nm in width were also extracted from *Phormium tenax* leaf fiber by acid hydrolysis [40]. The study confirmed the removal of hemicelluloses and lignin, and that the prostine phorium fiber containing both amorphous and crystallite regions were successfully treated with acid to obtain CNC structures utilising a two-step chemical procedure [40]. Furthermore, the applied hydrolysis parameters were capable of extracting microcrystalline material which is also suitable for hydrolysis from macrofiber such as *Phormium tenax*. It should be noted that producing cellulosic material is the preferred procedure for a high yield aqueous stable colloid suspension of cellulose nanocrystals [40].

Chemical processes such as acid hydrolysis, chlorination, alkaline extraction, and bleaching have been used for the extraction of cellulose from cotton, sisal, flax fiber, corn stover, and rice husk [41]. According to Ludueña *et al.* [41], they used the acid hydrolysis method for the extraction of cellulose in order to manufacture cellulose nanowhiskers (CNW) from different sources as mentioned above. All used in their study had produced CNW with different characteristics and diameters. These were cotton (~73.4 nm), sisal (~57.4 nm), flax (~39.4 nm),

corn stover (~38.4 nm), and rice husk (~12.4 nm). The crystallinity of the CNW produced from cotton was 94.0%, from sisal it was 85.9%, from flax it was 84.9%, from corn stover it was 80.6%, and form rice husk it was 76.0% [41]. Furthermore, the CNW extracted from rice husk revealed low aspect ratio together with low diameter which make them suitable materials for reinforcement in polymer matrices.

2.3 Functionalization of cellulose membranes

2.3.1 General overview

Cellulose membranes have played a critical role in various fields such as water purification, the food industry, the oil industry, medical applications, and biotechnology. The literature clarified that each field requires different functionality of the membranes for them to be applied usefully in a specific application [42]. It thus follows that there is a need for the fabrication of functionalized membranes for advanced applications. Different materials and chemicals have been used for the functionalization of cellulose membranes such as (2,2,6,6-Tetramethylpiperidin-1-yl) oxyl and (2,2,6,6-tetramethylpiperidin-1-yl) oxidanyl, commonly known as TEMPO-, amide-, amino-, and hydroxyl-based groups.

2.3.2 Preparation, morphology, and effectiveness of TEMPO-functionalized cellulose membranes

The main purpose for the surface modification of cellulose membranes is to change their surface functionality and improve the interaction of the membranes with pollutants. In most cases, TEMPO-oxidisation has been employed for the functionalization of cellulose in order to introduce the carboxylic groups. Karim *et al.* [42] studied the development of nanocellulose to achieve improved water permeability, better functionality, and improved mechanical stability. This was achieved by functionalizing cellulose nanocrystals with TEMPO (2,2,6,6-Tetramethylpiperidin-1-yl) oxyl–NaBr–NaClO combination to improve the metal adsorption capacity of the cellulose nanocrystals. The pH of the solution was adjusted to 10 by adding sodium hydroxide while the membranes were immersed in the solution for 180 seconds. Atomic force microscopy (AFM) showed enhancement in the roughness of the membranes due to using TEMPO modification. Furthermore, the membranes also showed enhancement in terms of total acidic content. Generally, it was found that the permeability of the TEMPO-functionalized membranes was not affected in water. It is well known that bromide at lower

contents is not easily absorbed, especially not in medical wastewater. As a result, there is a need to design systems that consist of an effective adsorbent or adsorbents. For instance, Liu and co-workers [43] investigated the adsorption of bromide ions at lower concentrations through the modification of cellulose beads with TEMPO and iron (III) (Fe [III]). In study, the cellulose beads were prepared by extrusion dropping technology. Generally, the main aim of modifying cellulose beads with TEMPO to introduce the carboxylate groups into the cellulose. The modification of cellulose beads took place or follows, cellulose was added into deionized water, with both TEMPO and sodium bromide added into the mixture of deionized water and cellulose beads. Finally, 10% sodium hypochlorite (NaClO) was added to the mixture. The pH of the solution was kept at 10 by introducing sodium hydroxide into the reaction mixture. The mixture was allowed to react over a four-hour period after which carboxylated cellulose was obtained. These carboxylated cellulose beads were then combined with iron (III) to form an iron-to-iron carboxylated cellulose beads complex. The fabrication of the complex was done by adding wet carboxylated cellulose bead (CCB) samples into the solution of iron (III) chloride ($FeCl_3$) and the mixture was stirred overnight at room temperature. The resultant yellow complex was first washed with distilled water, further washed with a water solution at a pH value of 3, and then further washed with distilled water. The surface morphologies of the investigated samples were analysed using SEM and the functionality of the CCB as well as Fe (III)-CCB complex was determined using Fourier Transport Infrared spectroscopy (FTIR). SEM of neat CB showed smooth surfaces whereas the surfaces of the complex (Fe-CCB) were rough and irregular. FTIR spectroscopy revealed that the CBs, CCBs, Fe-CBs, and Fe-CCBs displayed the well-known characteristic peaks of cellulose. It was concluded that the CCB material was able to combine with the metal ions in the form of iron for further usage in advanced applications.

According to Liu *et al*. [44], TEMPO-mediated oxidised cellulose nanofibers (TOCNFs) have shown potential within the bioremediation of metal ions from contaminated water due to their interaction with charged metal ions via electrostatic interactions involving surface carboxyl groups. Copper is known as a common pollutant in industrial effluents and was thus the target metal in the study. Isolation of TEMPO-oxidized cellulose nanofibers (TOCNFs) with different carboxylate group content was prepared from cellulose sludge. The slurry pulp residue was mechanically processed and distributed into a solution consisting of sodium bromide and TEMPO. Sodium hypochlorite was added dropwise to the suspension while maintaining the reaction pH at ca.10 by adding sodium hydroxide. Furthermore, with the option of two different

quantities of hypochlorite, two different degrees of oxidation were achieved. When all the (NaClO) was depleted, the filtration of oxidized pulp was executed by washing it numerous times with purified water until the filtered solution reached a neutral state. Using a micro-fluidiser, the purified pulp fiber were distributed in water as they disintegrated to accomplish a TOCNF water suspension. After the experiment, an electric conductivity titration method was used to achieve the TOCNF with the carboxylate content. It was concluded by the authors that the larger the surface area and the higher the carboxylated content were, the better they resulted in the effective adsorption of copper metal. The surface morphology of the investigated samples before and after copper adsorption was analysed by atomic force microscopy (AFM) and SEM images. The authors reported that there were no copper nanoparticles on the surface of the TOCNF before copper adsorption. However, to show the effectiveness of the TOCNF membrane(s), the SEM revealed copper nanoparticles with different sizes on the surface of the TOCNF.

The adsorption of lead ions by grafted TEMPO-oxidized cellulose nanofiber infused with magnetite was investigated by Abou-Zeid and co-workers [45,44]. The TEMPO-oxidized cellulose nanofibers were fabricated from bleached bagasse pulp utilising TEMPO-oxidation as well as mechanical defibrillation. Furthermore, the authors synthesised the magnetite nanoparticles using the so-called co-precipitation method. Different contents of the magnetite i.e., 0, 1, 3, and 5 wt.% in relation to the acrylic acid were introduced into the acrylic modified TEMPO-CNF to form nanocomposites. The morphology of the TEMPO-CNF and 5 wt.% of the magnetite nanocomposites was investigated using SEM. The TEMPO-CNF was observed as smooth, tubular, and interconnected structures while the nanocomposite showed a rough surface which may have been associated with grafting by acrylic acid. In terms of lead ions removal, a comparative investigation was done to demonstrate the effectiveness of the TEMPO-CNF magnetite composites in relation to time, namely 30 and 60 min. The investigation was conducted with 1wt% of magnetite incorporated into the TEMPO-CNF at a pH of 5.3. It was reported that there was a general increase in the adsorption of lead ions over time. This was attributed to more effective nanocomposites which were able to enhance the adsorption of the pollutant with time. The TEMPO-CNF showed less adsorption when compared with the magnetite nanocomposite TEMPO-CNF. The magnetite nanocomposite showed higher adsorption of lead ions due to the crosslinking between the polymeric chains which resulted in the potential to trap the ions in the solution.

Another investigation was done by the same authors [45,46] on the preparation of novel adsorbents based on cellulose nanofibrils for heavy metal removal by TEMPO-mediated oxidation and polyethyleneimine (PEI) grafting (TOCN-PEI) [42]. The PEI grafting into the TOCN was done utilising the glutaraldehyde crosslinking process. The raw cellulose was reported to have an average diameter of 10−30 μm and a length in the range of 100−200 μm. The addition of PEI into the TOCN showed that the PEI covered the TOCN uniformly with small pores occurring between the TOCN matrix. Raw cellulose showed low copper adsorption which was evidence that the non-functionalized materials had few or no binding sites. Furthermore, it became apparent that the raw cellulose-PEI was also a poor adsorber of copper metal ions. The authors further showed that the TEMPO-oxidized cellulose was the most effective system in terms of adsorption of Cu (II) ions when compared with raw cellulose and raw cellulose-PEI. The observed behaviour was ascribed to the presence of carboxylated groups emanating in the cellulose, with high adsorption of Cu ions due to the electrostatic effect.

2.3.3 Amide- and amino-functionalized cellulose-based materials

Various authors [43, 47-50] investigated the preparation of amide-functionalized cellulose systems to produce effective materials for the adsorption of pollutants. Liu *et al.* investigated an efficient, eco-friendly, amide-functionalized primarily cellulose-based porous adsorbent [43]. According to the authors, the resultant amide-functionalized material had numerous adsorption sites that ensued in the exceptionally efficient elimination of anionic dyes and copper ions from aqueous media. The amide-functionalized cellulose was achieved by mixing cellulose fiber and amide in a solution of sodium hydroxide and urea. The mixture was stirred and stored in dark conditions, resulting in the achievement of amide-functionalized cellulose materials. The authors reported that bisacrylamide, which was crosslinked with cellulose for the fabrication of amide-functionalized cellulose, had different adsorption sites which enhanced the adsorption of copper metal ions and dyes.

Mercury is classified as one of the most toxic metals as it is harmful to health and the environment. Mercury waste has been found in wastewater originating from industries and, as a result, there is a need to purify or clean wastewater that contains mercury. Sun *et al.* [47] used two methods for the adsorption of mercury metal which were the esterification of sugarcane bagasse cellulose with excess stearic acid and the grafting of poly-acrylamide brush

by ultraviolet radiation to prepare cellulose-based adsorbent material. The pre-treatment of the sugarcane bagasse fiber was done by pouring the fiber into 9wt.% of sodium hydroxide. The sugarcane bagasse fibers was modified with stearic acid by adding the pre-treated bagasse into a solution of ethanol containing stearic acid. The stearic acid-modified sugarcane bagasse fibers was mixed with 15 wt.% acrylamide (AM) and the mixture was sealed in a tube that was exposed to UV rays for 20 minutes. The surface morphology of the adsorbent material was analysed through an optical microscope (OM) and SEM-EDS and the interaction of the investigated samples was studied using infrared spectrometry (FTIR). The surface morphology of the functionalized sugarcane bagasse (SBF-g-SA)-g-PAM sample was found to be different from that of the sugarcane bagasse (SBF) sample. When the sugarcane bagasse was decrystallized, the SBF was found to be porous and fibers filament was observed after crystallization which enhanced surface reactivity and improved grafting reactivity. It was reported that modifying the cellulose with stearic acid improved the grafting of SBF with polyacrylamide (PMA). As a result, the (SBF-g-SA)-g-PAM system was made effective for the removal of mercury ions in solution. Other studies [48,49] also reported the incorporation of the amine functional groups on the surface of cellulose materials.

Jin *et al.* [50] investigated amino-functionalized cellulose nanocrystalline for adsorption of dyes. Cellulose nanocrystals were fabricated by sulfuric acid hydrolysis. The fabricated cellulose nanocrystals were introduced into the ethylenediamine at various contents. In summary, nanocrystalline cellulose was oxidized with sodium periodate and subsequently grafted with ethylenediamine to form amino groups on the surface of the cellulose. The surface morphology of the samples was analysed by atomic force microscopy (AFM), and it was reported that functionalization had little effect on the morphology of the cellulose nanocrystals. The amino-functionalized cellulose nanocrystals were found to be effective adsorbents of dyes as they showed high adsorption capability, more especially in an acidic medium.

Alatawi *et al.* [48] investigated the covalent binding of amino-functionalized epichlorohydrin (ECH) cross-linked with carboxymethyl cellulose (CMC) polymeric solid support with different degrees of functionalization. The study demonstrated that functionalized cellulose can also be employed in the treatment of urinary tract and kidney diseases besides being utilised for water purification. Urease immobilization was investigated to determine the effects of pH and temperature. The results showed that after 7 days, the immobilization of urease by amino-functionalization showed 75% initial activity when compared with free urease which did not

return its activity to the same extent as immobilized urease. However, it has improved the membrane surface hydrophilicity and subsequently reduced membrane biofouling in the membrane bioreactor (MBR) system [48]. The authors also prepared cellulose acetate (CA) nanocomposite membranes by embedding amino-functionalized nanodiamond (ND-NH_2) as well as polyethylene glycol grafted ND (ND-PEG) in the cellulose-based system. Cellulose nanocomposites were fabricated by incorporating various quantities of amino-functionalized nanocrystalline to produce effective membrane material inhibiting oil depositions. Essential flux, fouling activity, and anti-fouling properties against extracellular polymeric substances (EPS) were studied to compare prepared nanocomposite membranes with the pure CA membrane. Using SEM, the surface membrane and cross-section morphologies of neat CA were compared with the selected nanocomposite membranes containing 0.5wt.% of pristine and functionalized nanoparticles. It was reported that the optimum concentration of nanocellulose loading was less than 1.0 wt.%. Above this concentration pore-blocking of the fabricated membrane occurred which reduced porosity. It was further reported that the ultrafiltration (UF) performance of the membranes revealed that the 1 wt.% was the optimum concentration for water flux with 43% more than that of the neat membrane. Furthermore, the nanocomposite membrane showed oil rejection at a rate greater than 98.2%.

Huang *et al*. [51] prepared a new nanostructured amino-functionalized magnetic bacterial cellulose/activated carbon (BC/AC) composite bioadsorbent (AMBCAC) for the removal of Pb^{2+} and methyl orange (MO) from an aqueous solution. The findings showed that the equilibrium adsorption potential (Q_e) for Pb^{2+} increased after amino group introduction. The optimum pH for Pb^{2+} and MO adsorption was 5.0 and 3.0 respectively [51].

Liang *et al.* [52] investigated the synthesis of a new adsorbent based on cellulose (PQC, where P and QC designate polyethyleneimine and quaternized cellulose respectively) with quaternary ammonium and amino functional groups for enhanced capture of Cr (VI) in water. Cellulose was homogeneously quaternized for the preparation of PQC, and this was followed by grafting and/or cross-linking it with polyethyleneimine in the presence of epichlorohydrin [52]. The PQC followed the isotherm of Langmuir and had a maximum Cr (VI) uptake ability that was far higher than many other recorded adsorbents derived from cellulose [52]. This behaviour was attributed to physicochemical properties such as the robust porous structure and high density of functional groups as well as quaternary ammonium, amino, and hydroxyl which enhanced the functional groups that improved the availability to capture or reduce Cr (VI).

Moeinzadeh *et al*. [53] synthesized nanocomposite ultrafiltration (UF) membranes by adding different portions of amino-functionalized nanocrystalline cellulose (NCs) to enhance membrane anti-fouling resistance in opposition to oil depositions. The latter authors reported that, the porosity and hydrophilicity of the membranes were enhanced significantly with the use of NCs despite a decrease in the pore length of nanocomposite membranes. The UF performance effect showed that the nanocomposite membrane integrated with 1 wt.% of NCs which accomplished an optimum water flux improvement, which was approximately 43% more than the pristine membrane. Furthermore, such nanocomposite membranes also exhibited promising oil rejection and extremely good water flux recuperation at a lower cost.

Yu *et al*. [54] investigated the use of a multi-amino adsorbent for arsenic adsorption. Glycidyl methacrylate (GMA) was grafted onto the surface of cotton cellulose with ceric ammonium nitrate (CAN) being used as the initiator. The delivered epoxy agencies reacted with tetraethylenepentamine (TEPA) to deposit a multi-amino adsorbent. The SEM images of the alkali-treated cellulose, cellulose-g-GMA as well as cellulose-g-GMA-b-TEPA, revealed smooth surfaces for alkali-treated cellulose. The surface morphology of the cellulose-g-GMA was rougher than that of the alkali-treated cellulose. The latter authors reported that the optimum pH for adsorption was 5 for arsenate and 7 for arsenic. It was concluded that the GMA and TEPA had been successfully grafted onto the surface of cellulose and that the modification had improved the arsenic adsorption performances.

2.4 Preparation, morphology, and effectiveness of carbon nanotube-functionalized membranes for adsorption of contaminants

Carbon nanotube (CNT) synthesis and its functions has been one of the most studied fields in many disciplines such as chemistry, physics, materials science, and life sciences [55]. Carbon nanomaterials have been utilized in different fields due to their special properties such as high electrical conductivity and chemical resistance. CNTs have been shown to have great potential as superior adsorbents for removing a variety of organic and inorganic pollutants from water due to their large specific surface areas, compact scales, and hollow and layered structures [56]. However, as much as carbon nanotubes are utilised as adsorbent materials for removing pollutants from solutions, carbon nanotubes may be functionalized further to enhance their ability to remove contaminants [57]. For example, multi-walled carbon nanotubes (MWCNTs) undergo mild oxidation which allows the formation of oxygen-containing surface groups.

Furthermore, it has been shown that, to improve the wettability of MWCNTs, polar solvents may be utilised to enhance the effectiveness of the carbon nanotubes as adsorbent materials [55]. In another study [57] multi-walled carbon nanotube/cellulose acetate (MWCNT/CA) nanocomposite membranes were prepared by utilizing acetone as the solvent and deionized water as the non-solvent. To enhance the distribution of the MWCNTs in the matrix, MWCNTs were functionalized in a strongly acidic medium. The concentrations of carbon nanotubes employed for the fabrication of the membranes included 0.0005, 0.005, and 0.01 wt.%. The morphology of the prepared carbon nanotube cellulose acetate was analysed using field emission scanning electron microscopy (FESEM) [57]. It was found that there was a reduction in the number of voids with an increase in the content of carbon nanotubes. Furthermore, it was reported that there were no MWCNT agglomerates and that MWCNTs were uniformly dispersed. It was further mentioned that the addition of small concentrations of MWCNT, namely 0.0005 wt.% and 0.005 wt.%, enhanced permeability of water in the membrane. This observation was ascribed to the formation of connective passages between membrane pores which was due to the -COOH groups arising from the modified carbon nanotubes. An increase in MWCNT content (0.01 wt.%) resulted in a reduction in the porosity and in the surface area of the membrane which resulted in decreased permeability.

To investigate improved hydrophilicity and biocompatibility of MWCNT, Chang *et al*. [58] used soluble starch-functionalized multiwall carbon nanotube composites (MWCNT-starch). They prepared the MWCNTs grafted iron oxide system for the removal of dye in a solution. The MWCNT-starch oxide nanocomposites were fabricated by synthesizing iron nanoparticles on the surface of the MWCNT-starch. The fabrication of the magnetic MWCNTs took place through suspension of MWCNTs-starch in a solution of ferric chloride while the pH of the solution was kept at 10-11. The surface morphology of the magnetite composites was investigated using TEM. Micrographs of the non-magnetic MWCNT-starch showed that the carbon nanotubes were embedded with starch. For the magnetic MWCNT-starch system, iron oxide dispersed uniformly with no aggregates. Furthermore, the addition of iron oxides did not demolish the structure of the starch in the MWCNTs-starch system. The authors further reported that the size of iron oxide nanoparticles in the composites consisting of MWCNT-starch was smaller than that of the iron oxide nanoparticles in the MWCNT-iron oxide. The fact that MWCNTs displayed both adsorption and magnetic separation properties suggests that they can be used as magnetic adsorbents to extract organic pollutants from aqueous solutions. Furthermore, starch grafted on MWCNTs can serve as a template for the formation of ZnO,

TiO^2, or Ag nanoparticles. The investigated samples were tested against anionic dye (MO) and cationic dye (MB) and it was observed that there had been rapid adsorption of MO dye between 10−30 min. To determine the amount of dye adsorbed by the two systems, a pseudo second-order model was utilised as shown in **Equation 1**:

$$\frac{t}{q_t} = \frac{1}{kq_e^2} + \frac{t}{q_e} \qquad \textbf{(1)}$$

where *k* with the unit (mg g^{-1} min^{-1}) is denoted as the second-order rate constant, while q_t (mg g^{-1}) represents the amount of dye adsorbed at time t and q_e denotes the amount of dye adsorbed at equilibrium. The values for t and q_e were normally recorded from the intercept and slope of t/q_t versus t. When analysing the results, the authors found that the R-value was greater than 0.999, which indicated that the adsorption property of this systems may be explained by the pseudo second-order equation. According to the *k* and q_e values, more enhanced adsorption of MO occurred with the MWCNT-starch-iron oxide than with the MWCNT-iron oxide. This was attributed to the hydrophilicity of the starch in the composites which enhanced the dispersion of the carbon nanotubes in the composites and dye solution.

Gao *et al.* [59] investigated the use of poly (1-glycidyl-3-methylimidazolium chloride) (PGMIC)PGMIC, Fe_3O_4, and MWCNT to prepare magnetic polymer multi-wall carbon nanotubes (MPMWCNT) for the removal of anionic azo dyes. In the study the adsorbent system consisted of ionic liquid-based polyether, ferrous oxide, and multi-wall carbon nanotubes. The nanocomposites were fabricated by following the steps shown in Figure 2.1.

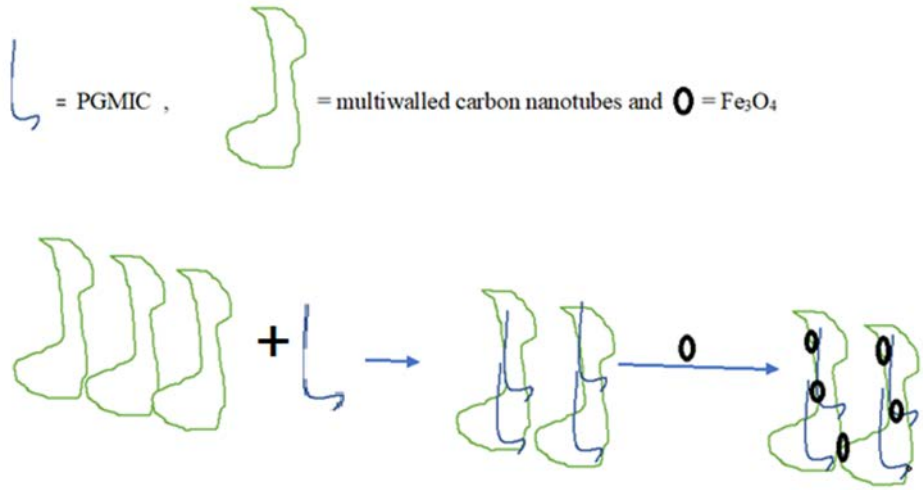

Figure 2.1: Schematic representation of nanocomposite fabrication steps

By utilising TEM, it was shown that the Fe_3O_4 occurred on the surface of the MWCNTs, which the authors attributed to the strong interaction between the two nanoparticles. Furthermore, it was observed that both the nanoparticles and the polymer were embedded successfully into the carbon nanotube surfaces. The effect of pH was also investigated for all the prepared samples, and it was found that the adsorption of the dye was most favourable at a low pH. It was concluded that the addition of polyether as well as ferrous oxide into the carbon nanotubes enhanced separation and adsorption efficacy. Furthermore, two diffraction peaks were observed in MPMWCNT from the XRD patterns, suggesting that the microstructures of the MWCNTs were not destroyed by the chemical treatment.

Gong *et al.* [56] investigated the synthesis of a magnetic multi-wall carbon nanotube (MMWCNT) nanocomposite for the removal of cationic dyes from water. Industrial multi-wall carbon nanotubes and iron oxide nanoparticles were used to fabricate the MMWCNT nanocomposite. MWCNTs were incorporated into the concentrate to purify the carbon nanotubes. The purified MWCNTs were added into the solution of ammonium ferrous sulfate and ammonium ferric sulfate (Fe^{2+}: Fe^{3+} ratio of 1:2). The pH of the solution was kept at 10−11. The surface morphology and the size of the investigated samples were analysed by utilising SEM. The SEM micrographs showed that the iron oxide nanoparticles were covered on the surface of the MWCNTs to fabricate the resultant nanocomposites. The surface of the samples was also investigated by BET, and it was found that the carbon nanotube nanocomposite adsorbent recorded a value of 61.74 m^2g^{-1}, while the MWCNTs recorded 44.29 m^2g^{-1}, which was lower than that of the nanocomposites. The XRD pattern of the nanocomposites showed four diffraction peaks (2Θ= 30.2 °, 35.6°, 43.3°, and 57.2°) that were attributed to maghemite and/or magnetite. The authors also reported that the adsorption percentages of dyes increased when the MWCNT content in the nanocomposites was increased. The removal of dye increased as follows: 30.1 to 99.16%, 17.11 to 98.33%, and 98.8% for MB, NR, and BCB respectively. The mechanism of adsorption of the MWCNTs was attributed to van der Waal's interactions between the hexagonal carbon atoms and the dye's aromatic structures.

2.4.1 Preparation, morphology, and effectiveness of graphene oxide functionalized cellulose for contaminant extraction in water

The utilisation of nanomaterials in different applications has increasingly gained attention due to advantages such as the existence of high active sites, the presence of functional groups, and

a wide surface area [60]. Graphene in particular has extraordinary properties and a wide range of applications in water purification [61]**.** According to Ain *et al.* [61], the primary graphene derivatives are graphene oxide (GO) and reduced graphene oxide (rGo). Many active functional groups, such as -OH, –COOH, -C = O and other hydrophilic groups, occur on the surface of graphene oxide [62,53]. According to Gusain *et al*. [63], graphene oxides and other oxidized carbons have high acidity and functional groups, allowing for excellent adsorption of cationic and basic compounds through electrostatic and hydrogen bonding interactions, while their pristine counterparts have hydrophobic surfaces and low adsorption.

Zhang *et al*. [65] stated that graphene oxide has a highly functionalized operative surface, making it a possible material for removing contaminants from water [66]. Various authors investigated the utilisation of graphene-based composites for removal of pollutants [67-77]. Ain *et al.* [61] prepared graphene oxide (GO) with iron nanoparticles (Fe^{3+}) inserted into the surface of the graphene oxide. Graphene oxide was fabricated by using Hummer's modified method while the magnetic graphene oxide (MGO) was prepared by using the co-precipitation method. SEM micrographs of the Fe_3O_4/graphene composites revealed uneven and heterogeneously distributed Fe_3O_4 in the graphene oxide matrix because of the agglomerates. XRD showed an increase in the *d*-spacing which was attributed to the incorporation of oxygen groups into the graphene because of oxidation. There were broad diffraction peaks in the XRD pattern of the nanocomposites which indicated that the size of the nanoparticles was small. The MGO dosage was investigated in relation to the adsorption performance in the range between 0.002 g/L to a high value of 0.016 g/L. It was reported that the adsorption capacity of the MGO nanocomposites decreased with an increase in the dose of the adsorbent. This behaviour was attributed to the availability of the adsorption sites and the surface area of the adsorbent material. It was further concluded that the MGO nanocomposite with the concentration between 0.014g/L and 0.016 g/L achieved the removal efficiency of 99.972%, 97.783%, 96.561%, 91.883%, 95.283% for Pb^{2+}, Cr^{3+}, Cu^{2+}, Zn^{2+} and Ni^{2+}, respectively.

Chen *et al.* [78] investigated the water purification ability of graphene oxide polyamide membranes. The membranes were prepared by interfacial polymerization of trimethyl chloride (TMC) with the content of GO ranging between 0.1−0.5 using polysulfone (PSF) as a substrate. According to the latter authors, the FTIR spectrum of the GO sample and graphite powder revealed that the surface of GO contained oxygen-containing functional groups and the usual GO peaks were visible in the XRD pattern. It was reported that higher concentration of the GO

resulted in good dispersion in the polyamide (PA) layer. At 0.3 content of the GO, it was observed from SEM that the GO had a wrinkled appearance as well as edges after application of electric field. This was due to the formation of edges and defect sites containing a lot of oxygen functional groups. The membrane at 0.3 of graphene oxide was found to demonstrate rejection rates for sodium sulfate (Na_2SO_4) (97.6%) and $MgSO_4$ (97.3%); however, there was a low rejection rate for sodium chloride (NaCl) (25.1%). There was a general improvement in antifouling property and selective divalent as well as monovalent ions, which are important properties for water purification. Based on these findings, one can conclude that the hydrophilicity and permeability of the membrane showed that the water flux of all the modified nanofiltration membranes was higher than that of the original nanofiltration membrane. Moreover, the flux of the nanofiltration membrane further increased after modification of the electric field.

Nanocomposites consisting of zirconium and graphite oxide were prepared by Luo *et al.* [79]. The composites were prepared using the green hydrothermal method and the prepared material exhibited three-dimensional hydrogel. Furthermore, the suspension of Reduced graphene oxide-zirconium (RGO-Zr) resulted in a black colour after freeze-drying which provided evidence that there was a conversion of GO to RGO. SEM revealed that the RGO-Zr had folded edges when compared with the GO. Furthermore, they were embedded into the surface of the reduced graphene oxide. This was due to enhancement in phosphate adsorption which occurred as a result of ZrO_2 dispersion on the RGO surface. According to the authors, the ability to adsorb phosphate was further enhanced when the temperature was increased. This behaviour was attributed to the acceleration of the phosphate ions on the surface of the adsorbent. A similar system consisting of graphene oxide-zirconium (GO-Zr) adsorbent for the removal of phosphate from water was investigated by Zong *et al.* [80]. The post-grafting method was utilised for the formation of the zirconia-functionalized method. The TEM results of the graphene oxide-zirconium (GO-Zr) adsorbent system showed that the ZrO_2 covered the surface of the GO in the adsorbent system when compared with neat GO. X-ray fluorescence (XRF) revealed a 12.5% content of ZrO_2 in the adsorbent system. The XRD pattern revealed a 2-theta value at 30^o, which was attributed to the amorphous part of the ZrO_2. The GO peak that is normally found around 2Ɵ value of 11.1^o showed reduction in its intensity which was ascribed to the fact that the Zr $(OH)_4$ was found on the surface of GO rather than being intercalated. The adsorption studies revealed that phosphate adsorption adhered to or followed the Langmuir adsorption isotherm which kinetically is pseudo-second order kinetics. Furthermore, the

adsorption of the GO-Zr system was better than that of the GO, and the adsorption of phosphate ion was more favourable in the acid system.

2.5 Thermal Stability of Cellulose-Based Membranes

The thermal stability of cellulose membranes and their functionalized membranes was investigated using thermogravimetric analysis (TGA). Various studies [81-86] have investigated the thermal stability of cellulose membranes and their functionalization, and it was found that the type of functionalization used, the preparation method of the membrane composites, the content of the functionalization, and the dispersion of the membrane composite(s) influenced the thermal stability of the membrane composites.

In one study the membranes were fabricated by phase inversion with the dispersion of titania nanoparticles into the cellulose acetate membranes [81]. TiO_2 nanoparticles were fabricated using the sonochemical method. The addition of TiO_2 (5−25 wt.%) into the cellulose acetate membranes showed improvement in thermal stability. It was argued that the enhancement in thermal stability was due to a better dispersion of the TiO_2 into the cellulose acetate membrane. The better dispersion that occurred was attributed to a coordination bond between Ti^{4+} and the acetate. It is well known that better dispersion results in high rigidity as a lot of energy is required to break the polymer chains. Furthermore, it became clear that an increase in TiO_2 content enhanced thermal stability as a result of more heat being absorbed by TiO_2 in the membranes.

Zhang *et al*. [82] prepared cellulose carbamate membranes using the solid-liquid phase method. Cellulose carbamate (CC) was produced from cellulose pulp and urea as well as from N,N-dimethylacetamide (DMAc). The authors achieved the regeneration of cellulose by dissolving cellulose carbamate (CC) into a solution of sodium hydroxide, and they then regenerated it using a process of coagulation that solidified the final product. They reported that cellulose enhanced thermal stability after regeneration and esterification.

Muhammad and co-workers [83] investigated the thermal stability of regenerated cellulose using the ionic liquid method. These authors found a reduction in activation of the thermal degradation for regenerated cellulose. Frone *et al*. [87] investigated the thermal stability of bacterial cellulose (BC) membranes with different surface modifiers. Bacterial cellulose

membranes were modified using 3-aminopropyl triethoxysilane (APS), vinyl-triethoxy silane (VS), acylation, as well as acrylation. The treated membranes had higher thermal stability than the untreated BC membranes. It was further observed that the thermal stability of the silane-treated samples had higher thermal stability than with other treatments. This was attributed to a rich Si char layer that probably formed on the surface of BC membranes and that subsequently protected the BC nanofiber from further degradation.

Silvério *et al*. [88] investigated the thermal stability of methylcellulose with cellulose nanocrystals loading at 2, 4, 6, 8 and 10%. The samples were fabricated by the casting method. There was a decrease in the thermal stability of methylcellulose (MC) and its nanocomposites at 120°C. This decrease was ascribed to moisture as well as the high retention capacity of the methylcellulose (MC).

2.6 Chemical resistance of fibers reinforced composites

Chemical resistances of fibers were investigated through by measuring by weight, volume, and dimensional change. Various studies were reported on the chemical resistance of cellulose membrane for advanced applications. Different factors were found to affect the chemical resistance of the fibers such as type of fibers and surface treatment of the fibers. Lee *et al*. reported on the chemical resistance of cross-linked cellulose acetate ultrafiltration membranes. The authors reported that a high degree of crosslinking was very important for the chemical resistance of the membranes. The authors reported that an enhanced crosslinking resulted in a better resistance against polar solvents such as ethanol and acetone. Vigneshwaran *et al*. the chemical resistance of natural fibers reinforced polyester composites. In this study, six various chemicals (viz hydrochloric acid, nitric acid, toluene, benzene, sodium hydroxide, calcium carbonate) were employed to the investigate the chemical resistance of the natural fibers reinforced composites. The jute fibers were treated with sodium hydroxide and silane. Generally, the authors reported that all composites showed positive results against the chemical resistance. According to the authors, it was suggested that the silane treated composites showed better resistance to all chemicals, with the highest weight gain observed on nitric acid (HNO3). Furthermore, Jawaid *et al*. reported on the chemical resistance of the hybrid composites fabricated from empty fruit bunches (EFB) and jute fibers, with the oil palm EFB noted as a skin, while the jute fibers were the core material of the system. The ratio of the EFB/Jute was noted as EFB/Jute 4:1. Various chemicals such as benzene, toluene, CCL4, hydrochloric acid,

nitric acid, acetic acid, sodium hydroxide, sodium carbonate and ammonium hydroxide. It was generally reported that all composites were found to be resistant to different chemicals and as a result there was no corrosion. Najafi *et al*. investigated the chemical reagents of the natural fiber reinforced polypropylene composites. The authors reported that the H2O2 soap solution as well as acetone showed little or no effect on all the investigated composites. Furthermore, the rice hulls composites were found to be significantly affected by sodium hydroxide, while other chemical were reported to be unsuccessful on other types of fibers (wood flour and kenaf fiber).

2.7 References

1. Zinge, C., & Kandasubramanian, B. (2020). Nanocellulose-based biodegradable polymers. *European Polymer Journal,* 113, 109758. https://doi.org/10.1016/j.eurpolymj.2020.109758
2. Patel, D.K., Dutta, S.D., & Ki-Taek, L. (2019). Nanocellulose polymer hybrids and their emerging applications in biomedical engineering and water purification. *The Royal Society of Chemistry adv.*, 9, 1914−19162.
3. Tranche, D. (2018). Nanocellulose as a promising sustainable material for biomedical applications. AIMS. *Material science,* 5, 201−205. https://doi.org/10.3934/matersci.2018.2.201
4. Mtibe, A., Linganiso, L.Z., Mathew, A.P., Oksman, K., John, M.J., & Anandjiwala, R.D. (2015). A comparative study on properties of micro and nano papers produced from cellulose and cellulose nanofibers. *Carbohydrate Polymers.* 118, 1–8. https://doi.org/10.1016/j.carbpol.2014.10.007
5. Siró, I., & Plackett, D. (2010). Micro fibrillated cellulose and new nanocomposite materials: a review. *Cellulose,* 17, 459–494. https://doi.org/10.1007/s10570-010-9405y
6. Valentini, F., Dorigato, A., Rigotti, D.A., & Pegoretti, A. (2019). Polyhydroxyalkanoates/fibrillated nanocellulose composites for additive manufacturing. *Journal of Polymers and the Environment. 27,1333–1341*. https://doi.org/10.1007/s10924-019-01429-8
7. Kiprono, S.J., Ullah, M.W., & Yang, G. (2018). Surface engineering of microbial cells: strategies and applications. *Engineering Sciences,* 1, 33–45. https://doi.org/10.30919/es.180330.

8. Seo, Y., Kim, J., Hoon, S., Kim, J., Chung, J.H., & Lim, K. (2018). Cellulose-based nanocrystals: sources and applications via agricultural by products. *Journal of Biosystems Engineering*, 43(1):59-71. https://doi.org/10.5307/JBE.2018.43.1.059
9. Xie, S., Zhang, X., Walcott, M.P., & Lin, H. (2018). Applications of cellulose nanocrystals: a review. *Engineering Sci*ences, 2, 4-16. https://doi.org/10.30919/es.1803302
10. Gan, P.G., Sam, S.T., bin Abdullah, M.F., & Omar, M.F. (2020). Thermal properties of nanocellulose-reinforced composites: a review. *Journal of Applied Polymer Science*. 137,48544. 101002/app.48544.
11. Mishra, R.K., Sabu, A., & Tiwari, S.K. (2018). Materials chemistry and the futurist eco-friendly applications of nanocellulose: status and prospect. *Journal of Saudi Chemical Society* 22, 949–978. https://doi.org/10.1016/j.jscs.2018.02.005
12. Lasrado, D., Ahankari, S., Kar, K. (2020). Nanocellulose-based polymer composites for energy applications: a review. *Journal of Applied Polymer Sci*ence, 48959. https://doi.org/10.1002/app.48959
13. Baldwin, I.T. (2010). Plant volatiles. Current Biology, 20,392–397. doi:10.1016/j.cub.2010.02.052
14. Maffei, M.E. (2010). Sites of synthesis, biochemistry and functional role of plant volatiles. *South African Journal of Botany*, 76,612–631. doi:10.1016/j.sajb.2010.03.003
15. Dudareva ,N., Negre, F., Nagegowda, D.A., Orlova, I. (2006). Plant volatiles: recent advances and future perspectives. *Critical R e views in Pl a n t Sciences* ,2 5 ,4 1 7 – 4 4 0. d o i.1 0 .1 0 8 0 / 07352680600899973
16. Shak, K.P.Y., Pang, Y.L., & Mah, S.K. (2018). Nanocellulose: recent advances and its prospects in environmental remediation. *Beilstein Journal of Nanotechnology*, 9, 2479–2498. https://doi.org/10.3762/bjnano.9.232
17. Mariani, L.M., Johnson, W.R., Considine, J.M., & Turner, K.T. (2019). Printing and mechanical characterization of cellulose nanofibril materials. *Cellulose*, 26, 2639–2651. https://doi.org/10.1007/s10570-019-02247-w
18. Jedrzejczak-Krzepkowska, M., Kubiak, K., Ludwicka, K.S., & Bielecki, S. (2016). Bacterial nanocellulose synthesis: recent findings. In: Initial, *Bacterial Nanocellulose* (pp. 19−46). Elsevier. 10.1016/B978-0-444-63458-0.00002-0
19. Stanisławska, A. (2016). Bacterial nanocellulose as a microbiological derived nanomaterial. *Advances in Materials Science*. 16, 45–57. https://doi.org/10.1515/adms-2016-0022

20. Jozala, A.F., Pértile, R.A.N., dos Santos, C.A., de Carvalho Santos-Ebinuma, V., Seckler, M.M., Gama, F.M.A. & Pessoa, A. (2015). Bacterial cellulose production by Gluconacetobacter xylinus by employing alternative culture media. *Applied Microbiology and Biotechnology*, 99, 1181–1190. https://doi.org/10.1007/s00253-014-6232-3
21. Dinh Vu, N., Thi Tran, H., Bui, N.D., Duc Vu, C., & Viet Nguyen, H. (2017). Lignin and cellulose extraction from Vietnam's rice straw using ultrasound-assisted alkaline treatment method. *International Journal of Polymer Science*,2,1-8. https://doi.org/10.1155/2017/1063695
22. Sun, J.X., Sun, X. F., Zhao, H., & Sun, R.C. (2004). Isolation and characterization of cellulose from sugarcane bagasse. *Polymer Degradation and Stability*, 84(2), 331–339. https://doi.org/10.1016/j.polymdegradstab.2004.02.008
23. Feng, Y.H., Cheng, T.Y., Yang, W.G., Ma, P.T., He, H.Z., Yin, X.C., & Yu, X.X. (2018). Characteristics and environmentally friendly extraction of cellulose nanofibrils from sugarcane bagasse. *Industrial Crops and Products*, 111, 285–291. https://doi.org/10.1016/j.indcrop.2017.10.041
24. Nie, S., Zhang, C., Zhang, Q., Zhang, K., Zhang, Y., Tao, P., & Wang, S. (2018). Enzymatic and cold alkaline pre-treatments of sugarcane bagasse pulp to produce cellulose nanofibrils using a mechanical method. *Industrial Crops and Products*, 124(August), 435–441. https://doi.org/10.1016/j.indcrop.2018.08.033
25. Raquez, J.M., Habibi, Y., Murariu, M., & Dubois, P. (2013). Polylactide (PLA)-based nano-composites. *Progress in Polym Science*, 38(10-11), 1504-1542.
26. Besbesa, I., Vilar, M.R., & Boufi, S. (2011). Nanofibrillated cellulose from alfa, eucalyptus and pine fibres: preparation, characteristics and reinforcing potential. *Carbohydrate Polymers*, 86, 1198-1206.
27. Acharya, S.K., Mishra, P., & Mehar, S.K. (2011). Effect of surface treatment on the mechanical properties of bagasse fiber reinforced polymer composite. *Bio-Resources*, 6(3), 3155e65.
28. Ng, H.M., Sin, L.T., Tee, T.T., Bee, S.T., Hui, D., Low, C.Y., & Rahmat, A.R. (2015). Extraction of cellulose nanocrystals from plant sources for application as reinforcing agent in polymers. *Composites Part B: Engineering*, 75, 176–200. https://doi.org/10.1016/j.compositesb.2015.01.008.

29. Sheltami, R.M., Abdullah, I., Ahmad, I., Dufresne, A., & Kargarzadeh, H. (2012). Extraction of cellulose nanocrystals from mengkuang leaves (*Pandanus tectorius*). *Carbohydrate Polymers*, 88(2), 772–779. https://doi.org/10.1016/j.carbpol.2012.01.062
30. Morais, J.P.S., Rosa, M.D.F., De Souza Filho, M.D.S.M., Nascimento, L.D., Do Nascimento, D.M., & Cassales, A.R. (2013). Extraction and characterization of nanocellulose structures from raw cotton linter. *Carbohydrate Polymers*, 91(1), 229–235. https://doi.org/10.1016/j.carbpol.2012.08.010.
31. Danial, W.H., Abdul Majid, Z., Mohd Muhid, M.N., Triwahyono, S., Bakar, M.B., & Ramli, Z. (2015). The reuse of wastepaper for the extraction of cellulose nanocrystals. *Carbohydrate Polymers*, 118, 165–169. https://doi.org/10.1016/j.carbpol.2014.10.072
32. Cao, X., Ding, B., Yu, J., & Al-Deyab, S.S. (2012). Cellulose nanowhiskers extracted from TEMPO-oxidized jute fiber. *Carbohydrate Polymers*, 90(2), 1075–1080. https://doi.org/10.1016/j.carbpol.2012.06.046
33. Johar, N., Ahmad, I., & Dufresne, A. (2012). Extraction, preparation and characterization of cellulose fiber and nanocrystals from rice husk. *Industrial Crops and Products*, 37(1), 93–99. https://doi.org/10.1016/j.indcrop.2011.12.016
34. Morán, J.I., Alvarez, V.A., Cyras, V.P., & Vázquez, A. (2008). Extraction of cellulose and preparation of nanocellulose from sisal fiber. *Cellulose*, 15(1), 149–159. https://doi.org/10.1007/s10570-007-9145-9
35. Ranganagowda, R.P.G., Kamath, S.S., & Bennehalli, B. (2019). Extraction and characterization of cellulose from natural areca fibers. *Material science research India*, 16(1), 86–93. https://doi.org/10.13005/msri/160112
36. Pasquini, D., Morais, E.D., Aprígio, A., Naceur, M., & Dufresne, A. (2010). Extraction of cellulose whiskers from cassava bagasse and their applications as reinforcing agent in natural rubber. *Industrial Crops & Products*, 32(3), 486–490. https://doi.org/10.1016/j.indcrop.2010.06.022
37. Rosa, S.M.L., Rehman, N., Miranda, M.I.G.D, Nachtigall, S.M.B., & Bica, C.I.D. (2012). Chlorine-free extraction of cellulose from rice husk and whisker isolation. *Carbohydrate Polymers*, 87(2), 1131–1138. https://doi.org/10.1016/j.carbpol.2011.08.084
38. Zhao, J., Zhang, W., Zhang, X., Zhang, X., Lu, C., & Deng, Y. (2013). Extraction of cellulose nanofibrils from dry softwood pulp using high shear homogenization. *Carbohydrate Polymers*, 97(2), 695–702. https://doi.org/10.1016/j.carbpol.2013.05.050

39. Park, N.M., Choi, S., Oh, J.E., & Hwang, D.Y. (2019). Facile extraction of cellulose nanocrystals. *Carbohydrate Polymers*, 223(June), 115114. https://doi.org/10.1016/j.carbpol.2019.115114
40. Flauzino Neto, W.P., Silvério, H.A., Dantas, N.O., & Pasquini, D. (2013). Extraction and characterization of cellulose nanocrystals from agro-industrial residue: soy hulls. *Industrial Crops and Products*, 42(1), 480–488. https://doi.org/10.1016/j.indcrop.2012.06.041
41. Ludueña, L.N., Vecchio, A., Stefani, P.M., & Alvarez, V.A. (2013). Extraction of cellulose nanowhiskers from natural fiber and agricultural byproducts. *Fiber and Polymers*. 14(7), 1118–1127. https://doi.org/10.1007/s12221-013-1118-z
42. Karim, Z., Hakalahti, M., Tammelin, T., & Mathew, A.P. (2017). In situ TEMPO surface functionalization of nanocellulose membranes for enhanced adsorption of metal ions from aqueous medium. *RSC Advances*, 7, 5232-5241.
43. Lui, J., Chen, T., Yang, Y., Bai, Z., Xia, L., Wang, M., Lv, X., & Li, L. (2020). Removal of heavy metal ions and anionic dyes from aqueous solutions using amide-functionalized cellulose-based adsorbents. *Carbohydrate Polymers*, 230, 115619.
44. Liu, P., Oksman, K., & Mathew, A.P. (2016). Surface adsorption and self-assembly of Cu (II) ions on TEMPO-oxidized cellulose nanofiber in aqueous media. *Journal of Colloid and Interface Science*, 464, 175–182. https://doi.org/10.1016/j.jcis.2015.11.033
45. Abou-Zeid,R.E., Kamal,K.H., Abd El-Aziz, M.E., Morsi,S.M., Kamel, S.(2018) Grafted TEMPO-oxidized cellulose nanofiber embedded with modified magnetite for effective adsorption of lead ions, *International Journal of Biological Macromolecules* .https://doi.org/10.1016/j.ijbiomac.2020.11.063
46. Zhang, N., Zang, G.L., Shi, C., Yu, H.Q., & Sheng, G.P. (2016.) A novel adsorbent TEMPO-mediated oxidized cellulose nanofibrils modified with PEI: preparation, characterization, and application for Cu (II) removal. *Journal of Hazardous Materials*, 316, 11–18. https://doi.org/10.1016/j.jhazmat.2016.05.018
47. Sun, N., Wen, X., & Yan, C. (2018). Adsorption of mercury ions from wastewater aqueous solution by amide functionalized cellulose from sugarcane bagasse. *International Journal of Biological Macromolecules*, 108, 1199–1206. https://doi.org/10.1016/j.ijbiomac.2017.11.027
48. Alatawi, F.S., Monier, M., & Elsayed, N.H. (2018). Amino functionalization of carboxymethyl cellulose for efficient immobilization of urease. *International Journal of*

Biological Macromolecules, 114, 1018–1025. https://doi.org/10.1016/j.ijbiomac.2018.03.142

49. Etemadi, H., Yegani, R., & Seyfollahi, M. (2017). The effect of amino-functionalized and polyethylene glycol-grafted nanodiamond on anti-biofouling properties of cellulose acetate membrane in membrane bioreactor systems. *Separation and Purification Technology*, 177, 350–362. https://doi.org/10.1016/j.seppur.2017.01.013
50. Jin, L., Li, W., Xu, Q., & Sun., Q. (2015). Amino-functionalized nanocrystalline cellulose as an adsorbent for anionic dyes. *Cellulose*,22(4). https://doi.org/10.1007/s10570-015-0649-4
51. Huang, X., Zhan, X., Wen, C., Xu, F., & Luo, L. (2018). Amino-functionalized magnetic bacterial cellulose/activated carbon composite for Pb2+ and methyl orange sorption from aqueous solution. *Journal of Materials Science and Technology*, 34(5), 855–863. https://doi.org/10.1016/j.jmst.2017.03.013
52. Liang, X., Liang, B., Wei, J., Zhong, S., Zhang, R., Yin, Y., Zhang, Y., Hu, H., & Huang, Z. (2020). A cellulose-based adsorbent with pendant groups of quaternary ammonium and amino for enhanced capture of aqueous Cr (VI). *International Journal of Biological Macromolecules*, 148, 802–810. https://doi.org/10.1016/j.ijbiomac.2020.01.184
53. Moeinzadeh, R., Jadval Ghadam, A.G., Lau, W.J., & Emadzadeh, D. (2019). Synthesis of nanocomposite membrane incorporated with amino-functionalized nanocrystalline cellulose for refinery wastewater treatment. *Carbohydrate Polymers*, 225, 115212. https://doi.org/10.1016/j.carbpol.2019.115212
54. Yu, X., Tong, S., Ge, M., Wu, L., Zuo, J., Cao, C., & Song, W. (2013). Synthesis and characterization of multi-amino-functionalized cellulose for arsenic adsorption. *Carbohydrate Polymers*, 92(1), 380–387. https://doi.org/10.1016/j.carbpol.2012.09.050
55. Rodríguez, A., Ovejero, G., Sotelo, J.L., Mestanza, M., & García, J. (2010). Adsorption of dyes on carbon nanomaterials from aqueous solutions. *Journal of Environmental Science and Health* [Part A]. *Toxic/Hazardous Substances and Environmental Engineering*, 45(12), 1642–1653. https://doi.org/10.1080/10934529.2010.506137
56. Gong, J.L., Wang, B., Zeng, G.M., Yang, C.P., Niu, C.G., Niu, Q.Y., Zhou, W.J., & Liang, Y. (2009). Removal of cationic dyes from aqueous solution using magnetic multi-wall carbon nanotube nanocomposite as adsorbent. *Journal of Hazardous Materials*, 164(2–3), 1517–1522. https://doi.org/10.1016/j.jhazmat.2008.09.072

57. El Badawi, N., Ramadan, A.R., Esawi, A.M.K., & El-Morsi, M. (2014). Novel carbon nanotube-cellulose acetate nanocomposite membranes for water filtration applications. *Desalination*, 344, 79–85. https://doi.org/10.1016/j.desal.2014.03.005
58. Chang, P.R., Zheng, P., Liu, B., Anderson, D.P., Yu, J., & Ma, X. (2011). Characterization of magnetic soluble starch-functionalized carbon nanotubes and its application for the adsorption of the dyes. *Journal of Hazardous Materials*, 186(2–3), 2144–2150. https://doi.org/10.1016/j.jhazmat.2010.12.119
59. Gao, H., Zhao, S., Cheng, X., Wang, X., & Zheng, L. (2013.) Removal of anionic azo dyes from aqueous solution using magnetic polymer multi-wall carbon nanotube nanocomposite as adsorbent. *Chemical Engineering Journal*, 223, 84–90. https://doi.org/10.1016/j.cej.2013.03.004
60. Wang, S., Sun, H., Ang, H.M., Tadé, M.O. (2013). Adsorptive remediation of environmental pollutants using novel graphene-based nanomaterials. *Chemical Engineering Journal*. 226, 336–347.
61. Ain, Q.U., Farooq, M.U., & Jalees, M.I. (2020). Application of magnetic graphene oxide for water purification: heavy metals removal and disinfection. *Journal of Water Process Engineering*, 33(October 2020), 101044. https://doi.org/10.1016/j.jwpe.2019.101044
62. Lujanienė,G..Šemčuk,S.,Lečinskytė,A.,Kulakauskaitė,I.,Mažeika,K.,Valiulis,D., Tumėnas,S.(2017).Magnetic graphene oxide-based nano-composites for removal of radionuclides and metals from contaminated solutions, *Journal of environmental radioactivity*. 166, 166–174.
63. Wang, J., & Chen, B. (2015.) Adsorption and coadsorption of organic pollutants and a heavy metal by graphene oxide and reduced graphene materials. Chemical Engineering Journal, 281, 379–388.
64. Gusain, R., Kumar, N., & Ray, S.S. (2020). Recent advances in carbon nanomaterial-based adsorbents for water purification. *Coordination Chemistry Reviews*. 405, 213111. https://doi.org/10.1016/j.ccr.2019.213111
65. Zhang, Y., Yan, L., Xu, W., Guo, X., Cui, L., Gao, L., Wei, Q., Du,B. (2014). Adsorption of Pb (II) and Hg (II) from aqueous solution using magnetic CoFe 2 O 4-reduced graphene oxide. *Journal of Molecular Liquids*, 191, 177–182.
66. Sharma, V.K., McDonald, T.J., Kim, H., & Garg, V.K. (2015). Magnetic graphene-carbon nanotube iron nanocomposites as adsorbents and antibacterial agents for water purification. *Advances in Colloid and Interface Science*, 225, 229–240. https://doi.org/10.1016/j.cis.2015.10.006

67. Su, H., Ye, Z.,Hmidi,N. (2017). High-performance iron oxide–graphene oxide nanocomposite adsorbents for arsenic removal. *Colloids and Surfaces A: Physicochemical and Engineering Aspects*. 522, 161–172.
68. Zinadini, S.,Vatanpour,V.,Zinatizadeh,A.A.,Rahimi,M.,Rahimi,Z.,Kian,M. (2015). Preparation and characterization of antifouling graphene oxide/polyethersulfone ultrafiltration membrane: application in MBR for dairy waste-water treatment. *Journal of Water Process Engineering*, 7, 280–294.
69. Han, Y., Xu, Z., & Gao, C. (2013). Ultrathin graphene nanofiltration membrane for water purification. *Advanced Functional Materials*, 23(29), 3693–3700. https://doi.org/10.1002/adfm.201202601
70. Liu, X., Zhou, Y., Nie, W., Song, L., & Chen, P. (2015). Fabrication of hydrogel of hydroxypropyl cellulose (HPC) composited with graphene oxide and its application for methylene blue removal. *Journal of Materials Science*, 50(18), 6113–6123. https://doi.org/10.1007/s10853-015-9166-y
71. Shen, J., Yan, B., Li, T., Long, Y., Li. N., & Ye, M.X. (2012). Study on graphene-oxide-based polyacrylamide composite hydrogels. *Composites Part A*, 43(9), 1476–1481. https://doi.org/ 10.1016/j.compositesa.2012.04. 006
72. Nair, A.K., & Jagadeesh, J.B. (2017). TiO2 nanosheet-graphene oxide based photocatalytic hierarchical membrane for water purification. *Surface and Coatings Technology*, 320, 259–262. https://doi.org/10.1016/j.surfcoat.2017.01.022
73. Peng, Y., Yu, Z., Li, F., Chen, Q., Yin, D., & Min, X. (2018). A novel reduced graphene oxide-based composite membrane prepared via a facile deposition method for multifunctional applications: oil/water separation and cationic dyes removal. *Separation and Purification Technology*. 200(February), 130–140. https://doi.org/10.1016/j.seppur.2018.01.059
74. Sun, X.F., Qin, J., Xia, P.F., Guo, B.B., Yang, C.M., Song, C., & Wang, S.G. (2015). Graphene oxide-silver nanoparticle membrane for biofouling control and water purification. *Chemical Engineering Journal*. 281, 53–59. https://doi.org/10.1016/j.cej.2015.06.059
75. Xu, C., Cui, A., Xu, Y., & Fu, X. (2013). Graphene oxide-TiO2 composite filtration membranes and their potential application for water purification. *Carbon*, 62, 465–471. https://doi.org/10.1016/j.carbon.2013.06.035
76. Zhang, P., Gong, J.L., Zeng, G.M., Song, B., Fang, S., Zhang, M., Liu, H.Y., Huan, S.Y., Peng, P., Niu, Q.Y., Wang, D.B., & Ye, J. (2019). Enhanced permeability of rGO/S-GO

layered membranes with tunable inter-structure for effective rejection of salts and dyes. *Separation and Purification Technology*, 220(December 2018), 309–319. https://doi.org/10.1016/j.seppur.2019.03.041

77. Zhu, C., Liu, P., & Mathew, A.P. (2017). Self-assembled TEMPO cellulose nanofiber: graphene oxide-based biohybrids for water purification. *ACS Applied Materials and Interfaces*. 9(24), 21048–21058. https://doi.org/10.1021/acsami.7b06358
78. Chen, X., Wang, W., Zhu, L., Liu, C., Cui, F., Li, N., & Zhang, B. (2021). Graphene oxide/polyamide-based nanofiltration membranes for water purification. *ACS Applied Nano Materials*, 4(1), 673–682. https://doi.org/10.1021/acsanm.0c02980
79. Lou X., Wang, X., Bao, S., Liu, X., Zhang, W., & Fang, T. (2016). Adsorption of phosphate in water using one-step synthesized zirconium-loaded reduced graphene oxide. *Scientific Reports*, 6, 39108. https://doi.org/10.1038/srep39108
80. Zong, E., Wei, D., Wan, H., Zheng, S., Xu, Z., & Zhu, D. (2013). Adsorptive removal of phosphate ions from aqueous solution using zirconia-functionalized graphite oxide. *Chemical Engineering Journal*, 221, 193–203. https://doi.org/10.1016/j.cej.2013.01.088
81. Abedini, R., Mousavi, S.M., & Aminzadeh, R. (2011). A novel cellulose acetate (CA) membrane using TiO2 nanoparticles: preparation, characterization and permeation study. *Desalination*, 277(1–3), 40–45. https://doi.org/10.1016/j.desal.2011.03.089
82. Zhang, S., Yu, C., Liu, N., Teng, Y., & Yin, C. (2019). Preparation of transparent anti-pollution cellulose carbamate regenerated cellulose membrane with high separation ability. *International Journal of Biological Macromolecules*, 139, 332–341. https://doi.org/10.1016/j.ijbiomac.2019.07.146
83. Muhammad, N., Man, Z., Khalil, M.A.B., Tan, I.M., & Maitra, S. (2010). Studies on the thermal degradation behavior of ionic liquid regenerated cellulose. *Waste and Biomass Valorization*, 1(3), 315–321. https://doi.org/10.1007/s12649-010-9026-6
84. Manjarrez Nevárez, L., Ballinas Casarrubias, L., Canto, O.S., Celzard, A., Fierro, V., Ibarra Gómez, R., & González Sánchez, G. (2011). Biopolymers-based nanocomposites: membranes from propionated lignin and cellulose for water purification. *Carbohydrate Polymers*, 86(2), 732–741. https://doi.org/10.1016/j.carbpol.2011.05.014
85. Kallioinen, M., Mänttäri, M., Nyström, M., & Nuortila-Jokinen, J. (2007). Effect of high filtration temperature on regenerated cellulose ultrafiltration membranes. *Separation Science and Technology*, 42(13), 2863–2879. https://doi.org/10.1080/01496390701558318

86. Mahendra, I.P., Wirjosentono, B., Tamrin, I.H., & Mendez, J.A. (2019). Thermal and morphology properties of cellulose nanofibers from TEMPO-oxidized lower part of empty fruit bunches (LEFB). *Open Chemistry*, 17(1), 526–536. https://doi.org/10.1515/chem-2019-0063
87. Conditions, E., Frone, A.N., Panaitescu, D.M., Chiulan, I., Nicolae, C.A., Casarica, A., Stanescu, P.O. (2018). Surface treatment of bacterial cellulose in mild, eco-friendly conditions. *Coatings*, 8(221), 1−17. https://doi.org/10.3390/coatings8060221
88. Silvério, H.A., Pires, W., Neto, F., Souza, I., Rosa, J.R., Pasquini, D., Maria, R., & Assunção, N.De. (2014). Mechanical, thermal, and barrier properties of methylcellulose/cellulose nanocrystals nanocomposites. *Polímeros*, 24(6), 683-688. http://dx.doi.org/10.1590/0104-1428.1691
89. Lee,J.S., Heo,S.A., Jo,H.J., Min,B.R.(2016). Prepartaion and characteristics of cross-linked cellulose acetate ultrafiltration membranes with high chemical resistance and mechanical strength. *Reactive and functional polymers*,99,114-121. http://dx.doi.org/10.1016/j.reactfunctpolym.2015.12.014
90. Vigneshwaran, S., Uthayakumar,M.,V. Arumugaprabu,V.(2019). Experimental examination of chemical resistance behavior of jute fiber composite. *International Journal of Recent Technology and Engineering*,8, 289-290. DOI:10.35940/ijrte.D1062.1284S219
91. Jawaid,M.,Abdul Khalil,H.P.S., Abu Bakar,A.,Noorunnisa khanum,P.(2011). Chemical resistance, void content and tensile properties of oil palm/jute fibre reinforced polymer hybrid composites. *Materials and designs*,32,1014-1019.
92. Tajvidi, M., Shekaraby,M.M., Motiee,N., Saeed Kazemi Najafi,S.K.(2006).Effects of chemical reagents on the mechanical properties of natural fiber polypropylene composites. *Polymer composites*,27,563-569.

Chapter 3: Materials and Methods

3.1 Materials

3.1.1 Maize stalks

Maize stalks were provided by a local farmer from Cofimvaba in the Eastern Cape, South Africa.

3.1.2 Chemicals used

Sodium hydroxide (NaOH) was supplied in pellet form by Sigma-Aldrich, South Africa. It was a chemically pure (CP) grade with an assay of 99% and a density of 2.13 g cm^{-3}. Sodium lauryl sulfate (SLS) (90% assay) was supplied in powder form by Merck chemicals, South Africa. This product has a density of 1.01 g cm^{-3} and its chemical formula is $CH_3(CH_2)_{11}OSO_3Na$. It was used as an emulsifier. Sodium chlorite ($NaClO_2$) with purity of 80% and density of 2.5 g cm^{-3} was procured from Sigma Aldrich, South Africa. Potassium hydroxide (KOH) was supplied in pellet form by Sigma-Aldrich, South Africa. It was a chemically pure (CP) grade with an assay of 99% and a density of 2.12 g cm^{-3}. A batch of single-walled carbon nanotubes (SWCNTs) was supplied by OCSiAl, Luxembourg. The nanotubes had a density of 1.35 g/cm3, purity of 75%, and metal impurities of 15%. The diameter was below 2 nm and the length was >1 micron. Dylon multi-purpose dye that is generally used for fabrics was supplied in powder form by Henkel, United Kingdom. The dye with a density of 5.8 g cm^{-3} was used to test the adsorption capacity of cellulose and cellulose nanocomposites. Bromophenol blue dye was purchased from Merck, Gauteng, South Africa. The chemical structure of this dye is $C_{19}H_{10}Br_4O_5S$ and it has a molecular weight of 669.99 g mol^{-1}.

3.2 Cellulose Nanofibril Isolation Process

Maize stalks were grounded into a coarse powder by ‘hamermeul’ and dried in a vacuum oven at 60°C for 24 hours. The dried maize stalk powder was then treated with 1.5% NaOH, 1.5% $NaClO_2$, and 1.5% KOH, respectively, at 80°C for an hour. Each treatment was repeated four times with repeated washes using deionized water until pH neutral was achieved. The powder

content during all these chemical treatments was kept in the range of 5-6 wt.%. The powder was dried in an oven at 40°C for 24 hours. The obtained powder (2wt%) was agitated in a blender, then subjected to mechanical grinding using supermass colloider (MKCA-39 Masuko Sangyo Co Ltd., Japan) at 1500 rpm for 25 min. until a gel-like substance was obtained. Figure 3.1 is a schematic representation of the cellulose nanofibrils isolation process.

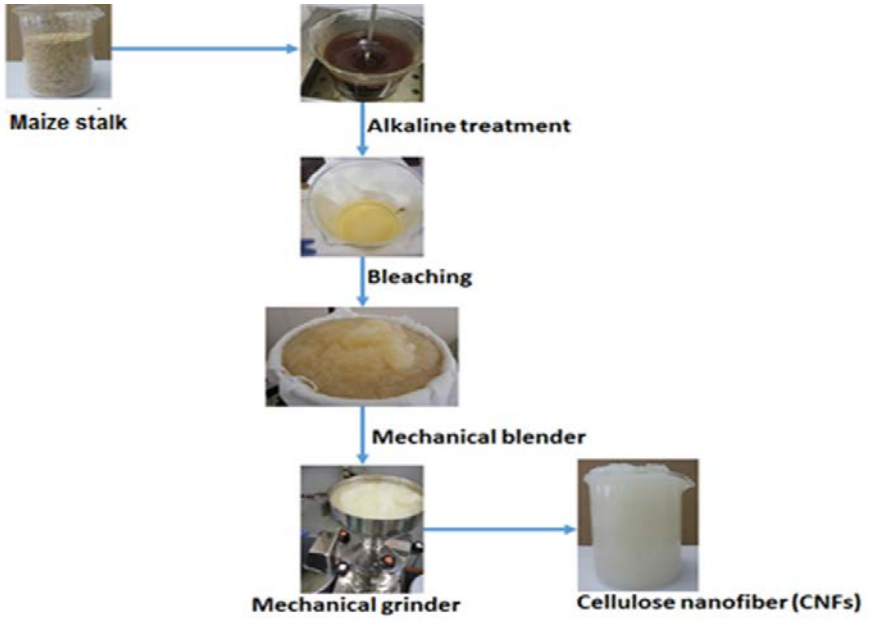

Figure 3.1: Cellulose nanofibrils isolation process

3.3 Preparation of Cellulose Membranes

3.3.1 Cellulose membrane

The isolated cellulose was agitated with a mechanical blender for 5 minutes. Cellulose suspension was filtrated using a Buchner funnel. After draining the water, cellulose membrane was removed from the Buchner funnel and dried at room temperature for 72 hours. The obtained cellulose membrane is illustrated in Figure 3.2.

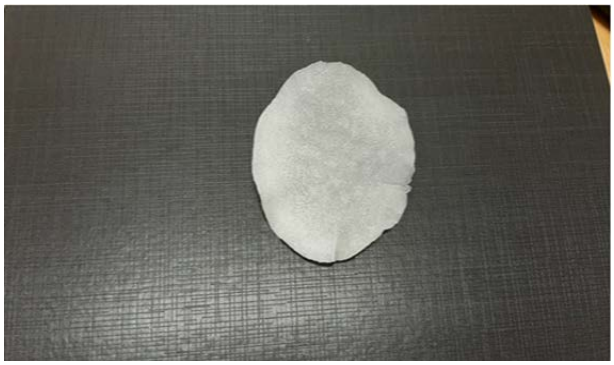

Figure 3.2: Cellulose membrane

3.3.2 Nanocomposite preparation

The nanocomposite membrane was prepared in three ratios. Carbon nanotubes were added into cellulose suspension, with ratios 1:1;1:0.5;1:0.3. Using a mechanical blender, the solution was blended and placed in a Buchner funnel. After draining the water, the cellulose nanocomposite was removed from the Buchner funnel and dried at room temperature for 72 hours. Figure 3.3 illustrates the cellulose nanocomposite membrane of which 0.5 g of SLS was used to improve the dispersion of the CNTs for all prepared nanocomposites from different ratios. The nanocomposites suspension with SLS was agitated using a mechanical blender for 20 minutes, then filtrated using the Buchner funnel. The obtained membrane was dried at room temperature for 72 hours.

Figure 3.3: CNT membrane

3.4 Dye Removal

Bromophenol and Dylon multi-purpose dyes were used as model dyes to determine the dye removal efficiency of the prepared cellulose and cellulose/CNTs composites. Test solutions were prepared by dissolving model dyes in deionized water. The prepared cellulose-based membranes (0.05 g) were placed in the 50 mL dye solutions with a concentration of 15 mg L^{-}

[1]. The adsorption rates of dye on membranes were monitored after 24 hours and determined by UV Vis spectrometer. The amount of the adsorbed dye, *Qe (mg g^{-1})*, was calculated using **equation 2**:

$$Q_e = \frac{(C_0 - C_e)V}{m} \qquad \textbf{(2)}$$

where *Qe* is the amount of dye adsorbed on the membranes at equilibrium, C_0 *(mg L^{-1})* is the initial concentration, C_e (*mg L^{-1}*) is the concentration of dye in the solution at equilibrium, *m (g)* is the mass of the membrane used, and *V (L)* is the volume of the dye. The dye removal percentage (%) from the solution was calculated using **Equation 3**:

$$R(\%) = \frac{C_0 - C_e}{C_0} \times 100 \qquad \textbf{(3)}$$

3.5 Water Absorption and chemical resistance

Water analysis was investigated using different samples at various time intervals. The analysis was done by placing a sample of known weight (W_i) into water at 24, 48, and 72 hours. The surfaces of the samples were placed on a dry cloth in order to dry the samples and the percentages of water absorption were determined using **Equation 4** below:

$$M(\%) = \frac{w_f - W_i}{Wi} \times 100\% \quad \textbf{(4)}$$

The chemical resistance of the cellulose membranes was studied using ASTM D 543-87 method. Chemicals such as sodium hydroxide (NaOH), calcium carbonate ($CaCO_3$) and nitric acid (HNO_3) were studied on the cellulose membrane and their membrane composites. Pre-weighed samples were dipped in chemicals for 24 h and the percentage weight loss/gain were determined.

3.6 Characterization Methods

3.6.1 Scanning electron microscopy (SEM)

SEM is an instrument that is used to observe the surface phenomena of various materials. In the SEM process a sample is shot by utilizing high energy electron and the outcoming electrons and/or X-rays are then analysed [see Figure 3.4]. The outcoming electrons provide information on the morphology, orientation, and crystallographic knowledge properties of a material [1,2]. Shimadzu ZU SSX-550 Superscan SEM was used to determine the morphology of the fractured

samples. All the analyses were done at room temperature. The samples were fractured by freezing them in liquid nitrogen and simply breaking the specimen into an appropriate size to fit the specimen chamber. The fractured samples were gold coated by sputtering to produce conductive coatings onto the samples before recording the SEM micrographs.

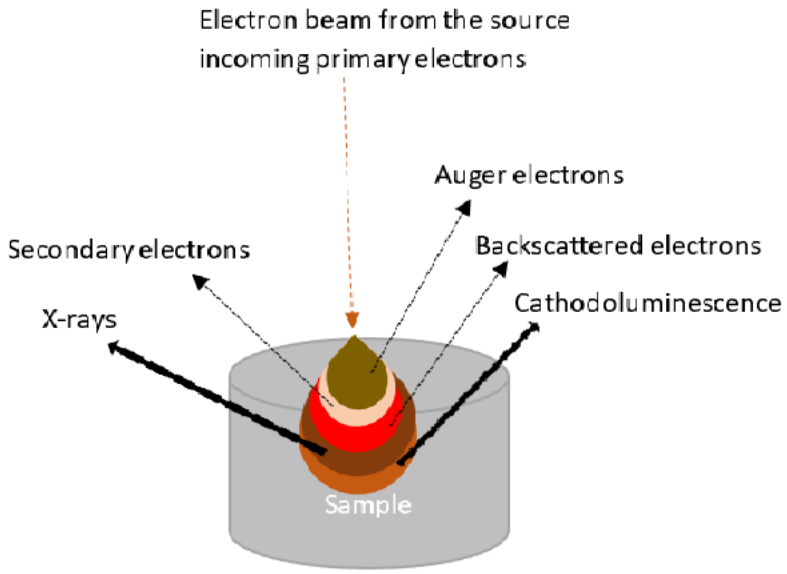

Figure 3.4: SEM instrument analysis process

3.6.2 Transmission electron microscopy (TEM)

Using transmission electron microscopy (TEM) it is possible to study the inner structure of fractured material and to analyse its features on an atomic scale − i.e., within the range of a few nanometers [3,4,5]. The TEM technique utilizes electrons to assemble enlarged images. This process is similar to SEM, but the working principle of TEM is different to that of SEM. Generally, TEM utilizes high E-beam energies within the range 60−350 keV that normally pass through a thin sample to fabricate an image onto the fluorescent screen. In the preparation of TEM samples they are sliced into thin sections that are less than 100 nm and the sliced sections are then pre-treated with staining before visualization. A Philips CM 200 transmission electron microscope (TEM) equipped with an AMT XR-60 CCD digital camera system was employed to produce images of the membranes. An accelerating voltage of 80 kV was used for the TEM analyses. Sample preparation was done as follows: a 10 µL droplet of cellulose membrane suspension (0.0 1 wt.%.) was deposited on a carbon-coated TEM grid. A small drop of 2.0%

uranyl acetate negative stain was then incorporated. The uranyl acetate excess solution was extracted from the system, allowing the blotted piece to dry on the grid.

3.6.3 X-ray diffraction (XRD)

XRD is the most widely used technique to distinguish the crystalline phases present in various materials [6]. Because each solid material has a unique X-ray diffraction pattern, this technique can be used to determine the phases and components present. The structural properties of these phases can also be measured using XRD analysis, such as grain size, crystallinity (relative to a single reference material), and the presence of more than one phase (for example, for polymer blends) [6,7]. The XRD technique involves concentrating an X-ray beam at an initial angle of 2 theta on the material(s), and then reading the strength of the diffracted ray with specific detectors. Following the reading, the incident ray's angle 2 θ is adjusted for a new reading up to a final 2 θ value. Bragg's law (see **Equation 5**) governs the diffracted beam through crystalline phases [6,7].

$$n\lambda = 2d \sin\theta \qquad \textbf{(5)}$$

where *d* is the distance between atomic layers in a crystal, while lambda λ is the wavelength of the incident X-ray beam and *n* is an integer [8]. The cellulose-based material and the films of all the CNFs were scanned in the reflection mode using an incident X-ray of CuKα with a wavelength of 1.54 A at a step width of 0.05° min^{-1} from 2 θ = 10-100°. The crystallinity index (CrI) was defined according to **Equation 6** as:

$$\text{CrI}(\%) = \frac{I_{002} - I_{100}}{I_{002}} \times 100 \qquad \textbf{(6)}$$

Crl is the crystallinity index

I_{002} stands for crystalline

I_{100} stands for amorphous material

3.6.4 Fourier Transform Infrared (FTIR) spectroscopy

Infrared (IR) spectroscopy is a technique that works with the infrared region of an electromagnetic spectrum [8,9]. IR spectroscopy operates with the light of a longer wavelength in combination with a lower frequency than visible light. This technique provides in-depth knowledge of the interaction of molecules within infrared light. The main utilisation of IR spectroscopy is to provide more information on the functional groups. FTIR-ATR was used to investigate the molecular structure and chemical bonds in cellulose and its nanocomposites. A Perkin Elmer Spectrum 100 infrared spectrometer was used for FTIR spectroscopy. Cellulose membrane was analysed in an attenuated total reflectance (ATR) detector over a 400−4000 cm^{-1} wavenumber range at a resolution of 4 cm^{-1}.

3.6.5 Ultraviolet-visible (UV-vis) spectroscopy

UV-vis spectroscopy is a technique that is used to determine the quantitative measurement of various solutions, especially for known concentrations of solutes [10]. The physical principle of the technique is such that the light of a known wavelength and its intensity is directed at a certain sample. The final intensity is measured by the detector after the light has passed through [11]. The amount of light absorbed by a certain sample at a particular wavelength can be determined by using Beer-Lambert's law **(Equation 7)**:

$$A = \log \frac{I_0}{I} = \varepsilon . c . L \qquad (7)$$

where *A* is for absorbance, ε is the molar absorptivity (L mol^{-1} cm^{-1}), c is the concentration of the solute, while *L* is the path length. The absorbance at 800 nm was measured by Agilent Technologies Cary 60 UV-Vis.

3.6.6 Thermogravimetric analysis (TGA)

Thermogravimetric analysis (TGA) is a technique that measures the mass of a sample as a function of temperature and/or time. The investigated sample is normally heated at a constant heating rate or held at a constant temperature [12]. Furthermore, the sample may be investigated under non-linear temperature programs which are those that are utilised in sample-

controlled TGA. The investigated temperature programme depends on the information needed for a particular sample. TGA measurement is shown as a TGA curve whereby the mass or percentage mass is plotted against time and/or temperature [13,14]. A Perkin Elmer TGA7 thermogravimetric analyser was used for the TGA analyses in this study. Under nitrogen, samples weighing between 5 and 10 mg were heated at a rate of 10°C min^{-1} from 30−600°C (flow rate 20 mL min^{-1}) and the corresponding loss was recorded.

3.7 References

1. McMahon, G. (2007). Analytical instrumentation: a laboratory guide. Portable and miniaturized instruments (p. 296), *Chichester: Wiley*.
2. A. Bogner, P.H. Jouneau, G. Thollet, D. Basset, C. Gauthier. (2007). A history of scanning electron microscopy developments: Towards “Wet-STEM” imaging. *Micron* ,38,309-401
3. Campbell, D., Pethrick, R.A., White, J.R., & Thornes, S. (2000). Polymer characterization: physical techniques. *Cheltenham: Stanley Thornes Publishers*.
4. Leng, Y. (2008). Materials characterization: introduction to microscopic and spectroscopic methods. *Singapore: John Wiley & Sons*.
5. Hosier, I.L., Vaughan, A.S., Mitchell, G.R., Siripitayananon, J., & Davis, F.J. (2004). Polymer characterization. In: F.J. Davis (Ed), Practical approach in chemistry: polymer chemistry. *New York: Oxford University Press*.
6. Buffeteau, T., Desbat, B., Eyquem, D. (1996). Attenuated total reflection of Fourier Transform Infrared microspectroscopy: theory and application to polymer samples. *Vibrational Spectroscopy*, 11, 29−36.
7. Mahendra, I.P., Wirjosentono, B.*, Tamrin, I.H., & Mendez, J.A. (2019). Thermal and morphology properties of cellulose nanofibers from TEMPO-oxidized lower part of empty fruit bunches (LEFB). *Open Chemistry*, 17, 526–536. https://doi.org/10.1515/chem-2019-0063
8. Buffeteau, T., Desbat,B., Eyquem.D.(1996). Attenuated total reflection Fourier transform infrared microspectroscopy: Theory and application to polymer samples. *Vibrational Spectroscopy*. 11,29-36.
9. Smith, B.C. (2011). Fundamentals of Fourier Transform Infrared spectroscopy. *New York: CRC Press.*

10. Saitó, R., Fujita, M., Dresselhaus, G., & Dresselhaus, M.S. (1992). Electronic structure of chiral graphene tubules. *Applied Physics Letter*., 60(18), 2204–2206.
11. Kataura, H., Kumazawa, Y., Maniwa, Y., Umeza,I.,Suzuki,S.,ohtsuka,Y.,Achiba,Y. (1999). Optical properties of single-wall carbon nanotubes. *Synthetic Metals*, 103(1), 2555–2558.
12. Mochane, M.J. (2011). Polymer encapsulated paraffin wax to be used as phase change material for energy storage. *MSc Thesis, University of the Free State, South Africa*.
13. Menczel, J.D., Bair, H.E., Vyazovkin, S., Gallagher, P.K., & Riga. A. (2009). Thermogravimetric analysis (TGA). In: J.D. Menczel, & R.B. Prime (Eds.), Thermal analysis of polymers: fundamentals and applications. *Hoboken, New Jersey*: John Wiley & Sons.
14. Wunderlich, B. (2005). Thermal analysis of polymeric materials. *Berlin: Springer*.

Chapter 4: Results and Discussion

4.1 Morphology of the Cellulose Membranes and their SWCNT Composites

Figure 4.1 depicts the SEM image of a cellulose membrane and carbon nanotube membrane composites. The neat cellulose membrane shows a typical web-like feature resembling structures which are more visible at the junction points (Figure 4.1a). There are clear, bright spots on the surface of the cellulose (Figure 4.1b) as evident by symbol A in the SEM. These spots may be attributed to the presence of carbon nanotubes in the membrane composite. Similarly, Maria and Mieno [1] observed that multi-walled carbon nanotubes were covering the surface of cellulose fiber, with some carbon nanotubes forming bridge-like structures. Figure 4.1c shows that, in the presence of sodium lauryl sulfate (SLS), there was a better dispersion of the carbon nanotubes within the cellulose matrix with few carbon nanotube bright spots being visible. The TEM images show agglomeration of the CNT (symbol A and C in Figure 4.2 (a) and (b)) in the absence of SLS, while in the presence of SLS carbon nanotubes were well dispersed in the cellulose matrix (Figure 4.2c) and in the process the porosity size of the membrane might have been reduced. The agglomeration of CNTs in the absence of SLS was attributed to the interaction between SWCNTs nanoparticles which led to agglomeration. According to the literature [2], conductive nanoparticles tend to be susceptible to enhanced surface interactions that make them undergo particle adhesion upon direct interaction by electrostatic and magnetic as well as van der Waal's forces. It is noted that carbon nanotubes' with high aspect ratio and flexibility provide a high possibility of the SWCNTs' entanglement and agglomeration [3]. The results in the current study suggested that the SLS was able to modify the SWCNTs, which was also evident in the smaller average particle size − i.e., 14.8 nm − of the carbon nanotubes in the presence of SLS when compared with non-modified carbon nanotubes (*viz*. 19 nm). Based on a better dispersion of the SWCNTs, it was concluded that the cellulose was incorporated onto SWCNTs which enhanced the dispersion of SWCNTs into the cellulose membrane matrix.

A better dispersion or compatibility of the SLS modified SWCNTs was further supported by the FTIR (Section 3.6.4) whereby there were no carbon nanotube peaks in the spectrum. The improvement in dispersion was attributed to a л-л interaction between SLS and SWCNTs that improved the SWCNT dispersion in the cellulose membrane. Furthermore, it is well-documented in the literature that the benzene ring also plays a noteworthy role in terms of high

dispersive efficiency, more especially for a surfactant such as dodecyl-benzene sodium sulfonate (NaDDBS) [3]. Zheng *et al.* [4] investigated the effect of anionic, cationic, and non-ionic surfactants on the diameter as well as morphology of the electro-spun nanofibers. It was reported that the diameter of the nanofibers reduced with the addition of surfactant and increased in the surfactant content, with the anionic surfactant in the form of sodium dodecyl sulfate (SDS) showing a smaller particle size, as a result enhancing the uniformity of the nanofibers.

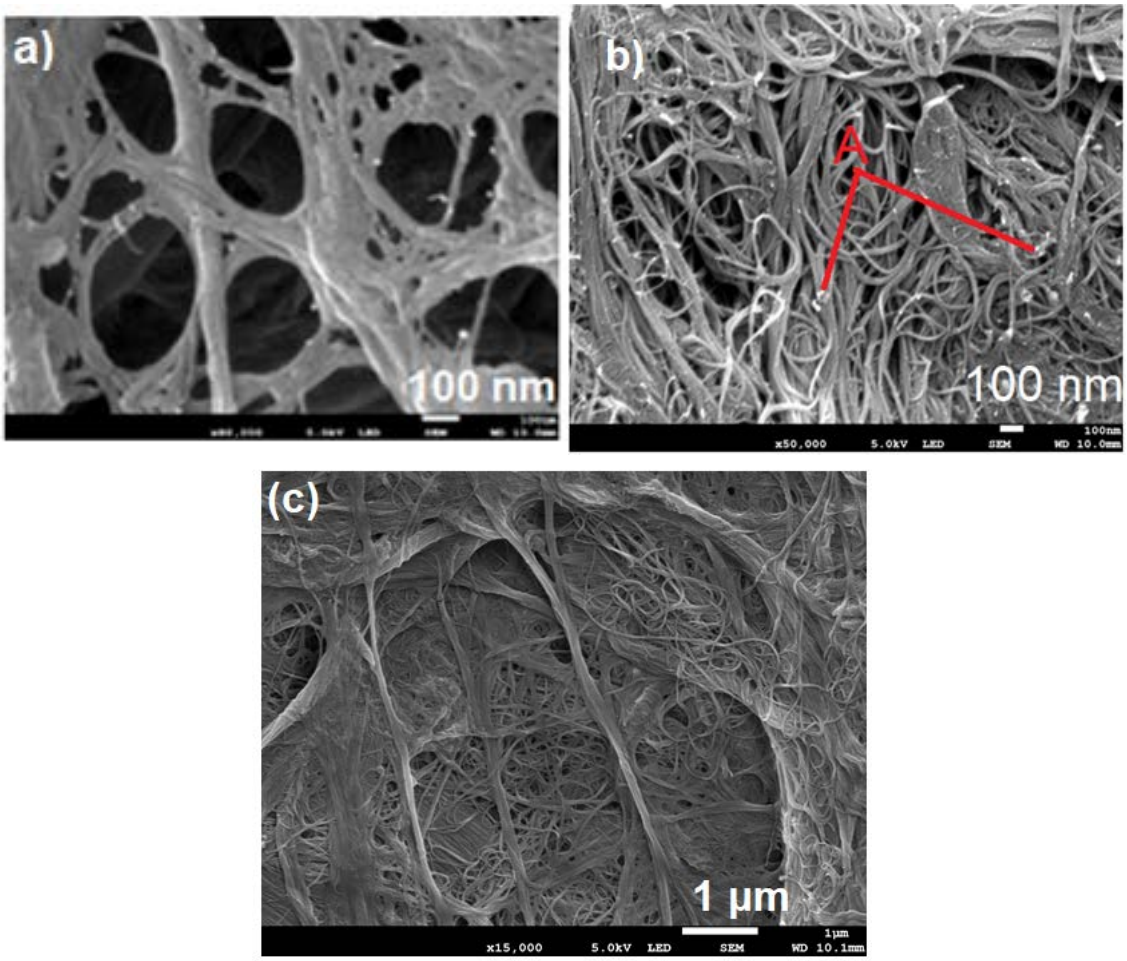

Figure 4.1: **SEM images of (a) cellulose, (b) cellulose/carbon nanotubes (CNT) composites, and (c) cellulose/carbon nanotubes (CNT)/sodium lauryl sulfate (SLS) composites**

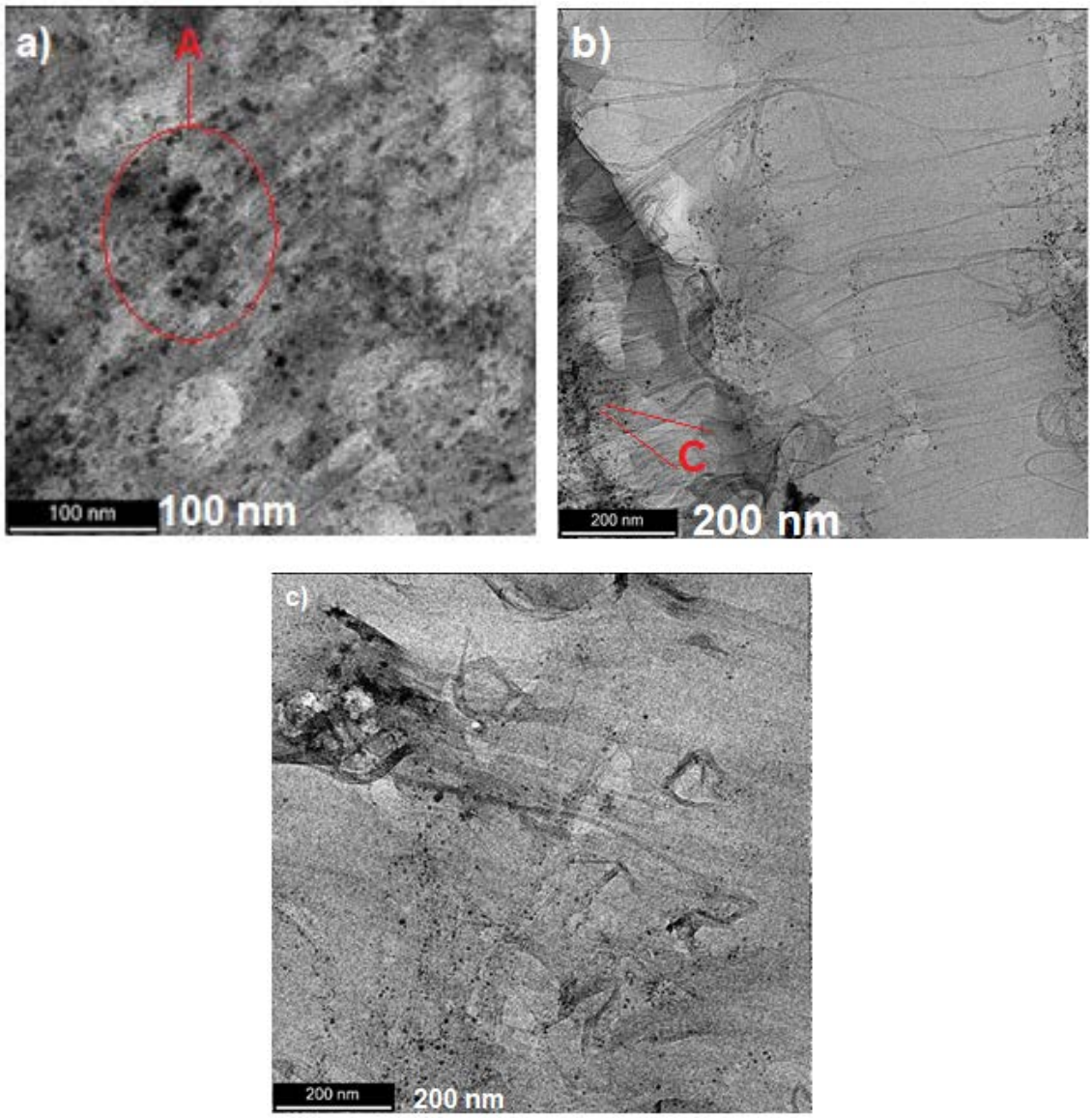

Figure 4.2: TEM images of (a) cellulose, (b) cellulose/CNT, and (c) cellulose/CNT/SLS composites

4.2 X-Ray Diffraction Analysis (XRD)

Figures 4.3 to 4.7 show the XRD diffractograms of cellulose membranes, cellulose/SWCNTs, and SWCNT-SLS/cellulose membrane composites. For all cellulose-based composites (Figure 4.3), the peaks that are observed (around 14.9° and 16.0°, and 23.4°) were attributed to amorphous cellulose I and crystalline cellulose, respectively [5]. The small peak shoulders (around 14.9° and 16.0°) corresponded to the $1\bar{1}0$and 110 diffraction planes in the cellulose, while the 23.4° and 35.0° peaks corresponded to the 200 and 004 planes, respectively. The incorporation of SWCNT and its modification in the form of SLS seemed to have little or no changes in the peak positions as illustrated in Figure 4.3 and Figure 4.4. However, there was a

reduction in the intensity of the peaks with the addition SWCNTs, which may suggest that there was a decrease in the crystallinity with the addition of SWCNT (Figure 4.3 and Figure 4.4), which was also evident by a reduction in crystallinity index (CI) (Table 4.1). The crystallinity index (*CI*) was determined as the height ratio between the intensity of the crystalline peak (I_{002} - I_{am}) and total intensity (I_{002}) from XRD curves using **Equation 6**

$$CI = \frac{[I_{200} - I_{am}]}{I_{200}} x\ 100\% \qquad \textbf{(6)}$$

where *CI* is the degree of crystallinity, I_{002} is the crystalline peak, and I_{am} is the amorphous state. The decrease in crystallinity may be attributed to the interaction between SWCNTs and cellulose, which affected the formation of crystalline regions negatively among cellulose chains and which led to a decrease in the degree of crystallinity. Furthermore, Table 4.1 indicates that the SLS modified SWCNTs/cellulose-based composites showed more reduction in crystallinity index when compared with the non-modified SWCNT cellulose-based composites. These results indicated that the non-modified SWCNT generally produced more ordered crystallites than the modified SLS: SWCNTs cellulose-based composites. The crystal sizes of the SWCNTs/cellulose-based composites were calculated from the main crystalline (200) plane using the Scherrer equation **Equation 8** with shape factor $K = 0.9$ as follows:

$$D_{hkl} = \frac{K.\lambda}{B_{hkl.\cos\theta}} \qquad \textbf{(8)}$$

where D_{hkl} = crystallite size in the direction normal to the hkl family of lattice plane, K = Scherrer constant, λ = wavelength of the radiation (1.54 Å), and B_{hkl} = full width at half-maximum in radius of the reflection of that family of lattice planes.

There is a clear correlation between the *CI* values and crystal sizes, with the decrease in crystal sizes being accompanied by the decrease in crystallinity indexes, especially for cellulose: SWCNT 1:0.3 and cellulose: SWCNT 1:0.5 membrane composites. The same behaviour was also observed for the SLS modified carbon nanotubes cellulose-based membranes with the cellulose: SWCNT: SLS 1:0.3:1 and cellulose: SWCNT: SLS 1:0.5:1 sample. This suggested that the cellulose at the interface of microfibrils was not totally crystalline, which implied partial crystallinity that became disordered with the conversion of microfibrils into CNFs.

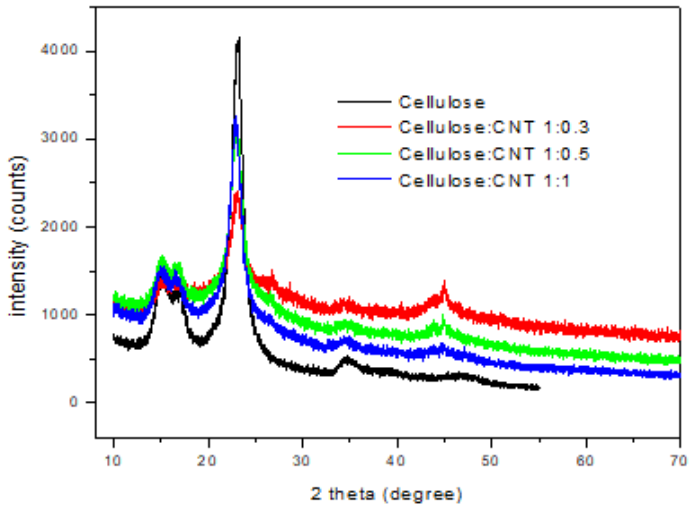

Figure 4.3: XRD curves of cellulose, cellulose: SWCNT 1: 0.3, cellulose: SWCNT 1:0.5 and cellulose: SWCNT 1:1

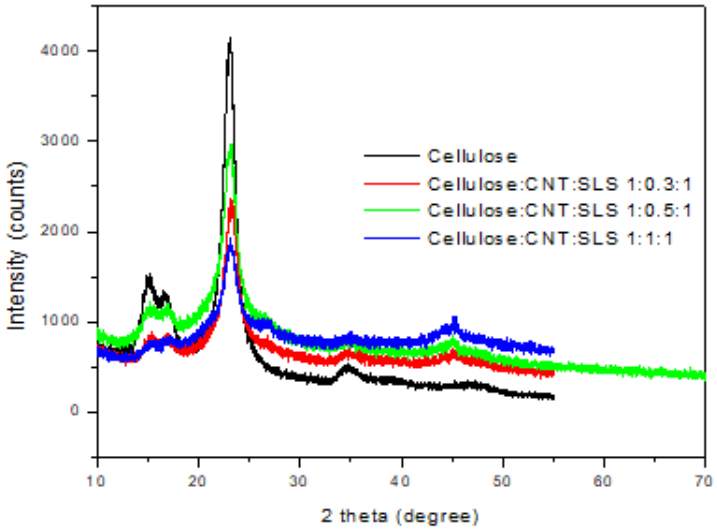

Figure 4.4: XRD curves of cellulose, cellulose: SWCNT: 1: 0.3:1, cellulose: SWCNT: SLS 1:0.5:1 and cellulose: SWCNT: SLS 1:1:1

The SLS modified carbon nanotubes showed a reduction in both the amorphous and crystalline regions of the cellulose when compared with neat cellulose and cellulose: SWCNT composites (see Figure 4.5 to Figure 4.7) (Symbol A to F). Furthermore, similar behaviour was observed for the neat cellulose and cellulose: SWCNT: SLS composites that also showed a significant reduction in the amorphous region as well as crystalline regions. Ideally, based on the reduction in amorphous region, one would have expected the crystallinity indices of the SLS-based composites to increase; however, based on the reduction in both regions, the overall crystallinity indices decreased. Poletto *et al.* [6] reported that both curaua and ramie showed

higher crystallinity indices accompanied by high crystallite sizes, which was ascribed to a decrease in the amorphous region. Tang *et al.* [7] reported that the crystallinity of neat cellulose was 71.0% while the crystallinity of TEMPO-oxidized cellulose was 69.5%, which was lower than that of neat cellulose. The reduction in crystallinity was attributed to the oxidation process, where the exposed hydroxymethyl groups that are generally found on the surface of cellulose crystals may have partially participated in the oxidation process [7], as a result decreasing the crystallinity. In the current study the in-plane regularity at 100 for the carbon nanotubes appeared at 45°, as is indicated in Figures 4.5 to 4.7, and this observation was reported in study [8]. The seems to be little or no effect on the peek position of SWCNT at 100 in the presence of cellulose.

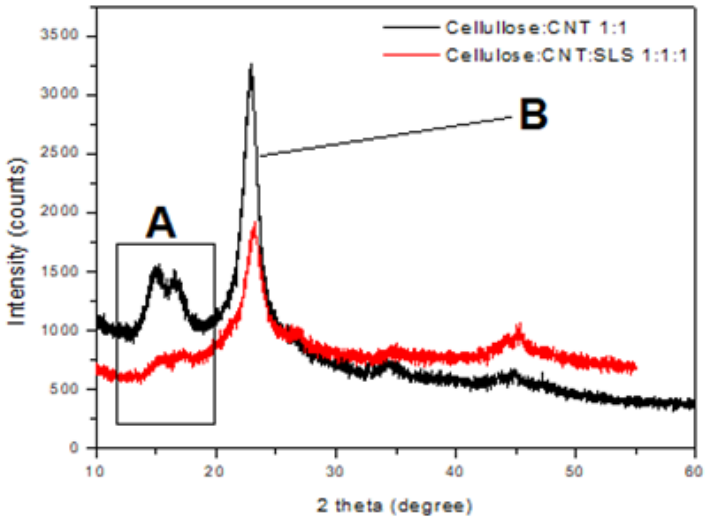

Figure 4.5: XRD curves of cellulose: CNT: 1:1 and cellulose: CNT: SLS 1:1:1

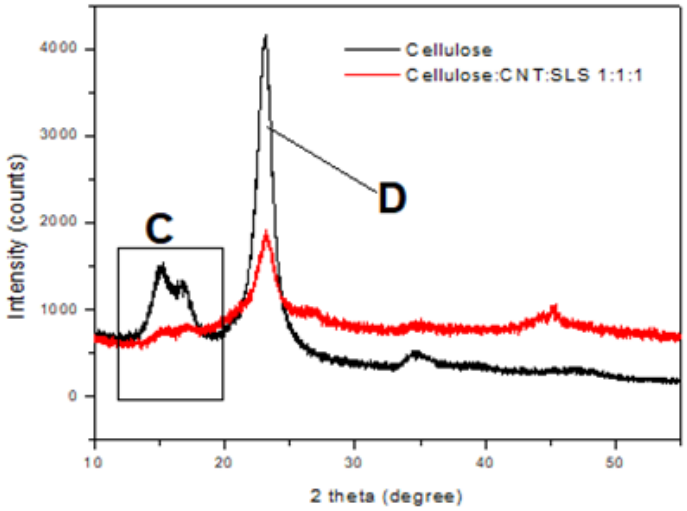

Figure 4.6: XRD curves of cellulose and cellulose: CNT: SLS 1:1:1

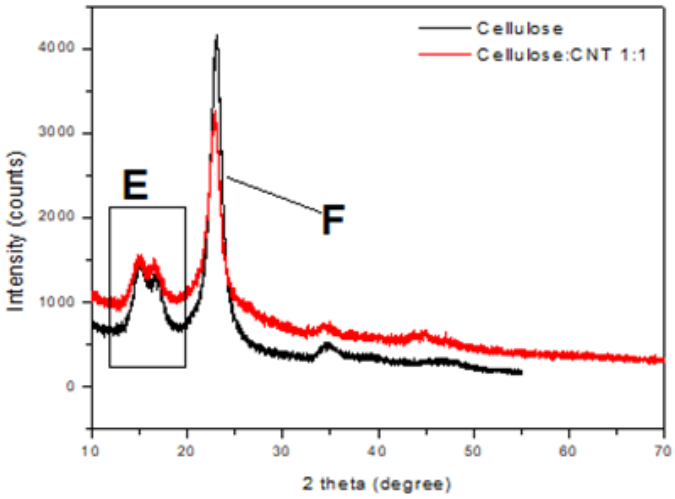

Figure 4.7: XRD curves of cellulose and cellulose: CNT 1:1

Table 4.1: Crystallinity index and crystallite sizes for the cellulose membrane and its SWCNT/cellulose composites

Membrane	Crystallinity index CI (%)	Crystallite size (nm)
Pure Cellulose	71.5	49.4
Cellulose: CNT 1:0.3	67.1	6.7
Cellulose: CNT 1:0.5	63.8	6.1
Cellulose: CNT 1:1	59.2	54.6
Cellulose: CNT: SLS 1:0.3:1	65.8	47.1
Cellulose: CNT: SLS 1:0.5:1	62.0	24.2
Cellulose: CNT: SLS 1:1:1	59.4	36.0

4.3 Fourier Transform Infrared (FTIR) Spectroscopy

Figures 4.8 to 4.9 illustrate the FTIR spectra of neat cellulose membranes, cellulose/CNT composites, and cellulose/modified SLS CNT composites. The absorption bands of cellulose-based materials are normally reported in two wavenumber ranges, i.e., 3500−2800 cm^{-1} and 1650−500 cm^{-1}. The detected peaks in the wave number range of 3334−2896 cm^{-1} are typical of polysaccharide stretching vibrations of O-H and C-H bonds [9,10,11]. In this study, neat cellulose showed a stretching vibration of the hydroxyl group in polysaccharides that was characterized by a large peak at 3334 cm^{-1} (Figure 4.8). According to the literature, this peak also comprises of the inter- and intramolecular hydrogen bond vibrations [12]. The CH stretching vibration of all hydrocarbon constituents in polysaccharides is linked to the band at 2896 cm^{-1} [9,10] for neat cellulose. Stretching and bending vibrations of $-CH_2$ and -CH, -OH

and C-O bonds in cellulose are represented by absorption bands at 1423, 1356, 1312, 1154, 1104, 1021 cm^{-1} and 894 cm^{-1} in cellulose [13,14]. The crystalline structure of cellulose is related with the band around 1423−1430 cm^{-1}, while the amorphous area of cellulose is ascribed to the band at 894 cm^{-1} [15,16].

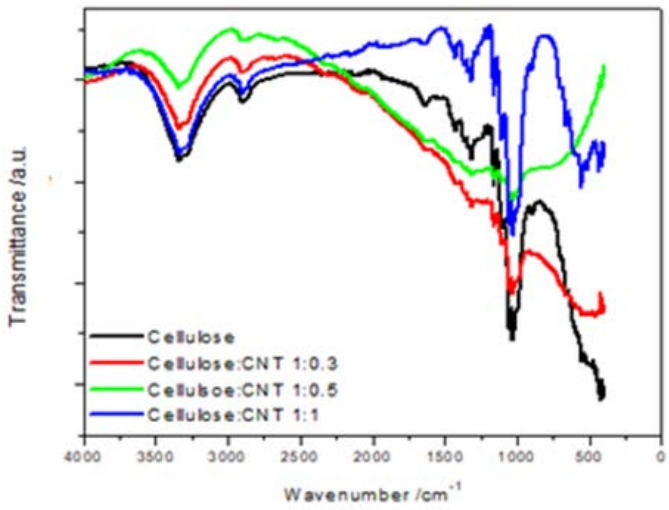

Figure 4.8: FTIR curves of cellulose, cellulose: CNT 1:0.3, cellulose: CNT 1:0.5 and cellulose: CNT 1:1

The functional groups of carbon nanotubes that were located at the wavenumbers − i.e., 3323 cm^{-1} and 1034 cm^{-1} − were attributed to the -OH and C-O stretching, respectively. However, in the cellulose/CNTs composites, the -OH and C-O stretching of CNTs were overlapping with those of the cellulose which occurred at 3334 cm^{-1} (-OH) and 1024 cm^{-1} (C-O). The addition of CNTs seemed to have little effect on the peaks of neat cellulose. However, there was a slight shift (Figure 4.9 symbol A) in the wavenumber (1641 cm $^{-1}$) of cellulose to lower wavenumber (1641 cm -1) in the presence of SWCNTs. This behaviour may be ascribed to the chemical bond in the membrane composites. This peak around 1641 cm^{-1} for cellulose was attributed to the absorption of water in the cellulose.

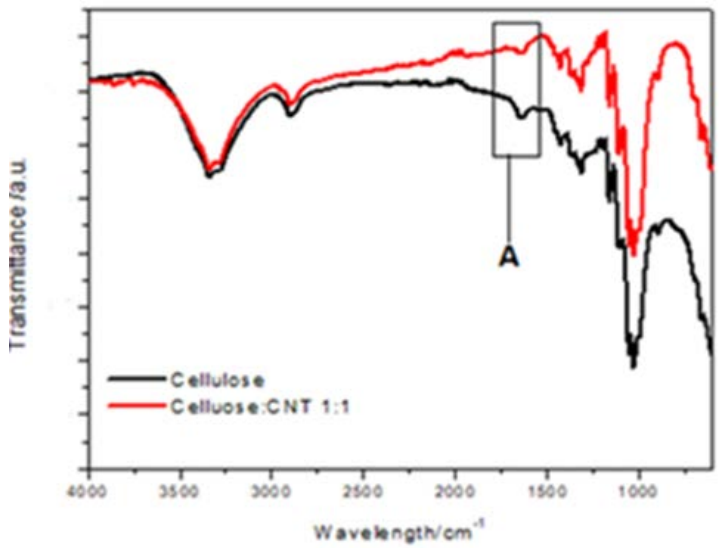

Figure 4.9: FTIR curves of cellulose and cellulose: CNT 1:1

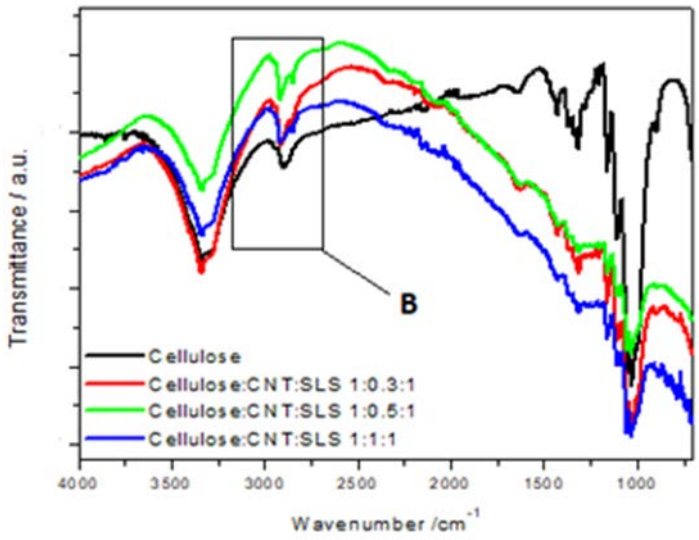

Figure 4.10: FTIR curves of cellulose, cellulose: CNT: 1:0.3:1, cellulose: CNT: SLS 1:0.5:1 and cellulose: CNT: SLS 1:1:1

Figure 4.10 illustrates the FTIR spectra of cellulose and cellulose: CNT: SLS membranes at various ratios of CNT and SLS. There was a clear reduction in the peak intensity of the cellulose in the CNT: SLS cellulose-based composites when compared with neat cellulose. The presence of SLS (chemical structure $C_{12}H_{25}NaO_4S$) in the composites was indicated by symmetric stretching 2843 cm^{-1} and asymmetric stretching 2910 cm^{-1}, as shown by symbol B in Figure 4.10. The asymmetric and symmetric peaks seemed to be absent in the non-SLS peaks, as is indicated by symbol C in Figure 4.11. Furthermore, as explained in the peak intensity of cellulose, it was also clear that the addition of SLS into CNT decreased the peak intensity when

compared with non-SLS composites, as is shown in Figure 4.11 symbol D. The decrease in the peak intensity in the presence of SLS was an indication of л-л interaction between SLS and CNT. The majority of the CNTs functional groups were not visible in the FTIR of the SLS/CNT cellulose composites which further emphasized that the dispersion of CNTs was improved in the presence of SLS. These results were well supported by the SEM investigation (section 4.1), which showed better dispersion of CNTs in the presence of SLS.

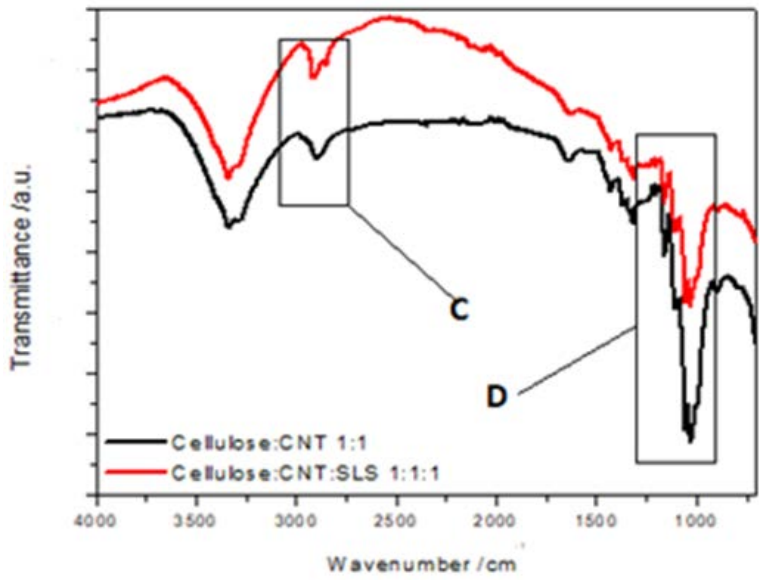

Figure 4.11: FTIR curves of cellulose: CNT: 1:1 and cellulose: CNT: SLS 1:1:1

4.4 Adsorption efficacy of cellulose, cellulose/SWCNT and cellulose/SWCNTs/SLS

Generally, the adsorption of unwanted/polluted materials depends on the physical and/or chemical process that is utilised. In the chemical interaction process, the extraction/adsorption of material interacts with the pollutant through an electrostatic force. Generally, a few steps are involved for chemical adsorption of pollutants in a solution, such as (i) transferring of bulk solution to the external surface of the adsorbent which takes place through pore diffusion from the outer surface of the adsorbent to the inner surface; and (ii) the adsorption of the pollutants on the active surfaces of the pores. The physical adsorption takes place through binding of the adsorbate on the surface of the adsorbent through forces of attraction [17]. Generally, the adsorption of pollutants by membranes occurs by merging the functional group onto the pore wall as well as the surface of the cellulose membrane. When a polluted solution passes through the membrane, the active sites in the membrane will bind with the target pollutants to extract

the contaminants from the solution (Figure 4.12). The removal of unwanted materials by carbon nanotubes takes place through four possible sites, namely outer grooves, inner grooves, interstitial channels, and the inner region of the carbon nanotubes (Figure 4.14). In the current study both anionic and cationic dyes were employed in order to investigate the method of adsorption for cellulose/SWCNT composites. Figure 4.13 to Figure 4.17 show the UV spectra of cellulose membranes and their SWCNTs cellulose membranes. Table 4.6 shows the adsorption efficiency of cellulose membranes against the bromophenol dye that was used. Table 4.2 indicates that cellulose: CNT 1:0.3 and its modified SLS system had the highest removal efficiency which was followed in efficiency by the neat cellulose membrane. As much as the cellulose: CNT composites have the highest efficiency, there is a slight difference efficiency of this system when compared with neat cellulose. Since both the dye and adsorbent system generally consist of negatively charged ions it is highly unlikely that the adsorption took place through electrostatic interaction [18-21]. However, it was highly possible that the adsorption of the dye took place through the porosity of the material. The fact that both the cellulose: CNT 1:0.3 and its modified SLS system had the highest removal efficiency made it very clear that it was the most porous system as it was able to initiate pore diffusion from the outer surface of the adsorbent system into the surface of the porous cellulose membrane. Generally, as much as the SLS modified system for cellulose: CNT 1:0.3 composites showed high removal efficiency of bromophenol dye, the presence of the SLS-based system seemed to hinder the formation of a porous structure in the cellulose membrane and, as a result, this reduced the adsorption of the dye. This behaviour showed that, in the presence of sodium lauryl sulfate, there was slow pore diffusion of the pollutants due to a limited porous structure in the membranes. El Badawi *et al.* [22] reported that the incorporation of modified CNTs led to a reduction in pore volumes, with the membrane having the largest CNT content resulting in the lowest permeation rate value.

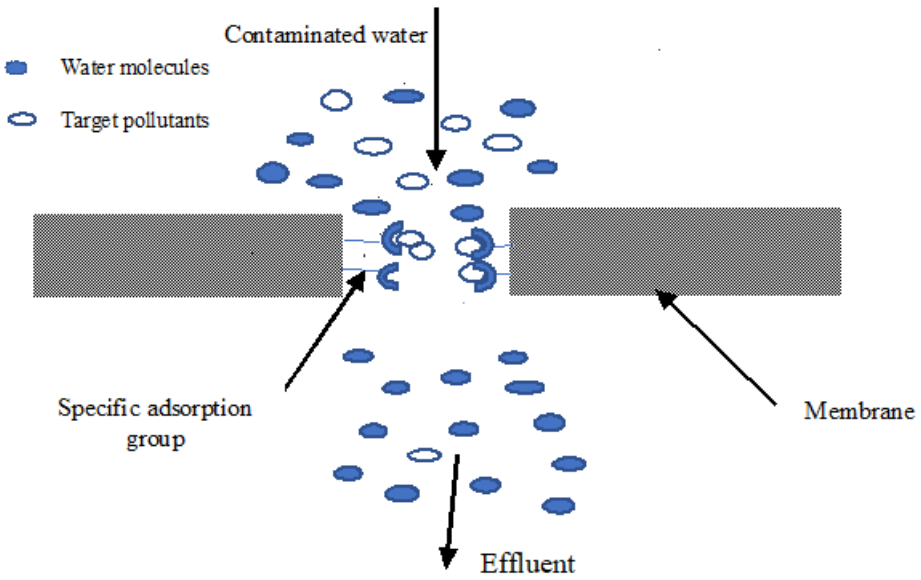

Figure 4.12: Schematic representation of the membrane adsorbent

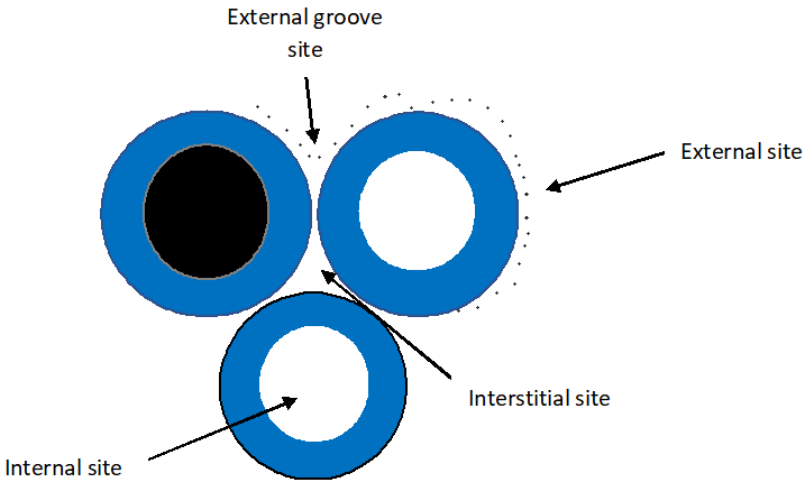

Figure 4.13: Various adsorption areas on the surface of SWCNT

The removal efficiency (R%) of the adsorbed dyes was calculated using **Equation 3**, where C_o (mg L^{-1}) is the initial concentration and C_e (mg L^{-1}) is the concentration of dye in the solution at equilibrium:

$$R(\%) = \frac{C_0 - C_e}{C_0} \times 100 \qquad (3)$$

Table 4.2: Summary of the removal efficacy of bromophenol and Dylon dye

Sample ID	Removal efficiency: Bromophenol blue %	Removal efficiency: Dylon dye %
Pure Cellulose	46.9	2.6
Cellulose: CNT 1:0.3	48.7	15.4
Cellulose: CNT 1:0.5	44.9	17.9
Cellulose: CNT 1:1	15.8	2.6
Cellulose: CNT: SLS 1:0.3:1	48.9	10.3
Cellulose: CNT: SLS 1:0.5:1	31.7	23.1
Cellulose: CNT: SLS 1:1:1	14.6	15.4

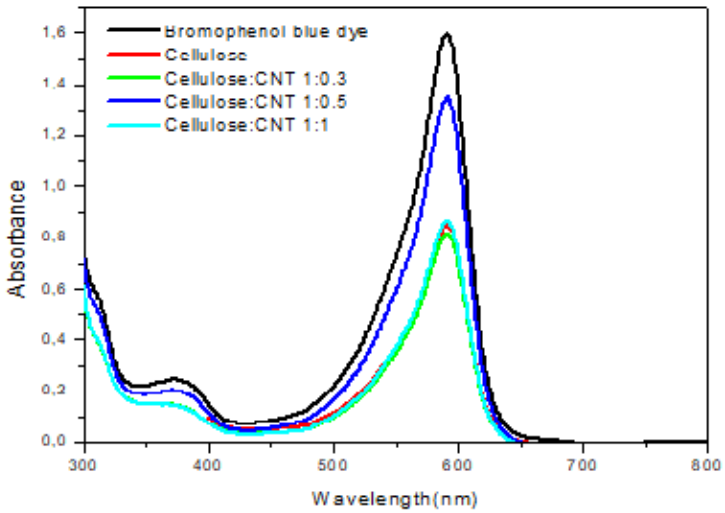

Figure 4.14: UV-vis curves of bromophenol blue dye, cellulose, cellulose: CNT 1:0.3, cellulose: CNT 1:0.5 and cellulose: CNT 1:1

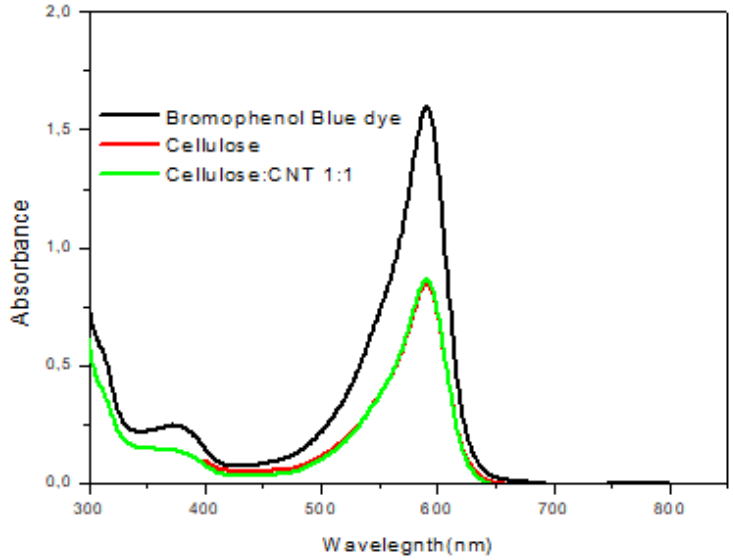

Figure 4.15: **UV-vis curves of bromophenol blue dye, cellulose, cellulose, and cellulose: CNT 1:1**

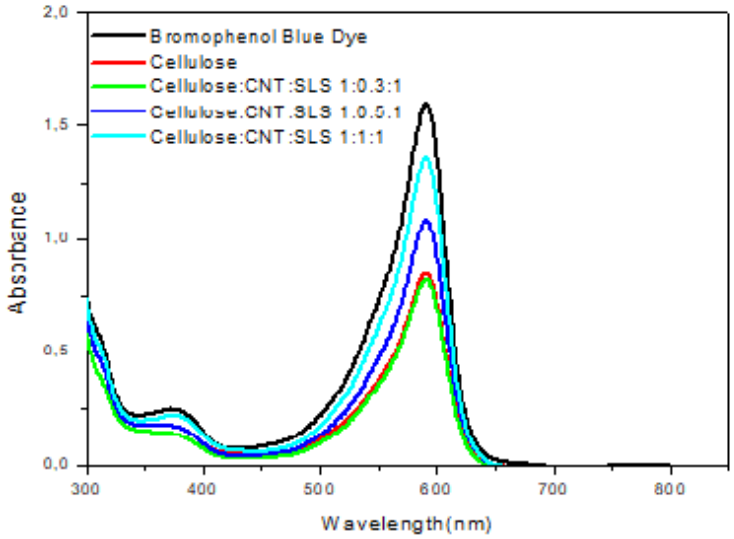

Figure 4.16: **UV-vis curves of bromophenol blue dye, cellulose, cellulose: CNT: SLS 1:0.3:1, cellulose: CNT: SLS 1:0.5:1 and cellulose: CNT: SLS 1:1:1**

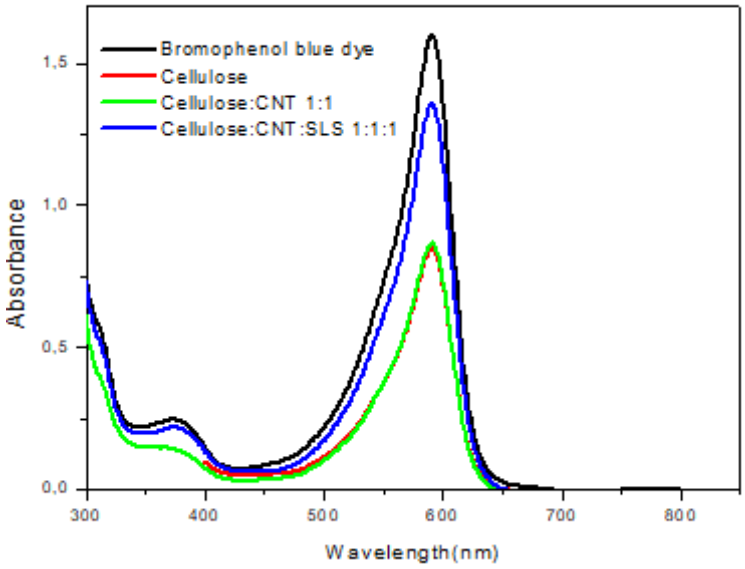

Figure 4.17: UV-vis curves of bromophenol blue dye, cellulose, cellulose: CNT 1:1 and cellulose: CNT: SLS 1:1:1.

The cellulose membrane's permeability was also tested using a Dylon dye as most commercial dyes are cationic. Table 4.2 indicates that the Dylon dye removal efficacy of all cellulose membranes/SWCNT and cellulose/SWCNTs/SLS was better compared with that of the neat the cellulose membrane, but it was completely different to what was observed in the case of anionic bromophenol blue. In this case it seemed as if the mechanism of adsorption was due to an electrostatic interaction whereby the negatively charged cellulose/SWCNT was attracted by the positively charged commercial dye. Furthermore, due to the presence of anionic SLS, the SLS-based composites showed a better removal efficacy than the cellulose/SWCNT. This might be attributed to the presence of more negatively charged SLS molecules in the system that were able to adsorb more of the positively charged dye. However, when the adsorption efficiency of the two dyes was compared with that of the cellulose/SWCNTs/SLS, the bromophenol blue dye was mostly absorbed by the system. One can argue that the porosity of the membranes played a major role in the adsorption of pollutants in this system. A careful inspection of the photographs in Figure 4.18 shows that bromophenol dye was better absorbed by the cellulose membranes than the commercial dye, which explains that porosity might have played a more significant role in the adsorption of the dye than electrostatic interaction.

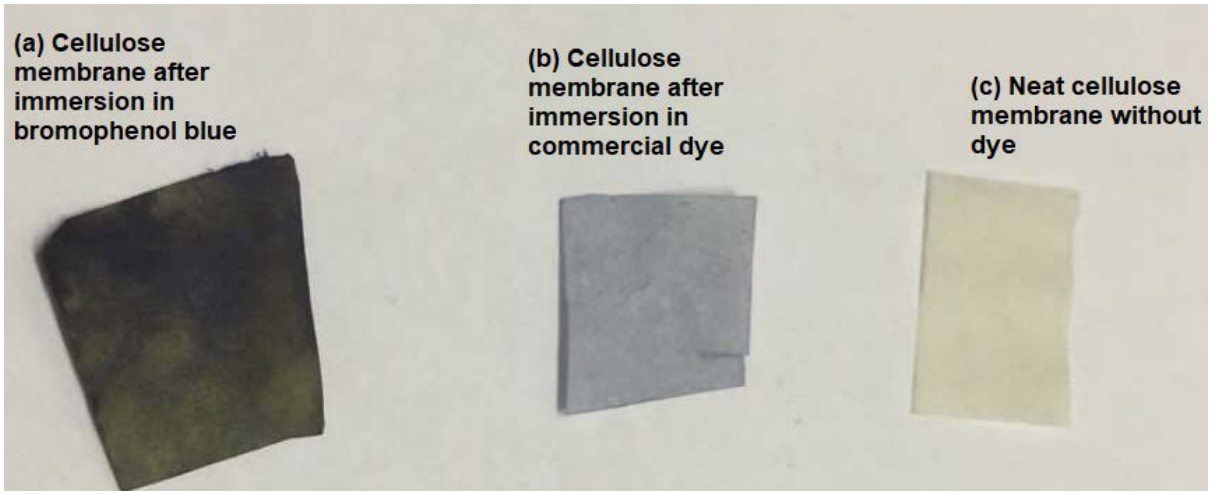

Figure 4.18: Photo images of the cellulose membranes after immersion in different dyes

4.5 Thermogravimetric Analysis

Figures 4.19 to 4.22 depict the TGA curves of cellulose, cellulose: CNT and cellulose: CNT: SLS composites. The neat cellulose membrane and its composites showed two degradation steps (Figure 4.19). The first degradation that occurred between 40^{o}C and 130℃ was attributed to the evaporation of the absorbed water from the cellulose, low molar mass components, and volatile materials. The second degradation that occurred between 200^{0}C and 400℃ was attributed to the degradation, dehydration, and decomposition of the cellulose membranes. According to the literature [23,24,25,26], the degradation of cellulose below 300℃ is known to occur faster because of the destruction of the hydrogen bonds. This behaviour changes the crystallinity and produces free radicals, namely the carbonyl as well as the carboxyl groups. Cellulose degradation between 300^{0}C and 390℃ produces products such ash, tar, and condensable as well as non-condensable gases.

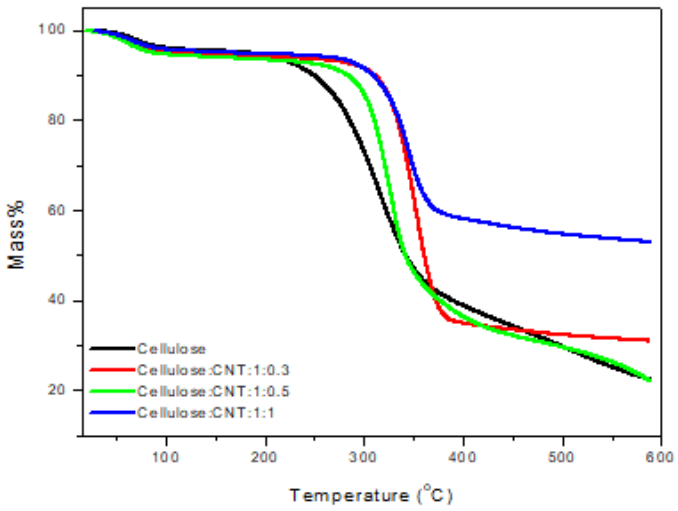

Figure 4.19: TGA curves of cellulose and cellulose: CNT 1:0.3, cellulose: CNT 1:0.5 and cellulose: CNT 1:1

The addition of CNTs at the ratio of 0.3, 0.5 and 1 into the cellulose enhanced the thermal stability of the cellulose as is depicted in Table 4.3 and Figure 4.19. This was due to the formation of the physical heat barrier against the diffusion of the volatile products out of the system, which was produced during thermal decomposition and, as a result, thermal stability was enhanced. Similar behaviour was reported in the literature [22- 26]. For example, the thermal stability of poly (ethylene 2,6-naphthalate)/CNT and poly (terephthalate of ethylene)/CNT) nanocomposites was reported [23]. It was observed from the study that the addition of the unmodified and modified carbon nanotubes into the poly (ethylene 2,6-naphthalate) enhanced the thermal stability of the polymer matrix, which was attributed to the formation of a heat barrier by the CNTs. Furthermore, the modified carbon nanotubes, which were modified with concentrated sulfuric acid and nitric acid to introduce the carboxylic acid groups onto the surface of the nanotubes, enhanced the thermal stability due to a better interfacial adhesion between the polymer and the carbon nanotubes. The char content for 0.3 of carbon nanotubes seems to be higher than that of 0.5 carbon nanotubes content. There is no clear explanation for such a behaviour

Table 4.3: Degradation temperatures at 10% and 40% for cellulose membranes

Samples	$T_{10\%}$	$T_{40\%}$
Cellulose	242.1	319.7
Cellulose: CNT (1:0.3)	313.9	353.2
Cellulose: CNT (1:0.5)	276.5	329.5
Cellulose: CNT (1:1)	306.0	372.7
Cellulose: CNT: SLS (1:0.3:1)	264.8	323.6
Cellulose: CNT: SLS (1:0.5:1)	221.7	270.6
Cellulose: CNT: SLS (1:1:1)	231.0	356.7

Figures 4.20 to 4.22 illustrate the thermal stability of neat cellulose membranes and SLS-modified CNT-based cellulose membranes. The modification of carbon nanotubes by SLS reduced the thermal stability of the unmodified CNT/cellulose composites in all investigated samples when compared with unmodified composites. For example, the $T_{10\%}$ for cellulose: CNT: SLS (1:0.3:1) showed a 15.6% reduction compared with cellulose: CNT (1:0.3), while the $T_{40\%}$ for cellulose: CNT: SLS (1:0.3:1) revealed an 8.4% reduction in relation to the unmodified cellulose: CNT (1:0.3). It seemed that the presence of sodium lauryl sulfate might have initiated the degradation of the overall composites due to the low degradation temperature of surfactants in the range of 200−300°C. Moreover, the presence of a lower thermal stability material in the form of SLS accelerated the degradation of the composites and, as a result, reduced thermal stability. Conversely, Sefadi *et al.* [27] reported an increase in thermal stability of the graphite-modified sodium dodecyl sulfate (SDS) reinforced ethylene vinyl acetate (EVA). This behaviour was attributed to a strong interaction between the chains of the polymer free radicals as well as volatile products and the filler. This strong interaction retarded the degradation of the polymer as well as the diffusion of the volatile materials out of the composite system, which improved thermal stability.

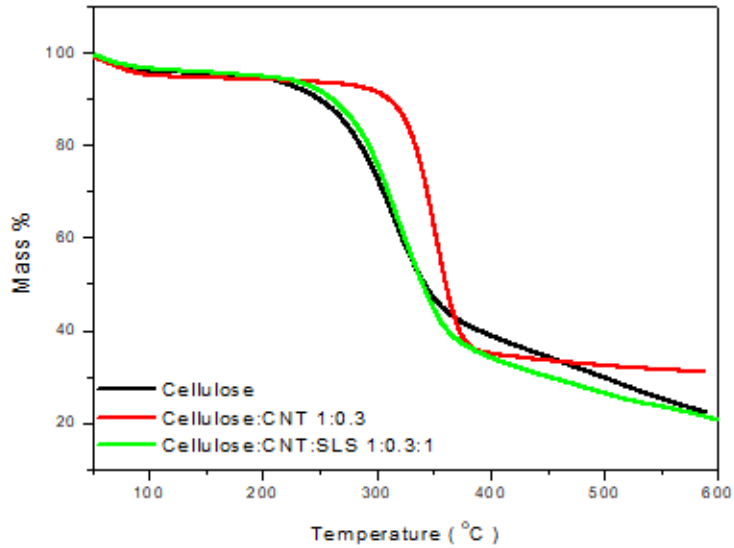

Figure 4.20: TGA curves of cellulose, cellulose: CNT 1:0.3 and cellulose: CNT: SLS 1:0.3:1

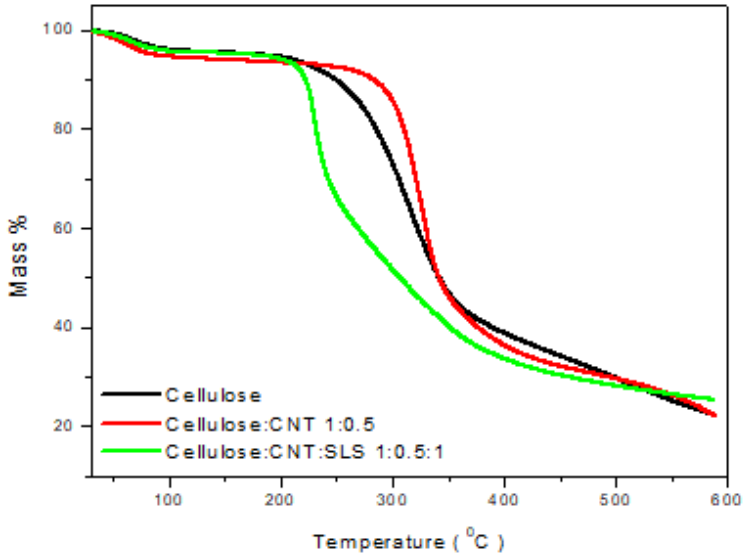

Figure 4.21: TGA curves of cellulose, cellulose: CNT 1:0.5, and cellulose: CNT: SLS 1:0.5:1

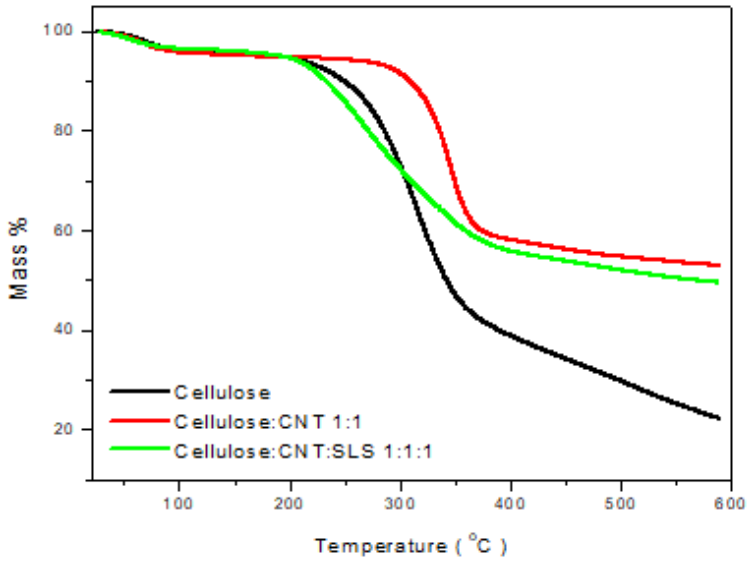

Figure 4.22: TGA curves of cellulose, cellulose: CNT 1:1 and cellulose: CNT: SLS 1:1:1.

4.6 The effect of Sodium Lauryl Sulfate (SLS) on the water absorption of cellulose/Carbon Nanotube Composites (CNT)

The nature of the interaction between water and cellulosic membranes has been a topic of fundamental curiosty for biological and environmental applications. Generally, it is well known that cellulosic materials have a high moisture tendency because of the presence and availability of hydroxy groups in cellulose. In most cases, the presence of water molecules in the cellulose membrane tends to influence interfacial bonding, which normally results in poor transfer between the cellulose membrane matrix and the reinforced fillers, which will eventually negatively affect the structural intergritiy of the membranes. Figure 4.23 schematically indictaes that the hydroxy groups (OH^-) of the cellulose membrane are completely exposed at the surface, and this means that they can easily form hydrogen bonds with nearby water molecules (H_2O). It is well documented in the literature that the formation of a hydrogen bond continuously changes the patterns in the liquid phase [28].

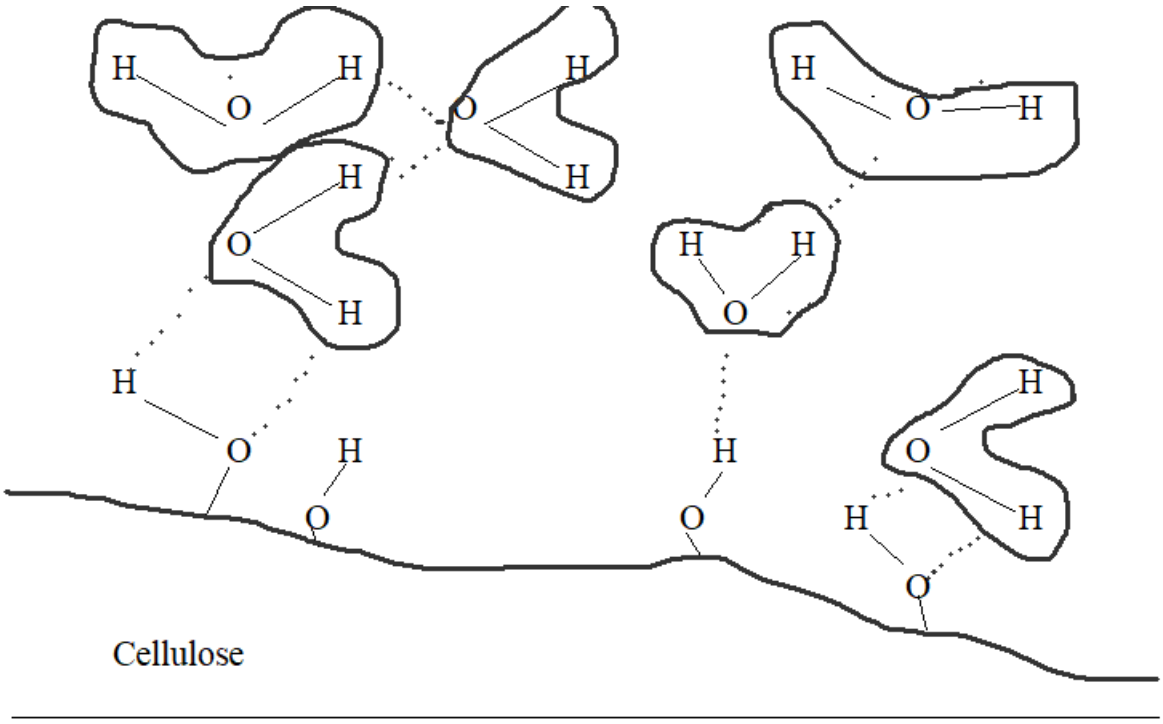

Figure 4.23: Schematic representation of the absorption of water (H_2O) by cellulose

Figure 4.24 illustrates the effect of sodium lauryl sulfate on the absorption of water by cellulose membrane/carbon nanotubes. Figure 4.25 also clearly depicts that the addition of carbon nanotubes into the cellulose mebranes enhanced the absorption of water into the composites when compared with neat cellulose. This is very interesting due to the hydrophobic nature of the carbon-based materials. However, it has been reported in the literature that nanocarbon-based materials have an intrinsic hydrophilic nature [29], which might have been the reason for the high water absorption rate in the presence of the single-walled carbon nanotubes. Generally, there was a reduction in water absorption in the presence of sodium lauryl sulfate (SLS) during all the investigated times (in hours) for samples. The main reason for this observation might be that SLS is amphiphilic, which means that it consists of a hydrophobic tail and a hydrophilic head (Figure 4.26). It is possible that the hydrophobic tail of the structure might have coated the surface of some of the OH-groups in cellulose, as a result reducing water absorption in the system. This results was in line with the removal efficiency (section 4.4) whereby the SLS-based composites showed less dye removal efficacy due to the presence of less porous strucutres in the membrane system. Futhermore, it became apparent that, when the time was increased from 24−72 hours, there was a possibility of micro cracking at the interface of cellulose/SWCNTs and/or cellulose/SWCNTs/SLS, which might have been due to swelling

in the membranes, resulting in enhanced penetration of water molecules into the composite. Zakaria *et al*. [30] reported that the neat bacterial cellulose (BC) showed the highest water absorption value of 79%. Furthermore, similar to the results in the current study, the bacterial cellulose silylated membrane absorbed less water, which was attributed to silane coating onto the BC membrane which produced a hydrophobic structures on the surface of the cellulose, thus reducing the absorption of water.

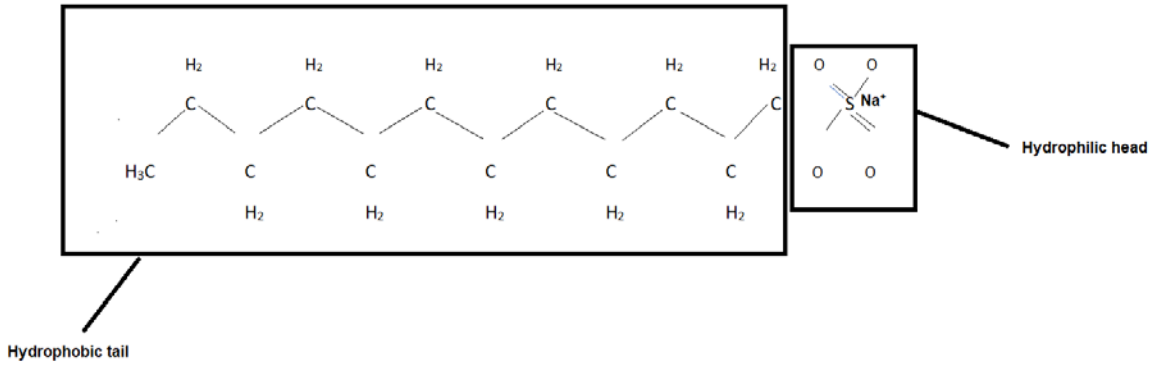

Figure 4.24: Structure of sodium lauryl sulfate (SLS)

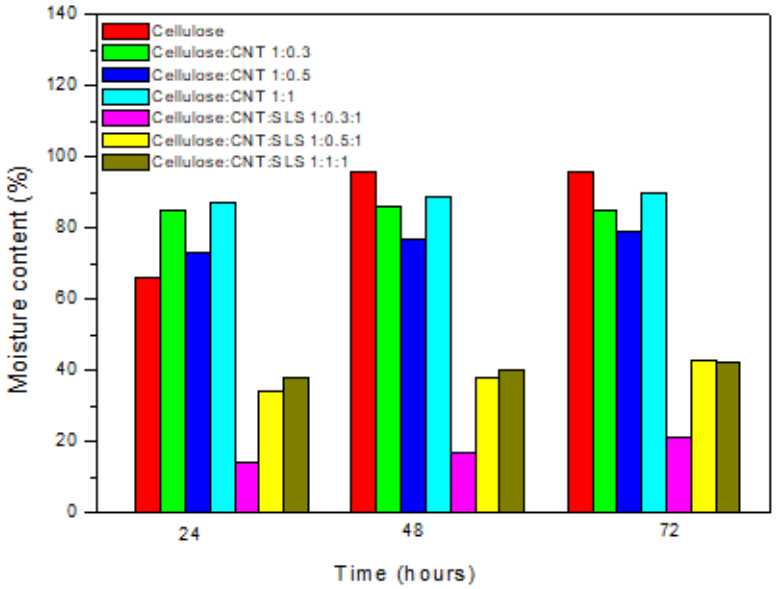

Figure 4.25: The effect of sodium lauryl sulfate on the water absorption of cellulose membranes

4.7 The effect of Sodium Lauryl Sulfate (SLS) on the chemical resistance of cellulose/Carbon Nanotube Composites(CNT)

The chemical resistance of the cellulose membranes was investigated by testing samples against different chemicals such as sodium hydroxide (NaOH) (10%), calcium carbonate ($CaCO_3$) (20%), and nitric acid (HNO_3) (40%). Figures 4.26 to 4.30 depict the chemical resistance of different cellulose-based membranes against sodium hydroxide, calcium carbonate, and nitric acid. The aim of investigating the effects of chemical absorption was to determine whether the cellulose and cellulose/CNT membranes might be employed in chemical resistance applications.

Generally, weight gain in the composite is an indication that the composite is chemically resistant [31]. It was observed that all the investigated samples showed weight gain when immersed in different chemicals. For example, Figure 4.26 and Figure 4.27 show the initial weight before immersion in the chemicals and, after 24 hours' immersion, there was an increase in weight. Similar results were obtained in the literature [32-35] as researchers reported an increase in weight when samples were immersed in chemicals. However, as much as the literature above showed improvement in chemical resistance, it became evident that, in some cases, the chemical used might decrease the chemical resistance of the fibers-based composites. For example, Noorunnisa Khanam *et al.* [35] reported chemical resistance for all investigated samples except carbon tetra chloride (CCl_4). The other chemicals utilised for their chemical tests were toluene, benzene, acetic acid (5%), HCl (10%), HNO_3 (40%), NaOH (10%), sodium carbonate (2%), and ammonium hydroxide (10%). The reduction in chemical resistance in the presence of carbon tetrachloride was attributed to the attack on the chlorinated hydrocarbons within the cross-linked polyesters, with the unsaturated polyester resin used as matrix in this study. The type of fibers and content of fibers incorporated into the polymer matrix had a different effect on the chemicals utilised for chemical resistance studies. For example, Tajvidi *et al*. [36] investigated the chemical resistance of natural fibers in the form of wood flour, newsprint, and kenaf in a fibers-reinforced polypropylene (PP) matrix. The samples consisting of 25% and 50% fibers were immersed for 7 days in chemicals such as NaOH (10%), HCl (10%), bleach solution (NaClO) (13%), H_2O_2 (3%), as well as an acetone and soap solution (1%). The results showed that the H_2O_2, soap, and acetone solutions had little effect on the chemical resistance of the samples irrespective of the natural fibers/PP composites. Furthermore, various fiber showed different behaviour regarding chemical resistance. For example, the natural fibers of rice hulls was strongly affected by the sodium hydroxide solution, whereas it was not effective against other fiber. It was shown that 25% of kenaf fibers in the

composite was quite defenceless against acid, which was evident by its weight loss. This behaviour was ascribed to the low acid resistance of the hemicelluloses and kenaf fibers which is well known to have a high hemicellulose content [37-38].

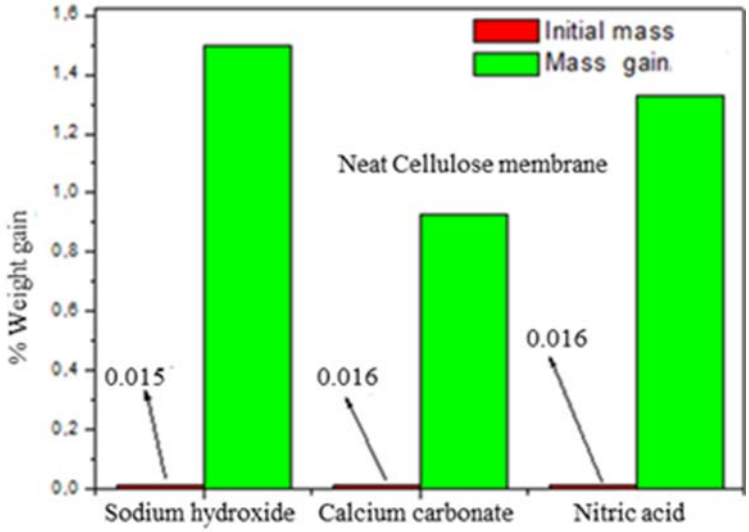

Figure 4.26: Chemical resistance results of the neat cellulose membrane tested against sodium hydroxide, calcium carbonate and nitric acid

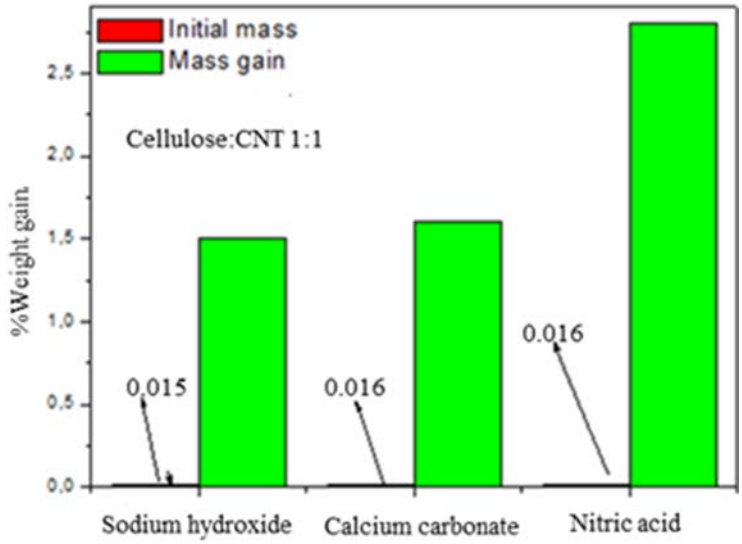

Figure 4.27: Chemical resistance results of neat cellulose: CNT 1:1 membrane tested against sodium hydroxide, calcium carbonate and nitric acid

Figures 4.28 to 4.30 depict a comparison between the results for the unmodified CNT/cellulose and the SLS-treated carbon nanotubes/cellulose membranes. Based on the data of all the chemical resistance graphs, it was evident that the samples tested with sodium hydroxide (10%) showed high values of chemical resistance for SLS-modified CNT/cellulose membranes

compared with the unmodified CNT/cellulose membranes in all investigated samples. The reason for this finding was not clear, but it seemed that the effect of common ions might have played a key role in this observation as both had sodium ions in their structure. The samples tested with both calcium carbonate and nitric acid showed higher values for the unmodified CNT/cellulose samples when compared with the SLS-modified CNT/cellulose composites. There was also no clear reason for this observation, but it has been reported in literature that more weight gain is an indication that the material is less chemically resistant [31]. This was a possibility in the current study, meaning that the modified samples were chemically more resistant than the unmodified samples. Singha *et al.* [39] reported less weight loss for silane-treated fiber, with 6% mercerized silane-treated fiber showing the lowest loss, followed by compositions such as 8, 10, 4, and 2%. Furthermore, Hossen *et al*. [31] reported that the composites showed chemical resistance, excluding carbon tetrachloride, with treated jute composites. They argued that this revealed better chemical resistance when compared with unmodified jute composites. Generally, in the composites that this study utilised the values of the chemical resistance were positive, which implies that there was a swelling of the composites with gel formation instead of them dissolving in these chemicals. Furthermore, the fact that there was no weight loss also meant that there was no erosion or corrosion of the composites.

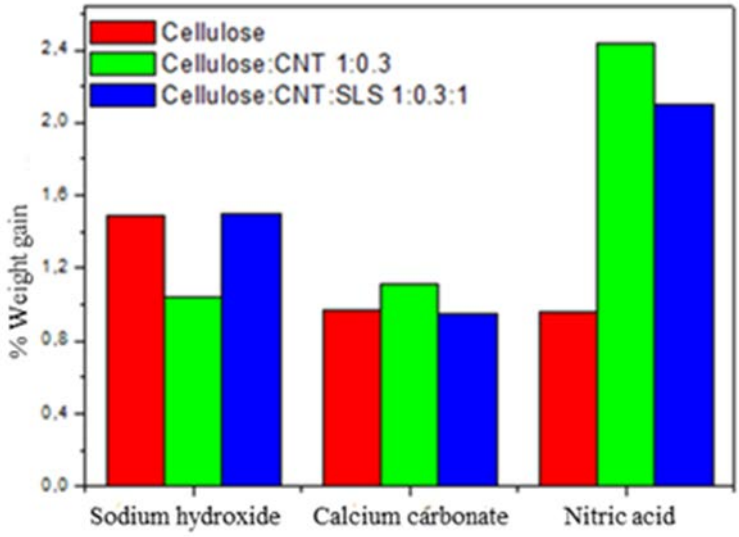

Figure 4.28: Chemical resistance results of neat cellulose, cellulose: CNT 1:0.3 membrane and cellulose: CNT: SLS 1:0.3:1 membrane tested against sodium hydroxide, calcium carbonate and nitric acid

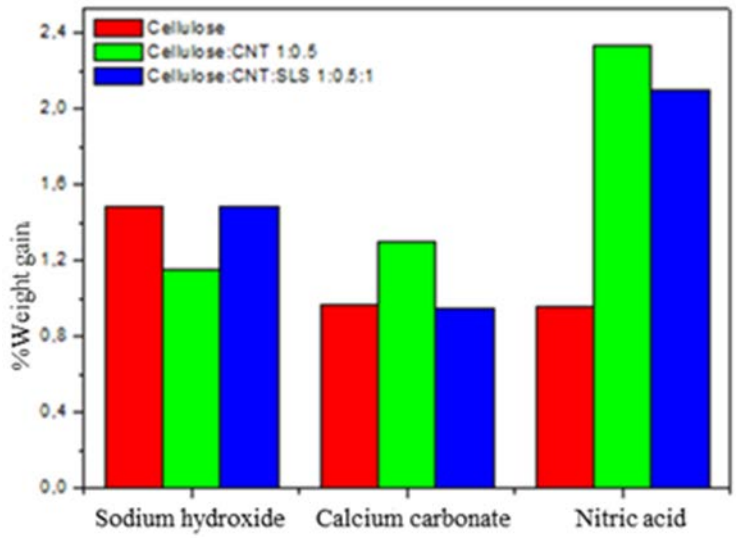

Figure 4.29: Chemical resistance results of neat cellulose, cellulose: CNT 1:0.5 membrane and cellulose: CNT: SLS 1:0.5:1 membrane tested against sodium hydroxide, calcium carbonate, and nitric acid

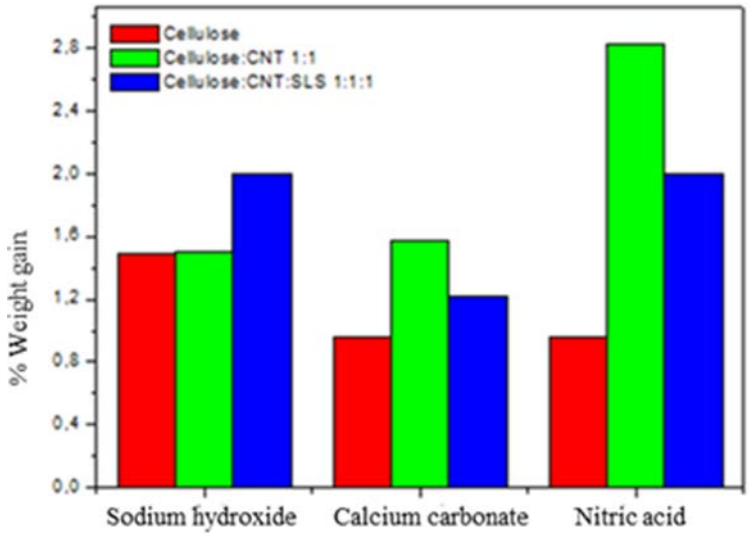

Figure 4.30: Chemical resistance results of neat cellulose, cellulose: CNT 1:1 membrane and cellulose: CNT: SLS 1:1:1 membrane tested against sodium hydroxide, calcium carbonate and nitric acid

4.8 References

1. Maria, K.H., & Mieno, T. (2017). Production and properties of carbon nanotube/cellulose composite paper. *Hindawi Journal of Nanomaterials,* Article ID 6745029, 11 pages. https://doi.org/10.1155/2017/6745029
2. Kawashima, S., Seo, J-WT, Corr, D., Hersam,M.C., Shah,S.P. (2014). Dispersion of CaCO3 nanoparticles by sonication and surfactant treatment for application in fly ash-cement systems. *Materials and Structures*, 47, 1011–1023.
3. Vaisman, L., Wagner, D., & Marom, G. (2006). The role of surfactants in the dispersion of carbon nanotubes. *Advances in Colloid and Interface Science*, 128–130, 37–46. http://dx.doi.org/10.1016/j.cis.2006.11.007
4. Zheng, J., Zhuang, M., Yu, Z., Zheng, G., Zhao, Y., Wang, H., & Sun, D. (2014). The effect of surfactants on the diameter and morphology of electrospun ultrafine nanofibers. *Journal of Nanomaterials*, 6,1-9. http://dx.doi.org/10.1155/2014/689298
5. Mohomane, S.M., Motloung, S.V., Koao, L.F., & Motaung, T.E. (2021). Effect of silica on alkaline bagasse cellulose and softwood cellulose. *Wood Research,* 66(1), 85−94. http://dx.doi.org/10.37763/wr.1336-4561/66.1.8594
6. Poletto, M., Heitor, L., Junior, O., & Zattera, A.L. (2014). Native cellulose: structures, characterization and thermal properties. *Materials*, 7, 6105−6119. http://dx.doi.org 10.3390/ma7096105
7. Tang, Z., Li, W., Lin, X., Xiao, H., Miao, Q., Huang, L., Chen, L., & Wu, H. (2017). TEMPO-oxidized cellulose with high degree of oxidation. *Polymers*, 9, 421. http://dx.doi.org 10.3390/polym9090421
8. Daicho, K., Saito, T., Fujisawa, S., & Isogai, A. (2018). The crystallinity of nanocellulose: dispersion-induced disordering of the grain boundary in biologically structured cellulose. *Applied Nanomaterials*, 1, 5774−5785.
9. Rosa, M.F., Medeiros, E.S., Malmonge, J.A., Gregorski, K.S., Wood, D.F., Mattoso, L.H.C. & Imam, S.H. (2010). Cellulose nanowhiskers from coconut husk fiber: effect of preparation conditions on their thermal and morphological behavior. *Carbohydrate Polymers*, 81, 83−92. https://doi.org/10.1016/j.carbpol.2010.01.059
10. Poletto, M., Pistor, V., Zeni, M., & Zattera, A.J. (2011). Crystalline properties and decomposition kinetics of cellulose fiber in wood pulp obtained by two pulping processes. *Polymer Degradation and Stability,* 96, 679−685. https://doi.org/10.1016/j.polymdegradstab.2010.12.007

11. Mandal, A., & Chakrabarty, D. (2014). Studies on the mechanical, thermal, morphological and barrier properties of nanocomposites based on poly (vinyl alcohol) and nanocellulose from sugarcane bagasse. *Journal of Industrial and Engineering. Chemistry*, 20, 462−473.
12. Popescu, M.C., Popescu, C.M., Lisa, G., & Sakata, Z. (2011). Evaluation of morphological and chemical aspects of different wood species by spectroscopy and thermal methods. *Journal of Molecular Structure*, 988, 65−72. https://doi.org/10.1016/j.molstruc.2010.12.004
13. Xu, F., Yu, J., Tesso, T., Dowell, F., & Wang, D. (2013). Qualitative and quantitative analysis of lignocellulosic biomass using infrared techniques: a mini-review. *Applied Energy*, 104, 801−809. https://doi.org/10.1016/j.apenergy.2012.12.019
14. Fackler, K., Stevanic, J.S., Ters, T., Hinterstoisser, B., Schwanninger, M., & Salmén, L. (2011). FT-IR Imaging Spectroscopy to localise and characterise simultaneous and selective white-rot decay within sprude woodcell. *Holzforschung*, 65, 411−420. https://doi.org/10.1515/hf.2011.048
15. Senapitakkul,V., Vanitjinda,G., Torgbo,S., Pinmanee,P.,Nimchua,T., Rungthaworn.P.(2020). Pretreatment of Cellulose from Sugarcane Bagasse with Xylanase for Improving Dyeability with Natural Dyes. *Acs omega*, 5, 28168−28177.
16. Szymanska-Chargot, M., Chylinska, M., Kruk, B., & Zdunek, A. (2015). Combining FT-IR spectroscopy and multivariate analysis for qualitative and quantitative analysis of the cell wall composition changes during apples' development. *Carbohydrate Polymers*,115, 93−103.
17. Li, B., Pan, Y., Zhang, Q., Huang, Z.,Liu, J., & Xiao, H. (2019). Porous cellulose beads reconstituted from ionic liquid for adsorption of heavy metal ions from aqueous solutions. *Cellulose*, 26(4),9163–9178. https://doi.org/10.1007/s10570-019-02687-4
18. Mohammed, N., Lian, H., Islam, M.S., Strong, M., Shi, A., Berry,R.M., Yu,H., Tam,K.H.(2021). Selective adsorption and separation of organic dyes using functionalized cellulose nanocrystals. Chemical Engineering Journal,417,129237. https://doi.org/10.1016/j.cej.2021.129237
19. Singh,S., Srivastava,V.C., Mall,I.D.(2013). Mechanistic study of electrochemical treatment of basic green 4 dye with aluminum electrodes through zeta potential, TOC, COD and color measurement, and characterization of residues. RSC Advances,1-33. DOI: 10.1039/C3RA41605D

20. Maleš,L., Fakin,D., Braˇciˇc,M., Gorgieva,S. (2020). Efficiency of Differently Processed Membranes Based on Cellulose as Cationic Dye Adsorbents. Nanomaterials,10,642. doi:10.3390/nano10040642
21. Nizam, N, U, M.,Hanafiah,M.M., Mahmoudi,E., Halim,A.A., Mohammed,A.W.(2021). The removal of anionic and cationic dyes from an aqueous solution using biomass-based activated carbon. Scientific reports,11,8623
22. Badawi, N.E., Ramadan, A.R., Esawi, A.M.K., & Morsi, M.E. (2014). Novel carbon nanotube-cellulose acetate nanocomposite membranes for water filtration applications. *Desalination*, 344, 79−85. http://dx.doi.org/10.1016/j.desal.2014.03.005
23. Kim, J.Y., Han, S.I., & Hong, S. (2008). Effect of modified carbon nanotube on the properties of aromatic polyester nanocomposites. *Polymer*, 49(15), 3335–3345. https://doi.org/10.1016/j.polymer.2008.05.024
24. Loof, D., Hiller, M., Oschkinat, H., & Koschek, K. (2016). Quantitative and qualitative analysis of surface modified cellulose utilizing TGA-MS. *Materials* 9(6), 1–14. https://doi.org/10.3390/ma9060415
25. Malaisamy, R., Mahendran, R., Mohan, D., Rajendran, M., & Mohan, V. (2002). Cellulose acetate and sulfonated Polysulfone blend ultrafiltration membranes: preparation and characterization. *Journal of Applied Polymer Science*, 86(7), 1749–1761. https://doi.org/10.1002/app.11087
26. Osorio, A.G., Silveira, I.C.L., Bueno, V.L., & Bergmann, C.P. (2008). H^2SO^4 /HNO^3/HCl-functionalization and its effect on dispersion of carbon nanotubes in aqueous media. *Applied Surface Science*, 255(5) [Part 1), 2485–2489. https://doi.org/10.1016/j.apsusc.2008.07.144
27. Sefadi, J.S., Luyt, A.S., Pionteck, J., Piana,F., & Gohs, U. (2015). Effect of surfactant and electron treatment on the electrical and thermal conductivity as well as thermal and mechanical properties of ethylene vinyl acetate/expanded graphite composites. *Journal of Applied Polymer Science*,132(2),1-10. http://dx.doi.org/10.1002/APP.42396
28. Hubbe,M.A.,Ayoub,A.,Daystar,J.S.,Venditti,R.A.,Pawlak,J.J.(2013).Review of cellulosic avsorbents.*BioResources*,8(4),6556-6629.
29. Stando,G., Łukawski,D., Lisiecki,F.,Janas,D.(2019). Intrinsic hydrophilic character of carbon nanotube networks. *Applied surface science*. 463,227-233. https://doi.org/10.1016/j.apsusc.2018.08.206.
30. Zakaria, M.N., Sukirah, A.R., Maizatulnisa, O., Ayuni, J., Khalisanni, K., & Rosmamuhamadani, R. (2017). Effect of growth times on the physical and mechanical

properties of hydrophobic and oleophilic silylated bacterial cellulose membranes. *AIP conference proceedings*, 1885, 02016. http://dx.doi.org/10.1063/1.5002354

31. Hossen, Md.F., Hamdan, S., Rahman, Md, R., & Sultan, Md.T. (2020). The effect of fibers chemical treatment on chemical resistance behavior of jute polyethylene composites for storage tank application. *Materials Science Forum*, 997, 49−55. http://dx.doi.org /10.4028/www.scientific.net/MSF.997.49.
32. Jawaid, M., Abdul Khalil, H.P.S., Abu Bakar, A., & Noorunnisa Khanam, P. (2011). Chemical resistance, void content and tensile properties of oil palm/jute fibers reinforced polymer hybrid composites. *Materials and Design*, 32, 1014−1019. https://doi.org/10.1016/j.matdes.2010.07.033
33. Vigneshwaran, S., Uthayakumar, M., & Arumugaprabu, V. (2019). Experimental examination of chemical resistance behavior of jute fibers composite. *International Journal of Recent Technology and Engineering*, 8, 289−290. http://dx.doi.org/10.35940/ijrte. D1062.1284S219.
34. Jawaid, M., Abdul Khalil, H.P.S., & Abu Bakar, A. (2011). Hybrid composites of oil palm empty fruit bunches/woven jute fibers: chemical resistance, physical and impact properties. *Journal of Composite Materials*, 45(24), 2515–2522. http://dx.doi.org 10.1177/0021998311401102.
35. Noorunnisa Khanam, P., Abdul Khalil, H.P.S., Ramachandra Reddy, G., & Venkata Naidu, S. (2011). Tensile, flexural and chemical resistance properties of sisal fibers reinforced polymer composites: effect of fibers surface treatment. *Journal of Environmental Polymer Degradation*, 19, 115–119. http://dx.doi.org/10.1007/s10924-010-0219-7
36. Tajvidi, M., Shekaraby, M.M., & Motiee, N. (2006). Effect of chemical reagents on the mechanical properties of Natural Fiber Polypropylene Composites. *Polymer Composites*,27 563−569. http://dx.doi.org/10.1002/pc.20227
37. Sjostrom, E. (1993). *Wood chemistry: fundamentals and applications* (2nd ed.). New York: Academic Press.
38. Han, J.S. (1998). Properties of non-wood fiber. In proceedings of the Korean Society of Wood Science and Technology Annual Meeting, the Korean Society of Science and Technology, Seoul, Korea, p. 3.
39. Singha, A.S., & Thakur, V.K. (2009). Morphological, thermal, and physicochemical characterization of surface modified pinus fiber. *International Journal of Polymer Analysis and Characterization*, 14(3), 271−289.

Chapter 5: Conclusions and Recommendations

Nanocellulose was extracted from maize stalks that had been sourced as agricultural waste to create a filtration membrane for wastewater treatment, specifically to investigate how nanocellulose structures affected the adsorption of different dyes contaminants and to understand the effect of carbon nanotubes on the adsorption efficacy of cellulose. It is suggested that such fabricated membranes may be useful in chemical applications due to the chemical resistant property of the cellulose membranes. The cellulose membranes were modified with carbon nanotubes and sodium lauryl sulfate (SLS) in order to enhance both their stability and absorption effectiveness. Generally, TEM and SEM showed a better dispersion of carbon nanotubes in the cellulose matrix in the presence of SLS. In the absence SLS there were clear agglomerates of the carbon nanotubes in the cellulose matrix. The presence of carbon nanotubes in the cellulose membrane matrix enhanced the thermal stability of the composites, while the presence of SLS in the cellulose/CNT decreased the thermal stability of the composites. It seemed that the presence of sodium lauryl sulfate might have initiated the degradation of the overall composites due to the low degradation temperature of surfactants in the range of 200−300°C. In light of the findings, it was concluded that the presence of CNT without SLS was able to act as a heat barrier, thereby blocking the volatiles from leaving the composites while also preventing the entrance of heat into the composites. Based on their removal efficiency, it was apparent that the cellulose membranes were able to absorb and thus remove a certain percentage of both the dyes, irrespective of the membrane used. In terms of the bromophenol dye-based system, it was concluded that the SLS-based composites were less effective in removing the bromophenol dye compared with the non-SLS-based composites, even though the cellulose: CNT: SLS 1:0.3:1 composites showed high removal efficiency. When comparing the potential removal efficiency for both dyes, it was clear that the bromophenol dye was more effectively adsorbed by the cellulose membranes, with high removal efficiency observed in the bromophenol dye system. However, the removal efficiency observed in this study was less than 50%, with the highest removal efficiency being 48.93%, which didn’t give us a higher adsorption efficiency. Future studies thus need to investigate the enhanced functionalization of cellulose membranes in order to improve their removal efficiency. This may be achieved by fabricating cellulose membranes with materials that are capable of achieving and enhancing large adsorption capacity, thus reaching high removal rates of pollutants. Additives such as activated carbon, graphene, and acetate have to be utilised in

future studies in order to compare their effectiveness against the carbon nanotubes that were utilised in the system employed by this study.

APPENDIX A

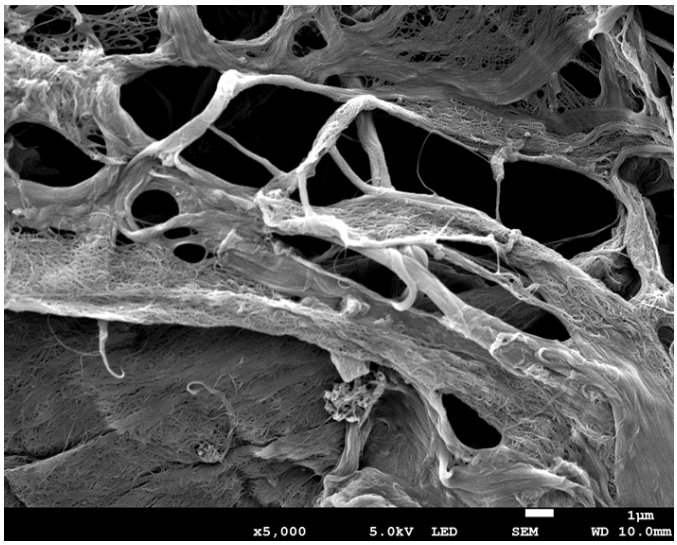

Figure A.1 SEM image of Cellulose: CNT 1:0.5

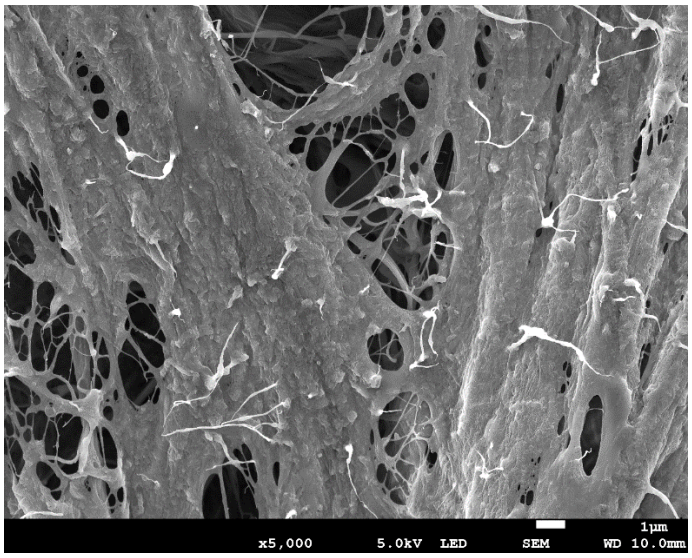

Figure A.2 SEM Image Pure Cellulose

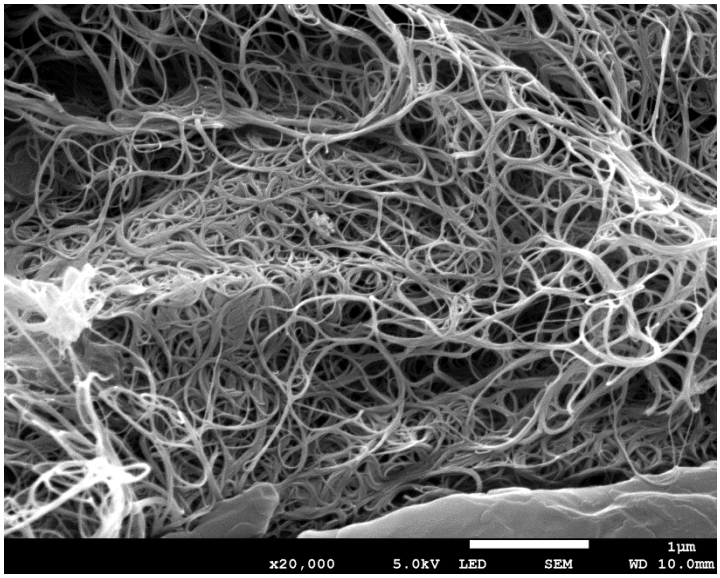

Figure A.3 SEM image of Cellulose: CNT: SLS 1:0.5:1

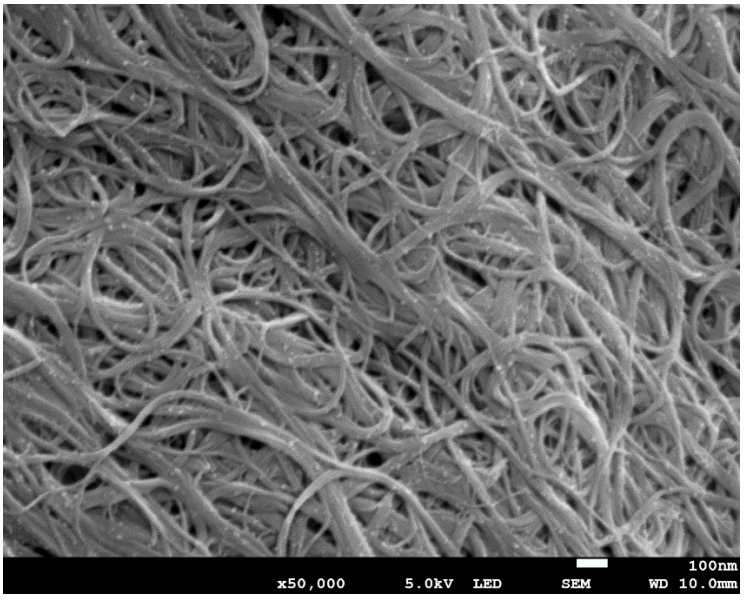

Figure A.4 Sem image of CNT: SLS 0.5:1

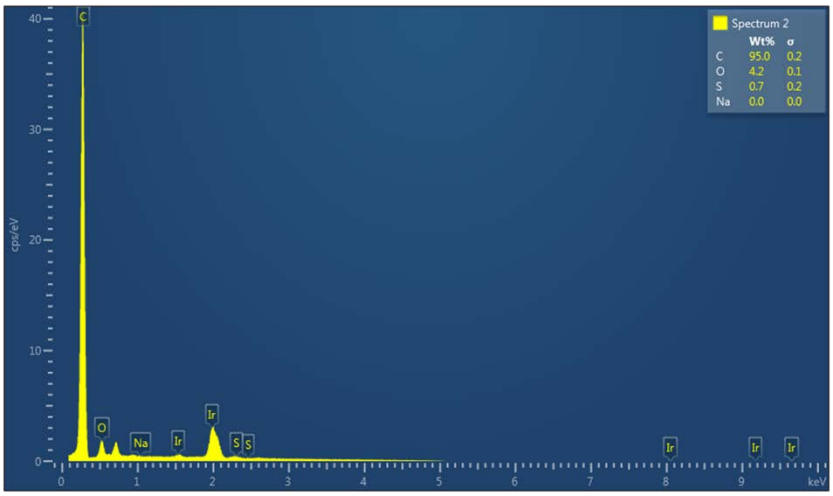

Figure A.5 EDS Report Cellulose:CNT

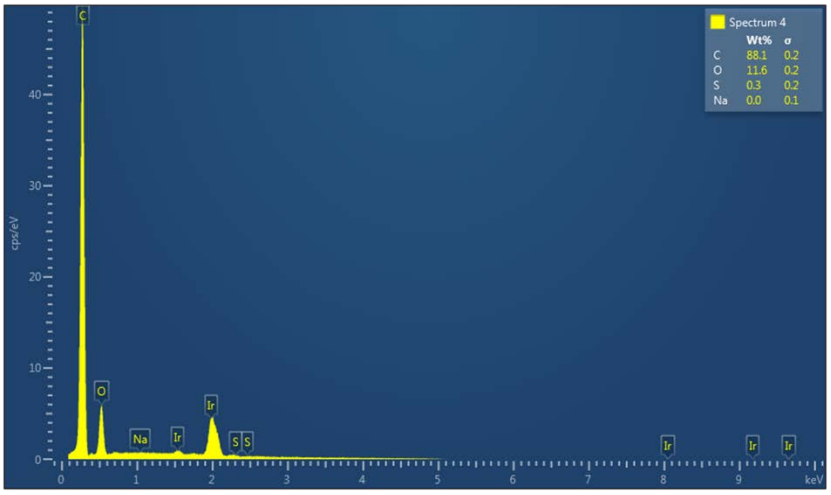

Figure A.6 EDS Report Pure Cellulose

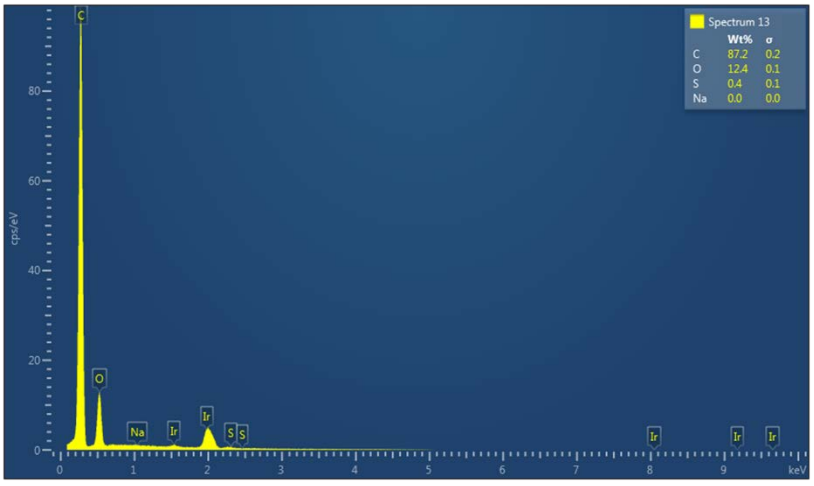

Figure A.7 EDS Report Cellulose: CNT: SLS